Study on development of CO[2] reactive ionic liquid-based facilitated transport membranes for CO[2] separation

Kasahara, Shohei

(Degree)
博士（工学）

(Date of Degree)
2014-09-25

(Date of Publication)
2015-09-01

(Resource Type)
doctoral thesis

(Report Number)
甲第6222号

(URL)
https://hdl.handle.net/20.500.14094/D1006222

Doctoral Dissertation

Study on development of CO_2 reactive ionic liquid-based facilitated transport membranes for CO_2 separation

CO_2 反応性イオン液体を用いた CO_2 選択透過型促進輸送膜の開発に関する研究

July 2014

Graduate School of Engineering

Kobe University

Shohei Kasahara

Contents

Chapter I

General introduction

I.1 Carbon dioxide capture technology

Prevention of global warming is a critical issue related to the conservation of the global environment. Because carbon dioxide (CO_2) is a major contributor to the greenhouse gas effect, the development of an energy-efficient and cost-effective technology for CO_2 capture has attracted considerable interest. The most widely used technology for CO_2 separation is the amine-based absorption process. However, aqueous-amine absorption processes suffer a number of serious disadvantages, including high energy costs, loss of solvent, and corrosion effects. Recently, membrane technology has become regarded as a potential alternative to conventional technologies because of various advantages, such as low capital and operating costs, low energy consumption, and ease of operation.[1-4] The number of patents in membrane technology for CO_2 separation has rapidly increased, year by year (Fig. I.1).[4]

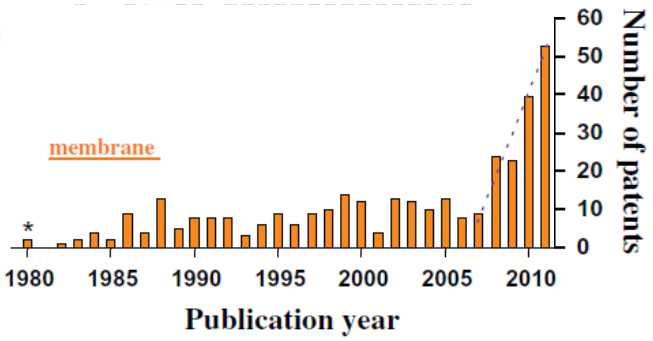

Fig. I.1 Number of patents published each year. The Espacenet website (http://www.epo.org/searching/free/espacenet.html)[5] was used to search for patents. Patents on CO_2 capture membranes were searched using (i) keywords (in title) "CO_2 membrane or carbon dioxide membrane" and (ii) combined keywords "membrane (in title) and CO_2 or carbon dioxide (in abstract)" and vice versa.[4]

However, practical use of CO_2 separation membranes remains challenging despite extensive research carried out in this area. One of the most serious problems for CO_2 separation membranes is their poor separation performance, in particular low CO_2 permeability. Poor CO_2 separation performances, such as low CO_2 permeability and low CO_2 selectivity, restrict the application of membranes in industrial processes because they require large membrane areas and multiple modules to produce a desired amount of CO_2 at high purity. Therefore, fabrication of a membrane with high CO_2 separation performance is highly desirable to enable compact processing and lower running and capital costs in line with industrial requirements.

I.2 CO_2 separation membranes

Both porous and nonporous membranes are commonly applicable in gas separations. Because porous membranes separate gases based on a molecular sieve mechanism, they are difficult to apply to CO_2 separation from light gases, such as hydrogen and nitrogen, which have molecular sizes that are similar to or smaller than CO_2. Therefore, nonporous membranes have recently attracted significant attention for separation of CO_2 from light gases. A brief introduction to previous studies regarding nonporous membranes is provided in the following sections.

I.2.1 Polymeric membranes

Among the several types of CO_2 separation membranes available, polymeric membranes have been widely investigated.[6-16] Advantages of polymeric membranes are their low fabrication costs and high mechanical toughness. However, they are rarely used in practical operation because of critical disadvantages: the CO_2 permeability and CO_2

selectivity against light gases are both very low.[6-16] In general, gas molecules permeate through polymeric membranes via the solution-diffusion mechanism. In this mechanism, gas permeation through a membrane can be described by the product of the gas solubility and the diffusion coefficient.[17] The gas permeability and selectivity are mainly controlled by the gas condensability and the kinetic diameter of the gas molecules, respectively. The size and condensability of several gases are listed in Table I.1.[18,19] As shown in Table I.1, the size of CO_2 is closely similar to that of the other light gases. In addition, the condensability of CO_2 is not markedly higher than that of the other gases, for example being just 2.4 times higher than N_2. For these reasons, polymeric membranes show low CO_2 permselectivity.

Table I.1 Penetrant parameters characterizing size (critical volume) and condensability (critical temperature)[7]

	Size (critical volume (cm^3/mole))	Condensability (critical temperature (K))
He	57.4	5.19
H_2	65.1	33.24
O_2	73.4	154.6
N_2	89.8	126.2
CO_2	93.9	304.21
CH_4	99.2	191.05
C_2H_4	130.4	282.40
C_2H_6	148.3	305.35
C_3H_6	181.0	364.9
C_3H_8	203.0	369.8

In 1991 and 2008, Robeson[9,20] reported that there was a trade-off relationship between the CO_2 permeability and CO_2/N_2 selectivity of polymeric membranes. As shown in the Robeson's plot (Fig. I.2), polymeric membranes have a clear upper bound in the relationship between the CO_2 permeability and CO_2/N_2 selectivity. This relationship indicates that it is difficult to improve both CO_2 permeability and CO_2/N_2 selectivity of

polymeric membranes by changing the polymers.

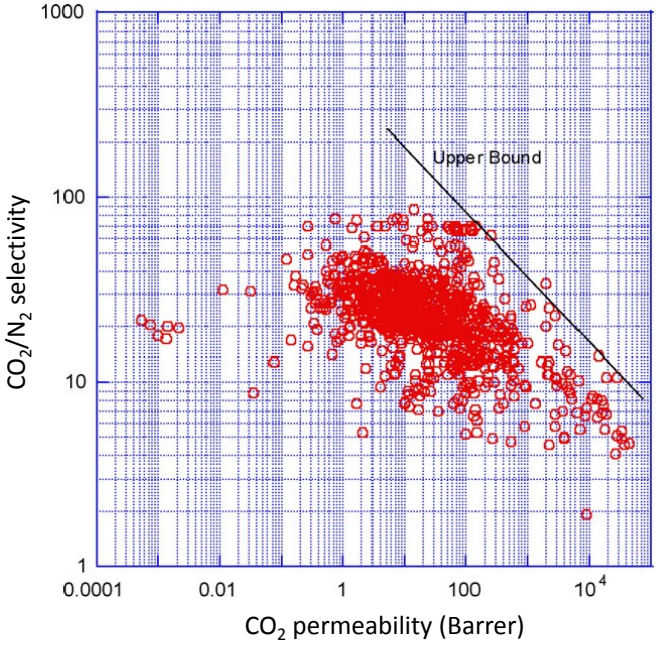

Fig. I.2 Upper bound correlation for CO_2/N_2 separation.[9]

I.2.2 Facilitated transport membranes

Recently, facilitated transport membranes (FTMs) have attracted attention as a promising CO_2 separation membrane.[21-33] FTMs are functionalized membranes that containing a chemical compound, a so-called "CO_2 carrier", which can selectively and reversibly react with CO_2. The permeation mechanism of FTMs is based on the reversible reaction of the target gas with a CO_2 carrier on the surface or inside the membranes and intra-diffusion of the CO_2-complex formed via reaction. The CO_2 carrier markedly improves CO_2 absorbability through chemical reaction with CO_2. In addition, because absorbability of gases other than CO_2 is not affected by the CO_2 carrier, the carrier dramatically increases CO_2 absorption selectivity. Therefore, as shown in Fig. I.3, FTMs display much higher CO_2 permeability and CO_2/N_2 selectivity than polymeric

membranes. In the next section, a brief introduction to previously developed FTMs is given.

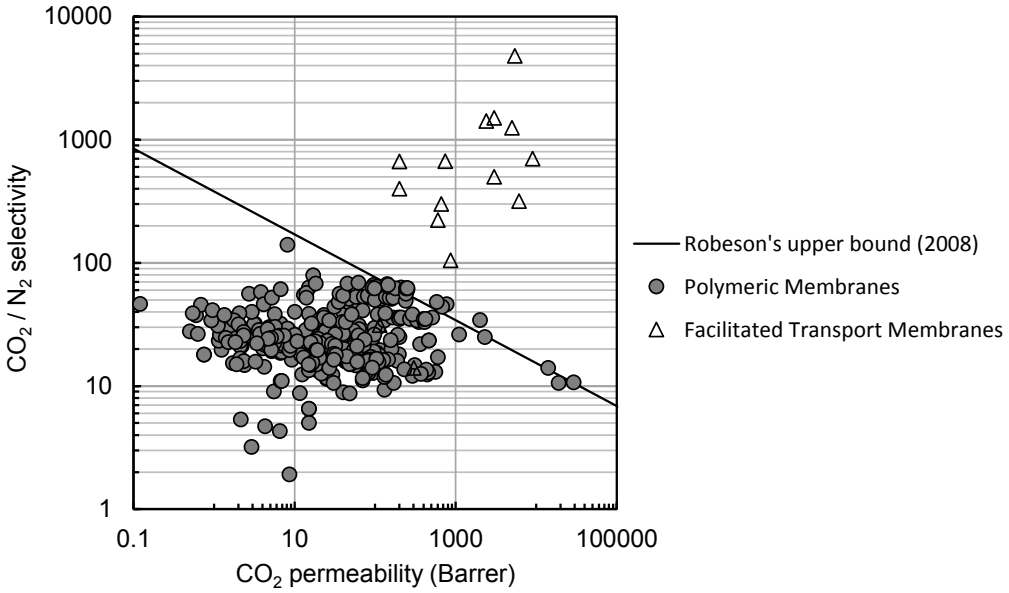

Fig. I.3 Comparison of gas separation performances for various membranes.[9,23-33]

I.2.2.1 CO_2 permeation properties of FTM

In general, two types of carriers have been developed for FTMs: a mobile carrier and a fixed carrier. FTMs that include mobile and fixed carriers are known as mobile carrier and fixed carrier membranes, respectively. The mobile carrier membrane contains a low molecular weight compound such as carbonate or amine as the mobile carrier. The most widely developed mobile carrier membranes are supported liquid membranes (SLMs), which are prepared by impregnating a carrier solution into a porous support membrane.[21,23,25,27,34-55] On the other hand, a fixed carrier membrane contains a polymeric amine such as polyvinyl amine or chitosan, where the amine groups function as the fixed carrier. Fixed carrier membranes are generally prepared by casting a polymer solution containing a polymeric amine with another polymer.[28,56-74] The gas

permeation mechanisms of the mobile carrier and fixed carrier membranes are shown in Fig. I.4.

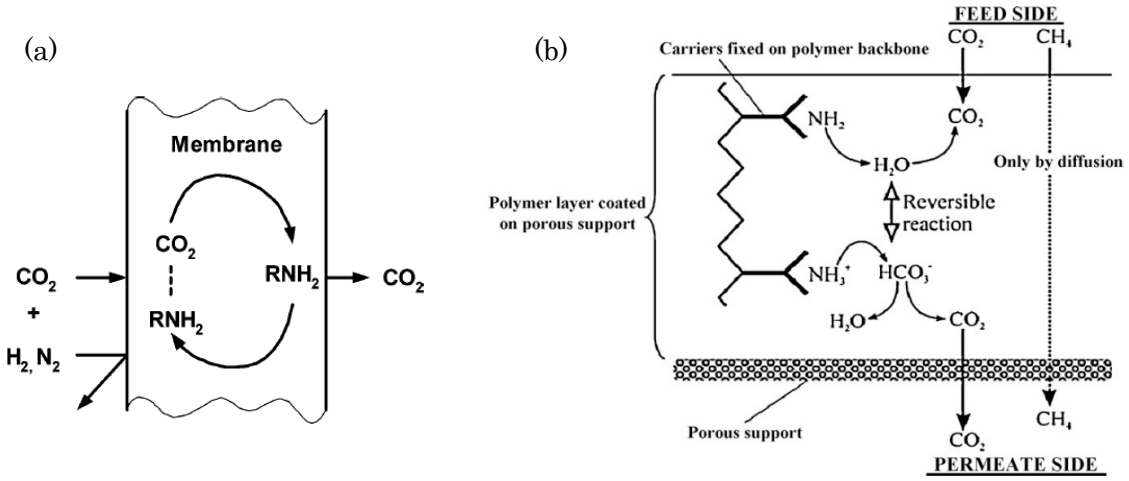

Fig. I.4 CO_2 permeation mechanisms for facilitated transport in (a) mobile carrier membranes[25] and (b) fixed carrier membranes[72].

Focusing on the CO_2 permselectivity, it is well known that mobile carrier membranes show much higher CO_2 permselectivity than fixed carrier membranes, because of the difference in carrier diffusivities.[75] In the case of mobile carrier membranes, the carriers can freely move within the membranes because the diffusion medium is a liquid. In contrast, in fixed carrier membranes, the carriers cannot freely move because they are fixed within the polymer matrix. Therefore, mobile carrier membranes provide much higher intra-membrane solute diffusivity than that of the fixed carrier membranes.

To overcome the low diffusivity of the fixed carrier membranes, superabsorbent polymers (SAPs) are mainly used as the major matrix of the fixed carrier membranes.[72-74] The fixed carrier membranes prepared with SAPs showed high CO_2 permselectivity under humid conditions.[74] However, the CO_2 permeability of the fixed carrier membranes

composed of SAPs was low under dry conditions. Therefore, the applicable conditions of the fixed carrier membranes are limited.

In summary, it can be said that the mobile carrier membrane is preferable to fabricate a CO_2 separation membrane with high CO_2 permeability and high CO_2/other light gas selectivity under wide applicable conditions.

I.2.2.2 Stability of SLMs

Although SLMs with a mobile carrier provide high CO_2 permeability as well as CO_2 selectivity, they still suffer serious disadvantages. Because a volatile carrier and/or solvent are generally used to prepare mobile carrier membranes, loss of volatile carrier and/or solvent from the membrane readily occurs. In addition, because the carrier solution is held within the porous supports by capillary forces, they readily leak from the porous support under the influence of a small pressure difference across the membrane. To overcome these disadvantages, many investigations have been carried out.

In 1967, Ward and Robb[34] first described an FTM as a mobile carrier membrane containing aqueous carbonate and hydrogen carbonate solution as the CO_2 carrier. Subsequently, to improve the CO_2 separation performance, other CO_2 carriers were developed and applied to the FTMs. Smith and Quinn[35], Donaldson and Nguyen[36], and Teramoto[43] investigated an FTM containing monoethanolamine as a mobile CO_2 carrier. Donaldson and Nguyen[36], Guha *et al.*[37], and Davis and Sandall[38] reported an FTM containing diethanolamine as a mobile CO_2 carrier. As described in these reports, the amine-based carriers showed high CO_2 permeability and selectivity. On the other hand, many researchers have investigated the improvement of the stability and durability of mobile carrier membranes. Leblanc *et al.*[44] suggested that carrier leakage from the

porous support can be improved by using an ion exchange membrane as a support because this can retain a carrier by electrostatic interaction. However, the loss of carriers cannot be completely prevented by using ion-exchange membranes.[27,45] Regarding the loss of the carrier solution caused by evaporation of the carrier and/or solvent during gas permeation operation, Chen *et al.*[21] developed a novel mobile carrier membrane containing a refractory material, such as glycerol, as a carrier solvent, and reported that the loss of the carrier can be completely prevented by using the refractory solvent. However, a membrane containing a refractory solvent showed low CO_2 permselectivity, because of low carrier concentration. This type of carrier solution was prepared by dissolving a solid state carrier such as sodium glycinate or carbonate in glycerol.[21,47,48] Therefore, the carrier concentration in the carrier solution was limited by the solubility of the carrier in the solvent.

I.2.2.3 Desirable carrier for a CO_2 facilitated transport membrane

In this section, a desirable carrier for a CO_2 selective FTM is proposed. In conventional mobile carrier membranes, a carbonate or an amine is used as a mobile carrier. Their CO_2 reaction mechanisms differ.[47] The reaction between carbonate and CO_2 requires water, while the amine can react with CO_2 regardless of the presence of water (Fig. I.5).[47] The reactions between each carrier and CO_2 can be described as follows.

In the case of carbonate type carriers:[34]

$$CO_2 + H_2O \rightleftarrows HCO_3^- + H^+ \quad \text{(I.1)}$$

$$CO_2 + OH^- \rightleftarrows HCO_3^- \quad \text{(I.2)}$$

$$HCO_3^- \rightleftarrows CO_3^{2-} + H^+ \quad \text{(I.3)}$$

$$H_2O \rightleftarrows H^+ + OH^- \quad (I.4)$$

The overall reaction can be described as follows:

$$CO_2 + H_2O + CO_3^{2-} \rightleftarrows 2HCO_3^- \quad (I.5)$$

In the case of amine type carriers:[25]

$$CO_2 + R\text{-}NH_2 \rightleftarrows R\text{-}NHCOOH \quad (I.6)$$

$$R\text{-}NHCOOH + R\text{-}NH_2 \rightleftarrows R\text{-}NHCOO^- + R\text{-}NH_3^+ \quad (I.7)$$

The overall reaction can be described as follows:

$$CO_2 + 2R\text{-}NH_2 \rightleftarrows R\text{-}NHCOO^- + R\text{-}NH_3^+ \quad (I.8)$$

The following reactions also occur under humid conditions:

$$R\text{-}NHCOOH + H_2O \rightleftarrows R\text{-}NHCOO^- + H_3O^+ \quad (I.9)$$

$$R\text{-}NHCOO^- + H_2O \rightleftarrows R\text{-}NH_2 + HCO_3^- \quad (I.10)$$

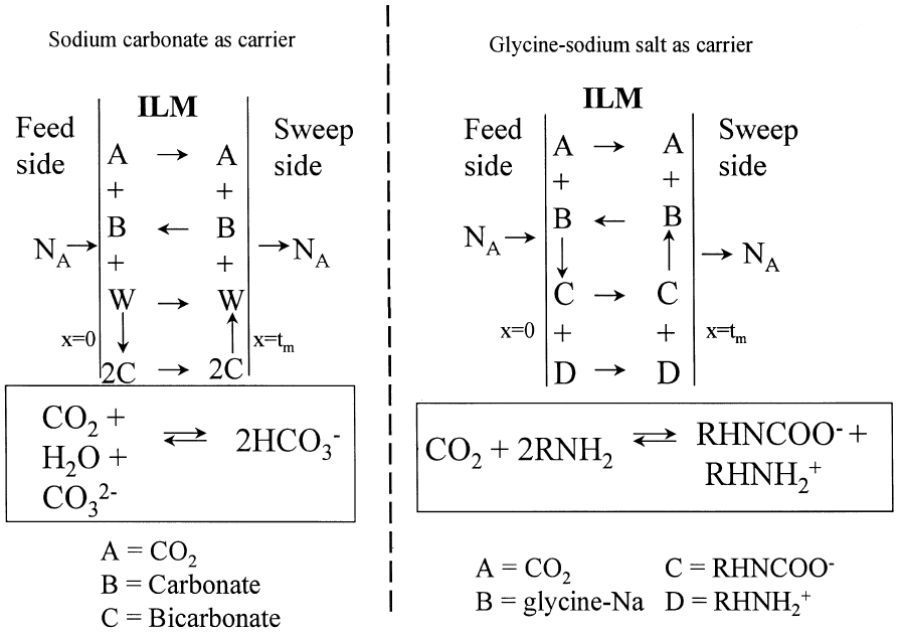

Fig. I.5 Schematics of the facilitated transport of CO_2 for sodium carbonate and sodium glycinate carriers. ILM, immobilized liquid membrane.[47]

Based on these reaction mechanisms, an amine carrier that can work under wide humidity conditions, including a dry environment, is preferable for CO_2 separation FTMs. However, if an amine carrier becomes solidified by crystallization under low humidity conditions, the mobility of the carrier is drastically decreased. Therefore, it is necessary to use an amine solution that maintains the liquid state over a wide temperature range. As mentioned in the above section, if the liquid carrier is volatile, it may be evaporated and lost from the membrane. Volatilization of the carrier would decrease CO_2 permeability and cause the formation of defects in the membrane during operation. Therefore, nonvolatility is also a necessary characteristic of a desirable CO_2 carrier. In addition to the above requirements, of course, a high carrier concentration is preferable, to set up a large CO_2 concentration gradient across the membrane, which is the driving force for CO_2 transportation through the membrane.

In summary, for a desirable CO_2 carrier in a CO_2 separation FTM having a high CO_2 permeability, CO_2 selectivity and good stability, the following four requirements can be proposed: (1) the carrier must exist in the liquid state over a wide temperature range; (2) the carrier is nonvolatile; (3) the carrier contains an amine group; and (4) the concentration of amine groups in the carrier is high.

I.2.3 Supported ionic liquid membranes

Recently, room temperature ionic liquids (RTILs) were used as a CO_2 separation media in novel SLMs. RTILs have negligible volatility, which is a promising property for overcoming shortages in the membrane. To overcome defect formation in SLMs caused by the evaporation of the solvent from the porous support, Scovazzo *et al.*[76] developed a supported ionic liquid membrane (SILM) and investigated its durability through a long-

term stability test. In their report, it was indicated that the CO_2 permeability and selectivity of SILMs remained constant during 106 days of continuous operation. They further reported that defect formation via evaporation could be completely prevented by using RTILs as a diffusion medium. However, the CO_2 permeability and selectivity of SILMs were low because the fabricated SILMs were not FTMs; i.e., no CO_2 carrier was incorporated in the SILMs and CO_2 permeated through the membrane via the solution-diffusion mechanism.[76-81]

Regarding FTMs fabricated using RTILs, Won *et al.*[82] developed an FTM for olefin/paraffin separation. The developed membrane was a SILM containing an RTIL in which silver salt was dissolved as an olefin carrier. Because the membrane showed higher olefin permeability and selectivity than other membranes without the carrier, they suggested that the olefin permeability and selectivity of the SILMs could be improved by the silver salt, which acted as an olefin carrier. Although this methodology would be applicable to develop CO_2 separation FTMs with desirable durability, no reports on the fabrication of FTMs containing RTILs with CO_2 carrier can be found. This is presumably because of the limited solubility of the CO_2 carrier in the RTILs. Won *et al.*[82] mentioned that fabrication of SILMs with high carrier concentration is difficult because of the carrier solubility in RTILs. However, it is well known that the physical and chemical properties of RTILs can be easily tuned by tailoring the structure of the cation and/or anion. Therefore, it should be possible to design an ionic liquid with a high CO_2 carrier solubility. Moreover, if an ionic liquid that can react with CO_2 could be tailored and applied to SILMs, it is expected that the reactive ionic liquid itself would act as a CO_2 carrier as well as a diffusion medium. Such FTMs would provide high CO_2 carrier concentrations because no solvent for CO_2 carrier would be required.

I.3 Amine-functionalized task-specific ionic liquids

I.3.1 Amine-functionalized task-specific ionic liquid-based membranes

Amine-functionalized task-specific ionic liquids (aTSILs) are types of RTIL, which have amino groups in their cation and/or anion groups. Of course, aTSILs have the unique properties of an ionic liquid such as nonvolatility, being in liquid state over a wide temperature range, high chemical and thermal stability, and so on. In addition, aTSILs have the potential to react chemically with CO_2. Therefore, aTSILs can be assumed a nonvolatile liquid CO_2 carrier with high amine group concentrations. That is, aTSILs satisfy the four requirements of desirable CO_2 carriers in FTMs described in I.2.2.3. In recent years, Hanioka *et al.*[83] developed a new class of FTMs in which aTSILs were used as a CO_2 carrier (aTSIL-FTMs). They reported that the aTSIL-FTMs facilitated CO_2 permeation through the membrane under humid conditions. On the other hand, Myers *et al.*[84] used an aTSIL-FTM under dry conditions and reported that an aTSIL-FTM prepared with *N*-aminopropyl-3-methylimidazolium bis(trifluoromethylsulfonyl)imide ($[C_3NH_2mim][Tf_2N]$) showed stronger temperature dependency on the CO_2 permeability than an SILM containing nonreactive, conventional RTILs (Fig. I.6).[84] From the results, they claimed that aTSIL-FTM worked as a CO_2 carrier and could facilitate CO_2 transport under dry conditions at elevated temperature. Although, as shown in Fig. I.6, the CO_2 permeability and selectivity of the aTSIL-FTM were relatively low, one can identify positive prospects for fabricating an FTM with a high CO_2 permeability and CO_2 selectivity under dry conditions by designing the chemical structure of aTSILs.

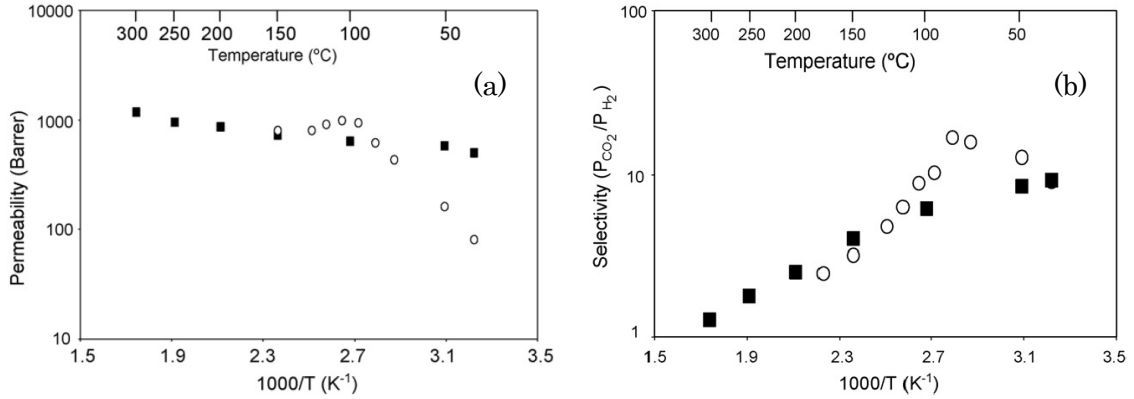

Fig. I.6 (a) CO_2 permeability and (b) CO_2/H_2 selectivity of supported ionic liquid membranes prepared with $[H_2NC_3H_6mim][Tf_2N]$ (circles) and 1-hexyl-3-methylimidazolium bis(trifluoromethyl-sulfonyl)imide (squares) as a function of temperature.[84]

I.3.2 CO_2 absorption capacity of aTSILs

Recently, many investigations on CO_2 absorbability of aTSILs have been carried out.[85-99] It was reported that the amount of CO_2 absorbed in an aTSIL with an amino group in the cation was not large (Fig. I.7).[86] From the result, it could be considered that the low CO_2 permeability and selectivity of the aTSIL-FTM with an amino group in the cation were due to the low CO_2 absorption by the aTSIL.

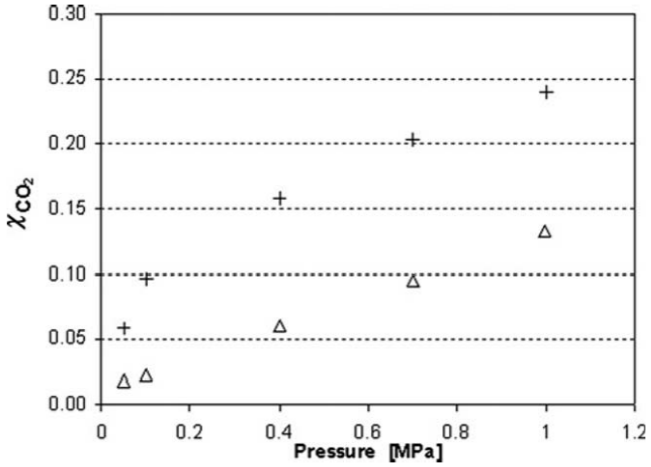

Fig. I.7 CO_2 solubility in 1-butyl-3-methylimidazolium dicyanamide (triangles) and a primary amine functionalized alkyl-imidazolium cation paired with dicyanamide anion (pluses) at 303 K.[86]

On the other hand, it has been reported that an aTSIL with an amino group in the anion had high CO_2 absorbability as well as a high CO_2 absorption capacity. In 2005, amino acid ionic liquids (AAILs) were developed as a kind of aTSIL with an amino group in the anion with novel functionality by Ohno *et al.*[100,101] The amino group in AAILs has the potential to react with CO_2, and in fact, AAILs showed quite high CO_2 absorption capacity.[88-95] It has been reported that the high CO_2 absorption capacity of trihexyltetradecylphosphonium prolinate, which is a type of AAIL, was maintained under wide temperature and humidity conditions (Fig. I.8).[94]

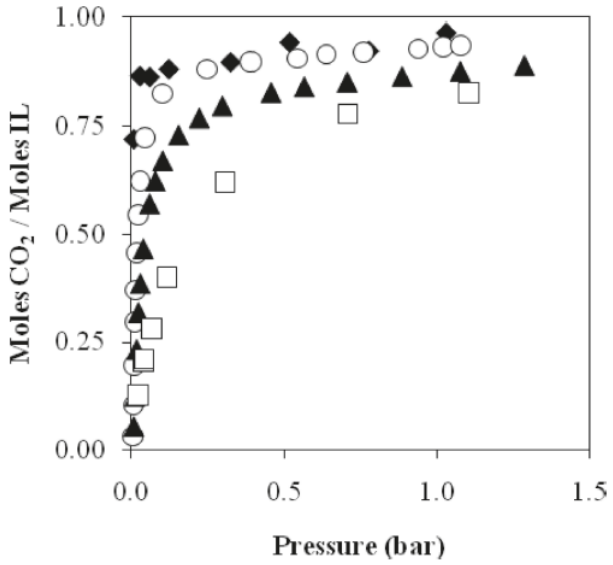

Fig. I.8 CO_2 absorption capacity of trihexyltetradecylphosphonium prolinate at 10 °C (diamonds), 60 °C (circles), 80 °C (triangles) and 100 °C (squares).[94]

I.3.3 Designing structure of aTSIL for improvement of CO_2 permselectivity

As mentioned above, the fabrication of a high performance membrane for CO_2 separation would reduce membrane requirements and lead to more compact processing equipment and lower capital costs. The CO_2 separation performance is determined by CO_2 permeability and other gas barrier properties. In this section, a methodology for

improving CO_2 permeability and other gas barrier properties of AAIL-based FTMs (AAIL-FTMs) is given.

In the case of nonporous membranes, gas permeability can be expressed as the product of the concentration gradient and the diffusion coefficient of the gas in the membrane.[17] In the case of SLMs, it is well known that both the concentration gradient of the gas in the membrane and the diffusion coefficient strongly depend on gas absorbability and the viscosity of the impregnated solution, respectively. This indicates that gas permeation properties of SLMs could be improved by enhancing the concentration gradient or the diffusion coefficient. Of these two approaches, the enhancement of the diffusion coefficient by decreasing the solution viscosity will increase not only the CO_2 permeability, but also that of other gases. Hence, CO_2 separation properties cannot be fundamentally improved by increasing the diffusion coefficient. On the other hand, the gas absorbability of the membrane can sometimes be controlled independently for each gas, a behavior typically observed in FTMs because FTMs are functionalized membranes that include a CO_2 carrier that can selectively react with CO_2. The CO_2 carrier causes a marked improvement in CO_2 absorbability by the membrane compared with other gases, through chemical reaction with CO_2. In addition, because other gases' absorbability is not affected by the CO_2 carrier, the introduction of the carrier dramatically increases CO_2 absorption selectivity. Moreover, it is expected that the inherent CO_2 permeation properties of the FTMs can be selectively improved by designing the chemical structure of the CO_2 carrier. The gas absorption properties of AAILs could be controlled by designing the structure of the AAILs because they are ionic liquids, i.e., "designer solvents"[100]. Here, a guideline is provided for designing the structure of an AAIL with suitable high CO_2 gas absorption properties but low

absorbability for other gases.

To improve the CO_2 absorption capacity of AAILs, Zhang *et al.*[98] developed dual amino-functionalized AAILs (dual-AAILs) and investigated their CO_2 absorption properties. They carried out CO_2 absorption tests by using dual-AAILs and normal AAILs supported on SiO_2, which have only one amino group in their anion, and reported that the dual-AAILs show twice the CO_2 absorption compared with normal AAILs.[89,98] This is because the dual-AAILs have two amino groups in both their cation and anion groups, which means that the dual-AAILs have two functional groups that can react with CO_2 per ionic liquid molecule. Years later, Peng *et al.*[99] developed three amino-functionalized AAILs (three-AAILs) that have three amino groups per ionic liquid molecule to further improve the CO_2 absorption capacity of AAILs. In addition, they carried out CO_2 absorption tests using a similar procedure to that of Zhang *et al.*[98] and revealed that the three-AAILs showed a higher CO_2 absorption capacity than dual-AAILs. The authors further claimed that CO_2 absorption capacity can be improved by increasing the number of amino groups in the molecule.

On the other hand, the N_2 absorption properties of RTILs have recently been investigated by many researchers.[102-104]

Camper *et al.*[102] developed a model for gas solubility of imidazolium-type RTILs to enable prediction of gas solubility from properties of RTILs. The gas solubilities calculated from the model were in good agreement with experimental data, which strongly depended on the molar volume of the RTILs. However, depending on the conditions, some errors were observed between the calculated values and experimental data.

Anderson *et al.*[103] investigated the effect of structure of RTILs on gas solubility of the

RTILs. They determined Henry's constant for RTILs from the absorption isotherms of several gases and calculated partial molar enthalpy and entropy. An RTIL with a suitable structure for CO_2 separation was suggested on the basis of the thermodynamic constant. They reported that gas solubility of RTILs is increased by increasing the molar volume of the RTILs.

Shannon *et al.*[104] modified the model developed by Camper *et al.*[102] on the basis of regular solution theory to enable its application to wider conditions. They investigated the relationship between the free volume of RTILs and gas solubility and solubility selectivity. They calculated the molar and Van der Waals volumes from density and molecular weight, and computer simulation, respectively. In addition, free volume was determined from the molar and Van der Waals volumes. Through comparison between experimental data and a value obtained from the modified model, it was revealed that the gas solubility of RTILs significantly depends on their free volume.

According to these reports, the gas solubility of RTILs depends significantly on their molar volumes or free volumes. RTILs have an inherent designer nature, in that many of their physicochemical properties, including their gas absorption properties, can be tuned by making appropriate variations to the cation and anion pair comprising the solvent. In particular, the molar and free volumes of RTILs can be easily adjusted by changing the size of their cation and/or anion groups.

In summary, it is expected that an AAIL that has a number of amino groups and small cation and anion groups would show preferable gas absorption properties in applications as a CO_2 separation membrane.

I.4 Polymeric ion-gel membranes

SILMs have serious disadvantages in that they are mechanically weak and cannot be used under pressurized conditions, which are requirements for gas separation membranes. There has been much research into methods to enhance the mechanical strength of these membranes while retaining their attractive diffusivity and solubility characteristics.[105-109]

To enhance the mechanical toughness of SILMs, Bara *et al.*[105] developed polymer membranes fabricated from self-crosslinkable RTILs as promising candidates. They used RTILs with polymerizable groups and prepared polymer membranes by converting the RTILs into dense poly(RTILs). The RTIL-based polymer membranes feature improved mechanical toughness compared with SILMs. However, their CO_2 permeability is similar to that of conventional polymer membranes. The authors attributed the low CO_2 solubility of the poly(RTILs) in part to the low CO_2 permeability. One year later, Bara *et al.*[106] developed alternative poly(RTIL) monomers to improve CO_2 solubility and successfully fabricated a poly(RTIL) membrane with superior CO_2 separation properties to previous poly(RTIL) membranes. However, the CO_2 separation property was only slightly higher than that of conventional polymer membranes, meaning that the CO_2 permeability was insufficient for practical use. These low CO_2 permeabilities of poly(RTIL) membranes are due to CO_2 diffusivity in a poly(RTIL) membrane being significantly limited because of the dense and rigid matrix formed by the cross-linked RTILs.

To overcome such diffusivity limitations, a gel containing a RTIL has been applied as a solvent (so called ion-gel) in recent investigations.[107-109] Hong *et al.*[107] developed polymer gel films including free RTILs in a polymer matrix and investigated the effect

of concentration of the free RTILs in the gel films on their CO_2 separation properties. The CO_2 permeability was dramatically increased by an increase in the concentration of free RTIL in the gel films, with constant CO_2/N_2 selectivity, which showed a slightly higher CO_2 separation performance than Robeson's upper bound. This behavior lies outside the limit of the trade-off relationship between permeability and selectivity and the authors proposed that this might be caused by gas solubility of the RTILs.

Bara *et al.*[108] investigated on the effect of free RTILs in gel films on their CO_2 solubility and diffusivity. They revealed that loading free RTIL into gel film causes an increase in diffusivity and a decrease in CO_2 solubility in the gel film, which causes an increase in CO_2 permeability and a decrease in CO_2/N_2 and CO_2/CH_4 selectivity.

Also, Carlisle *et al.*[109] investigated the effect of concentration of free RTILs and cross-linking monomer in the gel films on their CO_2 permeation properties, to enhance the gas diffusivity in gel films to a similar level to that of SILMs. They reported that the diffusivity can be improved by increasing free RTIL loading and/or reducing the concentration of cross-linking monomer, which causes a dramatic increase in CO_2 permeability.

As mentioned above, high diffusivity can be obtained by preparing a polymeric gel containing an RTIL as a solvent. However, the CO_2 permeation property of each gel film is slightly higher than or comparable with conventional polymer membranes. This is caused by the low CO_2 solubility of these RTILs.

AAILs have a high CO_2 absorption capacity because they can react with CO_2. Therefore, a polymeric ion-gel membrane with high diffusivity and high CO_2 solubility can be fabricated using an AAIL as a solvent instead of RTILs. There have only been two previous reports on gels containing AAILs.

Kagimoto *et al.*[110] developed thermotropic physical gels containing AAILs to fabricate a solid material with high ion density. These gels were fabricated simply by mixing AAILs with RTILs, without other additives such as gelators or polymer materials. The physicochemical properties of the gels were investigated. From both nuclear magnetic resonance (NMR) and mass spectra analyses, it was suggested that the AAIL-RTIL mixed solution formed a dispersed colloid. In addition, they revealed that the gels can be converted to liquid by heating.

Taguchi *et al.*[111] developed alternative thermotropic gels containing AAILs to fabricate a solid material that retains the original properties of AAILs, regardless of gelation. These gels were fabricated by adding a phosphonium-type zwitterion into an AAIL. They investigated the mechanism of gelation using wide-angle X-ray diffraction, NMR and fourier transform-infrared spectroscopy (FT-IR). As a result, it was revealed that the gels were formed by the dispersed aggregation of the phosphonium-type zwitterion. In addition, the dispersed particles were produced by ionophobic interaction, electrostatic interaction and hydrogen bonding.

The authors reported two types of gels containing AAILs. However, these gels were fragile and unsuitable for practical use in gas separations. To the best of my knowledge, there have been no reports of a polymer gel containing aTSILs. Hence, fabrication of a polymeric gel containing AAILs as a solvent is strongly expected to enable the production of a membrane with good CO_2 permeation properties and high pressure resistance.

I.5 Purpose of this study

In this study, fabrication of a new class of FTM with excellent CO_2 permeation properties was investigated by focusing on aTSILs as a CO_2 carrier in FTMs. The

chemical structures of aTSILs were designed to overcome the disadvantages of conventional FTMs.

As mentioned in the above section, AAILs have high CO_2 absorbability and are expected to be a promising material as a CO_2 carrier in FTMs. However, there have been no reports on utilizing AAILs as CO_2 carriers in an FTM for CO_2 separation. In this study, AAIL-FTMs were fabricated and the CO_2 permeation properties were investigated in detail. In fundamental investigations, the CO_2 absorbability and physicochemical properties of AAILs were measured. In particular, the viscosity of AAILs after CO_2 absorption was measured because it was reported that an increase in the viscosity of AAILs with CO_2 absorption is caused by hydrogen bonds among the AAIL-CO_2 complexes.[112,113] The increase in viscosity of the carrier solution in the SLMs decreases the diffusivity of dissolved gases in the SLMs and gas permeability.[94,95] Based on the physicochemical properties resulting from the fundamental investigations, the controlling factors for CO_2 permeability in an aTSIL-based membrane under various conditions were estimated to design the chemical structure of a desirable aTSIL CO_2 carrier. Following the results obtained from fundamental investigations, a proposed aTSIL with a preferable structure as a CO_2 carrier was synthesized, the CO_2 absorbability was examined, the physicochemical properties measured and then this was impregnated in a porous support to fabricate an FTM. The CO_2 permeation properties of the fabricated FTM with the designed aTSIL were investigated.

In addition, improvement of the pressure resistance of AAIL-FTMs was investigated using a gel containing AAILs as a solvent. Regarding gels containing AAILs, only two types of gels have been reported: one based on a mix of AAILs with RTILs and another containing a phosphonium-type zwitterion.[110,111] Both of these are types of

supramolecular gels without high mechanical toughness. To improve the pressure resistance of the aTSIL-FTMs, gels containing aTSILs should have high mechanical toughness. Therefore, a gel containing a polymeric matrix would be preferable. However, there have been no reports of a polymer gel containing aTSILs. Thus, in this thesis, fabrication of a polymeric ion-gel containing an AAIL as well as an ion-gel film for CO_2 separation was investigated. The CO_2 permeation properties of the fabricated ion-gel film containing AAILs were also evaluated.

I.6 Scope of this thesis

This thesis is divided into the following seven chapters.

Chapter I contains the introduction of the background of the CO_2 capture and a review of the previous work on CO_2 separation membranes. The aim, purpose, strategy and scope of this thesis are also given.

Chapter II describes the fabrication of AAIL-FTMs. To confirm the mechanism for CO_2 permeation through the AAIL-FTMs, the CO_2 partial pressure dependencies on the CO_2 permeability were investigated under dry conditions. The effects of the anion group of the AAIL on the CO_2 permeation properties of the AAIL-FTM were examined. The relationship between the CO_2 permeation properties and the water retention property of the AAILs was also investigated.

Chapter III describes the factors controlling CO_2 permeability of the aTSIL-FTMs. To clarify the mechanism behind the increase in the viscosity of AAILs after CO_2 absorption, the change in structure before and after CO_2 absorption was investigated. An aTSIL with a pyrrole type anion was synthesized to prevent the increase in viscosity after CO_2 absorption.

Chapter IV proposes a methodology to improve the CO_2 permselectivity of AAIL-FTMs by using AAILs with different chemical structures designed to control the gas absorption properties. AAILs with a series of cation group sizes were synthesized, and the effect of cation size on N_2 absorption was investigated. The relationship between N_2 absorption and the N_2 barrier properties of the AAIL-FTMs was investigated.

Chapter V describes the design criteria for AAILs with suitable gas absorption properties for a CO_2 separation membrane. An AAIL composed of small cation and anion groups, both of which have amino groups, was designed and synthesized to increase CO_2 absorption and decrease N_2 absorption. The CO_2 permeation properties of a membrane containing the synthesized AAIL were investigated under humid and/or elevated temperature conditions. A guideline for designing an AAIL with suitable gas absorption properties to fabricate a CO_2 selective membrane with excellent CO_2 permeation properties under humid and/or elevated temperature is proposed.

Chapter VI describes the fabrication of polymeric ion-gels containing an AAIL as a facilitated CO_2 transport medium. Polymeric ion-gels containing an AAIL as a solvent were fabricated to enhance the pressure resistance of the AAIL-FTMs. The mechanical strength of the gels was examined. In addition, ion-gel films containing AAILs were fabricated and their CO_2 permeation properties were investigated.

Chapter VII summarizes the conclusions of this thesis.

References

1. R. W. Baker and K. Lokhandwala, *Ind. Eng. Chem. Res.*, 2008, **47**, 2109.
2. P. Bernardo, E. Drioli and G. Golemme, *Ind. Eng. Chem. Res.*, 2009, **48**, 4638.
3. S. Basu, A. L. Khan, A. Cano-Odena, C. Liu and I. F. J. Vankelecom, *Chem. Soc. Rev.*, 2010, **39**, 750.
4. B. Li, Y. Duan, D. Luebke and B. Morreale, *Applied Energy*, 2013, **102**, 1439.
5. Espacenet website: <http://www.epo.org/searching/free/espacenet.html>.
6. H. Lin, E. Van Wagner, B. D. Freeman, L. G. Toy and R. P. Gupta, *Science*, 2006, **311**, 639.
7. J. Xia, S. Liu and T.-S. Chung, *Macromolecules*, 2011, **44**, 7727.
8. M. K. Barillas, R. M. Enick, M. O'Brien, R. Perry, D. R. Luebke and B. D. Morreale, *J. Membr. Sci.*, 2011, **372**, 29.
9. L. M. Robeson, *J. Membr. Sci.*, 2008, **320**, 390.
10. P. Bahukudumbi and D. M. Ford, *Ind. Eng. Chem. Res.*, 2006, **45**, 5640.
11. L. Wang, Y. Cao, M. Zhou, S. J. Zhou and Q. Yuan, *J. Membr. Sci.*, 2007, **305**, 338.
12. H. Sanaeepur, A. E. Amooghin, A. Moghadassi and A. Kargari, *Sep. Purif. Technol.*, 2011, **80**, 499.
13. T. Sakaguchi, S. Tominaga and T. Hashimoto, *Polymer*, 2011, **52**, 2163.
14. M. Calle and Y. M. Lee, *Macromolecules*, 2011, **44**, 1156.
15. A. W. Grabczyk and A. Jankowski, *J. Appl. Polym. Sci.*, 2011, **122**, 2690.
16. T. Sakaguchi, A. Takeda and T. Hashimoto, *Macromolecules*, 2011, **44**, 6810.
17. W. S. W. Ho and K. K. Sirkar, *Eds. Membrane Handbook*; Kluwer Academic Publishers: Boston, 1992.
18. J. Shieh and T. S. Chung, *J. Poly. Sci.: Part B: Poly. Phys.*, 1999, **37**, 2851.

19. H. Lin and B. D. Freeman, *J. Membr. Sci.*, 2004, **239**, 105.

20. L. M. Robeson, *J. Membr. Sci.*, 1991, **62**, 165.

21. H. Chen, A. S. Kovvali and K. K. Sirkar, *Ind. Eng. Chem. Res.*, 2000, **39**, 2447.

22. R. Yegani, H. Hirozawa, M. Teramoto, H. Himei, O. Okada, T. Takigawa, N. Ohmura, N. Matsumiya and H. Matsuyama, *J. Membr. Sci.*, 2007, **291**, 157.

23. M. Teramoto, K. Nakai, N. Ohnishi, Q. Huang, T. Watari and H. Matsuyama, *Ind. Eng. Chem. Res.*, 1996, **35**, 538.

24. A. S. Kovvali, H. Chen and K. K. Sirkar, *J. Am. Chem. Soc.*, 2000, **122**, 7594.

25. J. Huang, J. Zou and W. S. W. Ho, *Ind. Eng. Chem. Res.*, 2008, **47**, 1261.

26. C. A. Scholes, S. E. Kentish and G. W. Stevens, *Rec. Pat. Chem. Eng.*, 2008, **1**, 52.

27. H. Matsuyama, K. Matsui, Y. Kitamura, T. Maki and M. Teramoto, *Sep. Purif. Technol.*, 1999, **17**, 235.

28. H. Matsuyama, M. Teramoto, K. Matsui and Y. Kitamura, *J. Appl. Polym. Sci.*, 2001, **81**, 936.

29. N. Matsumiya, S. Matsufuji, M. Nakabayashi, K. Okabe, H. Mano and M. Teramoto, *Maku*, 2004, **29**, 66.

30. N. Matsumiya, S. Matsufuji, K. Okabe, H. Mano and M. Teramoto, *Maku*, 2004, **29**, 123.

31. K. Okabe, N. Matsumiya and H. Mano, *Sep. Purif. Technol.*, 2007, **57**, 242.

32. G. J. Francisco, A. Chakma, X. Feng, *J. Membr. Sci.*, 2007, **303**, 54.

33. P. Ji, Y. Cao, H. Zhao, G. Kang, X. Jie, D. Liu, J. Liu and Q. Yuan, *J. Membr. Sci.*, 2009, **342**, 190.

34. W. J. Ward and W. L. Robb, *Science*, 1967, **156**, 1481.

35. D. R. Smith and J. A. Quinn, *AIChE J.*, 1979, **25**, 197.

36. T. L. Donaldson and Y. N. Nguyen, *Ind. Eng. Chem. Fundam.*, 1980, **19**, 260.

37. A. K. Guha, S. Majumdar and K. K. Sirkar, *Ind. Eng. Chem. Res.*, 1990, **29**, 2093.

38. R. A. Davis and O. C. Sandall, *AIChE J.*, 1993, **39**, 1135.

39. G. Broun, E. Selegny, C. T. Minh and D. Thomas, *RFEBS Lett.*, 1970, **7**, 223.

40. S. Park, N. Heo, J. Kim and D. Suh, *Korean J. Chem. Eng.*, 1997, **14**, 312.

41. S. Park, N. Heo, G. Kim, I. Sohn and H. Kumazawa, *Sep. Sci. Technol.*, 2000, **35**, 2497.

42. S. Saha and A. Chakma, *J. Membr. Sci.*, 1995, **98**, 157.

43. M. Teramoto, *Ind. Eng. Chem. Res.*, 1995, **34**, 1267.

44. O. H. LeBlanc Jr., W. J. Ward, S. L. Matson and S. G. Kimura, *J. Membr. Sci.*, 1980, **6**, 339.

45. J. D. Way, R. D. Noble, D. L. Reed, G. M. Ginley and L. A. Jarr, *AIChE J.*, 1987, **33**, 480.

46. H. Chen, A. S. Kovvali, S. Majumdar and K. K. Sirkar, *Ind. Eng. Chem. Res.*, 1999, **38**, 3489.

47. H. Chen, G. Obuskovic, S. Majumdar and K. K. Sirkar, *J. Membr. Sci.*, 2001, **183**, 75.

48. A. S. Kovvali and K. K. Sirkar, *Ind. Eng. Chem. Res.*, 2002, **41**, 2287.

49. A. S. Kovvali and K. K. Sirkar, *Ind. Eng. Chem. Res.*, 2001, **40**, 2502.

50. R. Quinn, J. B. Appleby and G. P. Pez, *J. Membr. Sci.*, 1995, **104**, 139.

51. M. G. Shalygin, A. Y. Okunev, D. Roizard, E. Favre and V. V. Teplyakov, *Colloid J.*, 2006, **68**, 518.

52. A. H. Gorji and T. Kaghazchi, *J. Membr. Sci.*, 2008, **325**, 40.

53. L. Bao and M. C. Trachtenberg, *J. Membr. Sci.*, 2006, **280**, 330.

54. M. H. A. Marzouqi, M. A. Abdulkarim, S. A. Marzouk, M. H. El-Naas and H. M.

Hasanain, *Ind. Eng. Chem. Res.*, 2005, **44**, 9273.

55. A. H. Gorji, T. Kaghazchi and A. Kargari, *Chem. Eng. Technol.*, 2009, **32**, 120.
56. A. Diaf, R. M. Enick and E. J. Beckman, *J. Appl. Polym. Sci.*, 1993, **50**, 835.
57. T. Yamaguchi, L. M. Boetje, C. A. Koval, R. D. Noble and C. N. Bowman, *Ind. Eng. Chem. Res.*, 1995, **34**, 4071.
58. M. Yoshikawa, K. Fujimoto, H. Kinugawa, T. Kitao and N. Ogata, *Chem. Lett.*, 1994, 243.
59. H. Matsuyama, A. Terada, T. Nakagawara, Y. Kitamura and M. Teramoto, *J. Membr. Sci.*, 1999, **163**, 221.
60. Y. Zhang, Z. Wang and S. Wang, *Fuel Chem. Div. Prepr.*, 2002, **47**, 73.
61. Y. Zhang, Z. Wang and S. Wang, *Chem. Lett.*, 2002, 430.
62. J. Shen, J. Qiiu, L. Wu and C. Gao, *Sep. Purif. Technol.*, 2006, **51**, 345.
63. Y. Zhang, Z. Wang and S. Wang, *J. Appl. Polym. Sci.*, 2002, **86**, 2222.
64. L. Deng, T. Kim and M. Hagg, *J. Membr. Sci.*, 2009, **340**, 154.
65. L. A. El-Azzami and E. A. Grulke, *J. Membr. Sci.*, 2008, **323**, 225.
66. M. S. A. Rahaman, L. Zhang, L. Cheng, X. Xu and H. Chen, *RSC Adv.*, 2012, **2**, 9165.
67. M. Wang, Z. Wang, J. Wang, Y. Zhu and S. Wang, *Energy Environ. Sci.*, 2011, **4**, 3955.
68. M. Sandru, T. Kim and M. Hagg, *Desalination*, 2009, **240**, 298.
69. L. A. El-Azzami and E. A. Grulke, *Ind. Eng. Chem. Res.*, 2009, **48**, 894.
70. J. Zhao, Z. Wang, J. Wang and S. Wang, *J. Membr. Sci.*, 2006, **283**, 346.
71. Y. Zhang, Z. Wang, J. Wang and S. Wang, *Desalination*, 2006, **193**, 299.
72. T. Kim, B. Li and M. Hagg, *J. Polym. Sci.: Part B: Polym. Phys.*, 2004, **42**, 4326.
73. H. Bai and W. S. W. Ho, *Ind. Eng. Chem. Res.*, 2009, **48**, 2344.
74. J. Zou and W. S. W. Ho, *J. Membr. Sci.*, 2006, **286**, 310.

75. E. L. Cussler, R. Aris and A. Bhown, *J. Membr. Sci.*, 1989, **43**, 149.

76. P. Scovazzo, D. Havard, M. McShea, S. Mixon and D. Morgan, *J. Membr. Sci.*, 2009, **327**, 41.

77. P. Scovazzo, J. Kieft, D. A. Finan, C. Koval, D. DuBois and R. Noble, *J. Membr. Sci.*, 2004, **238**, 57.

78. P. Scovazzo, D. Camper, J. Kieft, J. Poshusta, C. Koval and R. Noble, *Ind. Eng. Chem. Res.*, 2004, **43**, 6855.

79. L. J. Lozano, C. Godinez, A. P. Rios, F. J. Hernandez-Fernandez, S. Sanchez-Segado and F. J. Alguacil, *J. Membr. Sci.*, 2011, **376**, 1.

80. J. E. Bara, T. K. Carlisle, C. J. Gabriel, D. Camper, A. Finotello, D. L. Gin and R. D. Noble, *Ind. Eng. Chem. Res.*, 2009, **48**, 2739.

81. L. A. Neves, J. G. Crespo and I. M. Coelhoso, *J. Membr. Sci.*, 2010, **357**, 160.

82. J. Won, D. B. Kim, Y. S. Kang, D. K. Choi, H. S. Kim, C. K. Kim and C. K. Kim, *J. Membr. Sci.*, 2005, **260**, 37.

83. S. Hanioka, T. Maruyama, T. Sotani, M. Teramoto, H. Matsuyama, K. Nakashima, M. Hanaki, F. Kubota and M. Goto, *J. Membr. Sci.*, 2008, **314**, 1.

84. C. Myers, H. Pennline, D. Luebke, J. Ilconich, J. K. Dixon, E. J. Maginn and J. F. Brennecke, *J. Membr. Sci.*, 2008, **322**, 28.

85. E. D. Bates, R. D. Mayton, I. Ntai and J. H. Davis, *J. Am. Chem. Soc.*, 2002, **124**, 926.

86. L. M. Sanchez, G. W. Meindersma and A. B. Haan, *Trans IChemE, Part A, Chem. Eng. Res. Design*, 2007, **85**, 31.

87. P. Sharma, S. D. Park, K. T. Park, S. C. Nam, S. K. Jeong, Y. I. Yoon and I. H. Baek, *Chem. Eng. J.*, 2012, **193-194**, 267.

88. C. Wang, X. Luo, X. Zhu, G. Cui, D. Jiang, D. Deng, H. Li and S. Dai, *RSC Adv.*, 2013, **3**, 15518.

89. J. Zhang, S. Zhang, K. Dong, Y. Zhang, Y. Shen and X. Lv, *Chem. Eur. J.*, 2006, **12**, 4021.

90. Y. Zhang, P. Yu and Y. Luo, *Chem. Eng. J.*, 2013, **214**, 355.

91. Y. Y. Jiang, G. N. Wang, Z. Zhou, Y. T. Wu, J. Geng and Z. B. Zhang, *Chem. Commun.*, 2008, 505.

92. Z. Feng, F. C. Gang, W. Y. Ting, W. Y. Tao, L. A. Min and Z. Z. Bing, *Chem. Eng. J.*, 2010, **160**, 691.

93. B. E. Gurkan, J. C. Fuente, E. M. Mindrup, L. E. Ficke, B. F. Goodrich, E. A. Price, W. F. Schneider and J. F. Brennecke, *J. Am. Chem. Soc.*, 2010, **132**, 2116.

94. B. F. Goodrich, J. C. de la Fuente, B. E. Gurkan, Z. K. Lopez, E. A. Price, Y. Huang and J. F. Brennecke, *J. Phys. Chem. B*, 2011, **115**, 9140.

95. B. F. Goodrich, J. C. de la Fuente, B. E. Gurkan, D. J. Zadigian, E. A. Price, Y. Huang and J. F. Brennecke, *Ind. Eng. Chem. Res.*, 2011, **50**, 111.

96. B. Gurkan, B. F. Goodrich, E. M. Mindrup, L. E. Ficke, M. Massel, S. Seo, T. P. Senftle, H. Wu, M. F. Glaser, J. K. Shah, E. J. Maginn, J. F. Brennecke and W. F. Schneider, *J. Phys. Chem. Lett.*, 2010, **1**, 3494.

97. C. Wang, X. Luo, H. Luo, D. Jiang, H. Li and S. Dai, *Angew. Chem. Int. Ed.*, 2011, **50**, 4918.

98. Y. Zhang, S. Zhang, X. Lu, Q. Zhou, W. Fan and X. Zhang, *Chem. Eur. J.*, 2009, **15**, 3003.

99. H. Peng, Y. Zhou, J. Liu, H. Zhang, C. Xia and X. Zhou, *RSC Adv.*, 2013, **3**, 6859.

100. K. Fukumoto, M. Yoshizawa and H. Ohno, *J. Am. Chem. Soc.*, 2005, **127**, 2398.

101. H. Ohno and K. Fukumoto, *Acc. Chem. Res.*, 2007, **40**, 1122.

102. D. Camper, J. Bara, C. Koval and R. Noble, *Ind. Eng. Chem. Res.*, 2006, **45**, 6279.

103. J. L. Anderson, J. K. Dixon and J. F. Brennecke, *Acc. Chem. Res.*, 2007, **40**, 1208.

104. M. S. Shannon, J. M. Tedstone, S. P. O. Danielsen, M. S. Hindman, A. C. Irvin and J. E. Bara, *Ind. Eng. Chem. Res.*, 2012, **51**, 5565.

105. J. E. Bara, S. Lessmann, C. J. Gabriel, E. S. Hatakeyama, R. D. Noble and D. L. Gin, *Ind. Eng. Chem. Res.*, 2007, **46**, 5397.

106. J. E. Bara, C. J. Gabriel, E. S. Hatakeyama, T. K. Carlisle, S. Lessmann, R. D. Noble and D. L. Gin, *J. Membr. Sci.*, 2008, **321**, 3.

107. S. U. Hong, D. Park, Y. Ko and I. Baek, *Chem. Commun.*, 2009, 7227.

108. J. E. Bara, R. D. Noble and D. L. Gin, *Ind. Eng. Chem. Res.*, 2009, **48**, 4607.

109. T. K. Carlisle, G. D. Nicodemus, D. L. Gin and R. D. Noble, *J. Membr. Sci.*, 2012, **397-398**, 24.

110. J. Kagimoto, N. Nakamura, T. Kato and H. Ohno, *Chem. Commun.*, 2009, 2405.

111. S. Taguchi, T. Matsumoto, T. Ichikawa, T. Kato and H. Ohno, *Chem. Commun.*, 2011, **47**, 11342.

112. K. E. Gutowski and E. J. Maginn, *J. Am.Chem. Soc.*, 2008, **130**, 14690.

113. H. Gao, Y. Zhang, H. Wang, J. Liu and J. Chen, *J. Phys. Chem. A*, 2010, **114**, 10243.

Chapter II

Fabrication of amino acid ionic liquid-based facilitated transport membranes for CO_2 separation

II.1 Introduction

AAILs, which have a "reactive" amino acid anion, were recently developed as RTILs with novel functionality.[1,2] The amino group in AAILs has potential for reaction with CO_2. In fact, it has been reported that tetrabutylphosphonium glycinate ($[P_{4444}][Gly]$) has a very high CO_2 absorption capacity.[3,4] Remarkably, $[P_{4444}][AA]$s can absorb large amounts of CO_2 under both dry and humid conditions. Therefore, AAILs have great potential for use as a CO_2 carrier over a wide moisture range. Here, I present novel CO_2 selective FTMs containing AAILs (AAIL-FTMs). The CO_2 permeability and CO_2/N_2 selectivity of AAIL-FTMs were investigated under low moisture conditions.

In addition, in the development of a CO_2 selective AAIL-FTM, knowledge regarding the key properties of AAILs that contribute to CO_2 permeation is very important. In this chapter, I also synthesized a series of AAILs. The tetrabutylphosphonium-type AAILs were used because the AAILs based on phosphonium cation has their better thermal stability.[5] On the other hand, I chose the four amino acids (glycine, alanine, serine and proline). The reason choosing these amino acids are as follows. The AAILs based on glycine, alanine and serine anions were used in the literature written about the CO_2 absorption.[3] In the literature, $[P_{4444}][Gly]$ and $[P_{4444}][Ala]$ showed good CO_2 absorption

properties. The [P_{4444}][Ala], which has almost same CO_2 absorption property to [P_{4444}][Gly], provides the knowledge of the effect of CO_2 absorption properties on CO_2 permeability. [P_{4444}][Ser], which had been also used in the literature,[3] has high viscosity. So [P_{4444}][Ser] was used to investigate the effect of diffusivity in the AAIL-FTMs. On the other hand, it was reported that [P_{4444}][Pro] could absorb large amount of CO_2 under wide pressure range.[4] In addition, the high CO_2 absorption property was independent of the existence of water.[4] I directed my attention to the specific CO_2 absorption properties of [P_{4444}][Pro] and selected it as one of the AAILs investigated in this research. In this chapter, I prepared AAIL-FTMs with [P_{4444}][Gly], [P_{4444}][Ala], [P_{4444}][Ser] and [P_{4444}][Pro]. The CO_2 permeability of the AAIL-FTMs was investigated and discussed based on the physical and physicochemical properties of the AAILs, such as viscosity, hygroscopicity and water-holding ability.

II.2 Experimental

II.2.1 Materials

Tetrabutylphosphonium hydroxide ([P_{4444}][OH], 40 wt% in water), 1-ethyl-3-methylimidazolium hydroxide ([Emim][OH], 10 wt% in water), 1-ethyl-3-methylimidazolium bis(trifluoromethylsulfonyl)imide ([Emim][Tf_2N], ≥ 98%) and acetonitrile (99.9%) were purchased from Sigma-Aldrich Co. (St Louis, MO, USA). Glycine (99.8%), alanine (>99.0%), serine (>99.0%), proline (>99.0%) and DL-2,3-diaminopropionic acid hydrochloride (DAPA, >98.0%) were purchased from Tokyo Chemical Industry Co. (Tokyo, Japan). Methanol (99.8%) was purchased from Wako Pure Chemicals Industry Ltd. (Osaka, Japan). They were used as received. Poly(vinyl alcohol)-poly(acrylic acid) copolymer (PVA/PAA copolymer) was supplied from Kyodo Yakuhin Co.

Ltd. (Tokyo, Japan).

Tetrabutylphosphonium type AAILs (tetrabutylphosphonium glycinate ([P_{4444}][Gly]), tetrabutylphosphonium alaninate ([P_{4444}][Ala]), tetrabutylphosphonium serinate [P_{4444}][Ser], and tetrabutylphosphonium prolinate ([P_{4444}][Pro])) were synthesized following a neutralization procedure reported previously.[3] An aqueous solution of [P_{4444}][OH] was added to a slight excess of an equimolar amino acid aqueous solution to prepare [P_{4444}][AA] salts, with water as a byproduct. The product was dried *in vacuo* for 24 h at 313 K. Subsequently, an appropriate amount of acetonitrile/ethanol mixture was added to recrystallize and remove unreacted glycine. The filtrate was evaporated to remove solvents. The reaction ratios were 95.5, 93.2, 94.8 and 99.9% for [P_{4444}][Gly], [P_{4444}][Ala], [P_{4444}][Ser] and [P_{4444}][Pro], respectively.

[Emim][Gly] was synthesized using a similar procedure to that used for [P_{4444}][AA]s except for the source solution, for which a commercial aqueous solution of [Emim][OH] was used. The reaction ratio of [Emim][Gly] was 80.8%.

The structures of the resulting [P_{4444}][AA]s and [Emim][Gly] were confirmed by ^{1}H-NMR spectroscopy (Bruker Advance 500, Bruker BioSpin, Kanagawa, Japan) and FT-IR (ALPHA FT-IR Spectrometer, Bruker Optics, Tokyo, Japan) measurements, as shown in appendix.

CO_2 and N_2 gases of 99.9% purity were used for gas permeation tests. A hydrophilic PTFE microporous membrane was purchased from Sumitomo Electric industries, Ltd. (Osaka, Japan). It has an average pore size of 0.2 μm and a film thickness of 37.5 μm. It was used as a support of the FTM with DAPA as a CO_2 carrier (DAPA-FTM) membranes prepared in this study. On the other hand, a hydrophilic PTFE microporous membrane with an average pore size of 0.1 μm and a film thickness of 37.5 μm was used as a support

for the AAIL-FTMs and [Emim][Tf_2N]-based supported ionic liquid membrane.

II.2.2 Preparation of membranes

The details of preparation method of AAIL-FTMs and the supported ionic liquid membrane of [Emim][Tf_2N] was as follows. A hydrophilic PTFE microporous membrane was immersed into the ionic liquid ([P_{4444}][Gly], [P_{4444}][Ala], [P_{4444}][Ser], [P_{4444}][Pro], [Emim][Gly] or [Emim][Tf_2N]) and whole of them were decompressed for 1,800 or 3,600 s in order to completely replace air in the PTFE membrane to ionic liquid. The ionic liquid impregnated PTFE membrane was taken out and wiped an excess ionic liquid on the surface.

The details of preparation method of the DAPA-FTM was as follows. PVA/PAA copolymer, DAPA and CsOH were dissolved in water by stirring the solution for 24 h at 298 K. The molar ratio of CsOH to DAPA was adjusted to 2 so that two amine groups in DAPA might be converted to deprotonated amine groups. The prepared solution was centrifuged at 5,000 rpm at room temperature for 1,800 s to remove small bubbles, which might cause membrane instability. Then the solution was cast onto a hydrophilic microporous PTFE membrane using an applicator with a gap setting of 500 μm. The cast membrane was dried at 298 K overnight. The concentrations of copolymer and DAPA in the dried membrane were 52.0 and 24.0 wt.%, respectively. Finally, the coated layer was crosslinked by heat treatment for 2 h at 393 K for crystallization.

II.2.3 Procedures for gas permeability measurement

A diagram of the experimental apparatus is shown in Fig. II.1. The gas transport properties of the membrane were measured using a flat-type permeation cell (Fig. II.2)

placed in a thermostat oven (YAMATO Scientific Co., Ltd., Japan) adjusted to a desired temperature. The permeation cell (GTR TEC Co., Japan) was made of stainless steel and had an effective permeation area of 2.88 cm^2.

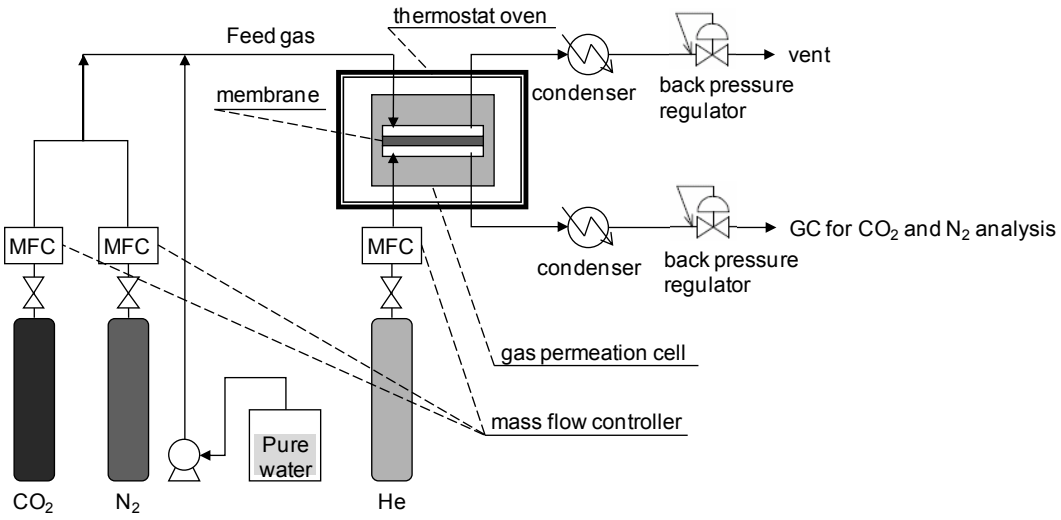

Fig. II.1 Schematic diagram of the apparatus for gas permeation test.

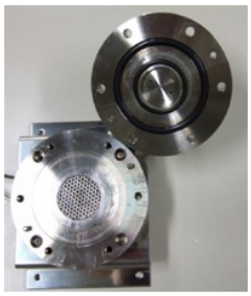

Fig. II.2 Stainless steel flat-type permeation cell.

A model feed gas was prepared by mixing CO_2, N_2 and/or steam. The flow rates of CO_2 and N_2 were controlled by mass flow controllers (Hemmi Slide Rule Co., Ltd., Japan), and the water flow rate was adjusted by a reciprocating metering pump (Nihon Seimitsu Kagaku Co., Ltd., Japan). The total flow rate of the feed gas was adjusted to 1.49×10^{-4} mol/s at 298 K, 101.3 kPa. The feed gas was pre-heated by a coiled heat exchanger and introduced into the cell. The feed side pressure was kept constant at atmospheric

pressure. Helium was supplied to the permeate side of the cell as a sweep gas through a coiled heat exchanger at a flow rate of 2.98×10^{-5} mol/s at 298 K, 101.3 kPa. The pressure on the sweep side was also kept constant at almost atmospheric pressure. Water vapor in the streams from both the feed and permeate sides of the permeation cell was removed by condensers, and the flow rates of the dried streams were measured by soap-film flow meters (HORIBA STEC Ltd., Japan). The dried sweep gas was sent to a gas chromatograph (GC-8A, Shimadzu Co., column: activated carbon, 1 m) to determine the composition of permeate. Each test was performed for more than 3 h until the differences between successively CO_2 and N_2 peak areas measured by GC became less than 1%.

II.2.4 Measurement of physicochemical properties of ionic liquids

Hygroscopicity and water-holding ability of the ionic liquids were measured by thermogravimetry. For hygroscopicity measurements, the water contents of $[P_{4444}][AA]$s, [Emim][Gly] and $[Emim][Tf_2N]$ at 373 K under humid conditions were measured using a thermogravimetry-differential thermal analyzer with a humidity generator (TG-DTA/HUM, Rigaku Co., Tokyo, Japan). A desired amount of sample was placed in the cell, and dry nitrogen was fed initially. The temperature of the cell was heated to 423 K at 0.0167 K/s and kept constant for 10 h to remove any residual free water from each ionic liquid. Subsequently, the cell temperature was dropped to 373 K at 0.033 K/s and kept constant for 1 h to reach a steady state. After 1 h, humid gas at 2.5% relative humidity (RH) was introduced into the cell. The condition in the cell was maintained for 5.5 h and the weight of the sample continuously monitored. The water content in the ionic liquids at each condition was calculated by subtraction of the weight of dried ionic liquid at 423 K. To measure the water contents under the different conditions, the RH

was changed sequentially to 5.0, 10.0 and 20.0%. Every measurement was performed for 5.5 h. The water-holding abilities of $[P_{4444}][AA]$s were also measured using TG-DTA/HUM. The temperature of the cell was heated to 323 K and kept constant for 5 h to desorb the free water in each AAIL. The desorption behavior of the free water was measured as the weight loss of the AAILs.

Viscosity of the AAILs was measured with a rheometer (MCR501, Anton Paar Co., Ltd.), using a cone-plate geometry at a constant shear rate of 100 s^{-1}. First, the viscosity was measured from 303 K to 373 K. After the temperature reached 373 K, the temperature was immediately cooled down to 303 K and the viscosity was again measured.

II.3 Results and discussion

II.3.1 Gas permeation properties of AAIL-FTMs

AAILs form a complex with CO_2 and absorb large amounts of CO_2. However, permeability of CO_2 through a FTM is affected by rates of complex formation and decomposition as well as the amount absorbed. If complex decomposition between CO_2 and an AAIL hardly occurs, CO_2 permeation through the membrane becomes very slow. In general, complex decomposition is accelerated in vacuum and at elevated temperature. In this study, the gas permeability at elevated temperature was investigated initially.

Fig. II.3 shows the effect of temperature on CO_2 and N_2 permeabilities of $[P_{4444}][Gly]$-FTM and [Emim][Gly]-FTM under dry conditions. In this figure the results for $[Emim][Tf_2N]$-SILM are also shown for comparison. The CO_2 permeabilities for $[P_{4444}][Gly]$-FTM and [Emim][Gly]-FTM drastically increased up to 5,000 and 8,300 Barrer respectively (1 Barrer = 1×10^{-10} $cm^3(STP)\cdot cm\cdot cm^{-2}\cdot s^{-1}\cdot cmHg^{-1}$) with increasing

temperature. On the other hand, the permeabilities of N_2 for both of the AAIL-FTMs were increased slightly. As a result, the CO_2/N_2 selectivity also significantly increased, up to 48 for $[P_{4444}][Gly]$-FTM and 146 for [Emim][Gly]-FTM. This is the first report of the realization of such high CO_2 permeabilities and CO_2/N_2 selectivities under dry conditions. AAILs thus show excellent promise as a CO_2/N_2 separation platform.

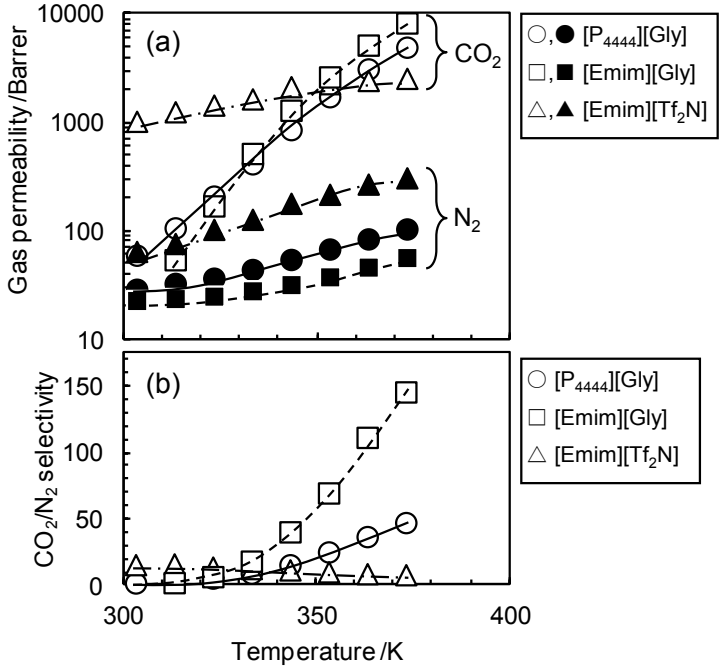

Fig. II.3 Temperature dependences of (a) CO_2 (open symbols) and N_2 (closed symbols) permeabilities and (b) CO_2/N_2 selectivity of $[P_{4444}][Gly]$-FTM, [Emim][Gly]-FTM and $[Emim][Tf_2N]$-SILM (CO_2/N_2 = 10/90 mol/mol, feed-side pressure (P_F) = sweep-side pressure (P_S) = 101.3 kPa, RH = 0%).

Focusing on the results for $[Emim][Tf_2N]$-SILM, both CO_2 and N_2 permeabilities increased slightly with temperature; i.e. the temperature dependence was based on diffusion. The slopes of the plots of N_2 permeability for the AAIL-FTMs were almost the same as for $[Emim][Tf_2N]$-SILM; i.e. N_2 permeation through AAIL-FTMs was also diffusion controlled. The unusual dependence of CO_2 permeability on temperature with

the AAIL-FTMs suggests that AAIL-FTMs definitely reacted with CO_2 and facilitated CO_2 transport even under dry conditions; i.e. CO_2 permeation would be controlled by dissociation of CO_2-AAIL complexes at the permeate side of the membrane.

To confirm the facilitated permeation of CO_2 through AAIL-FTMs under dry conditions, the effect of CO_2 partial pressure on gas permeability was investigated. It is well known behavior for FTMs that CO_2 partial pressure markedly influences CO_2 permeability.[6-8] The behavior reflects carrier saturation with CO_2 in FTMs. Fig. II.4 shows CO_2 partial pressure dependencies for the AAIL-FTMs and [Emim][Tf_2N]-SILM. As shown in Fig. II.4, the CO_2 permeability of only the AAIL-FTMs markedly increased with decreasing CO_2 partial pressure. From the results shown in Figs. II.3 and II.4, there is no doubt that the AAILs facilitated CO_2 permeation under dry conditions.

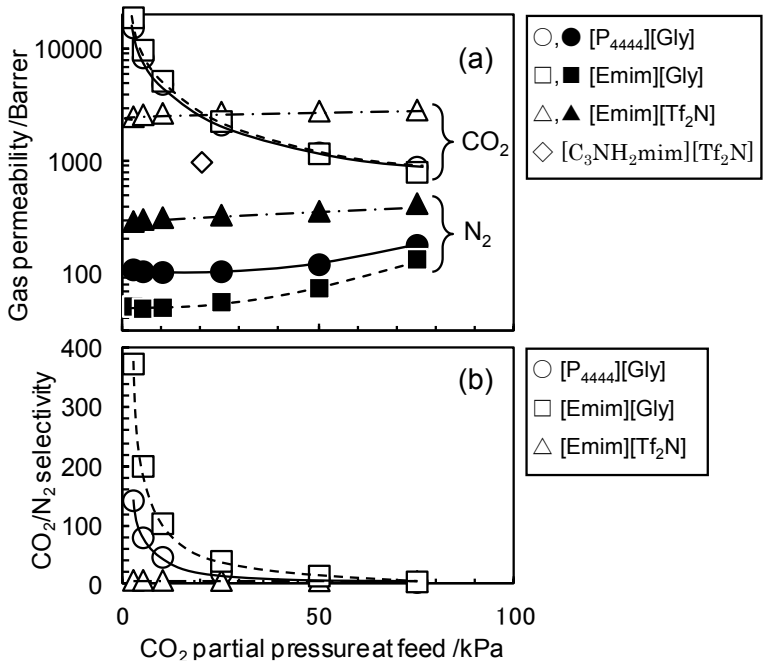

Fig. II.4 CO_2 partial pressure dependences of (a) CO_2 (open symbols) and N_2 (closed symbols) permeabilities and (b) CO_2/N_2 selectivity of [P_{4444}][Gly]-FTM, [Emim][Gly]-FTM and [Emim][Tf_2N]-SILM (T = 373.15 K, P_F = P_S = 101.3 kPa, RH = 0%). The performances of the [C_3NH_2mim][Tf_2N] membrane measured under same condition quoted from data reported in the literature[9] is also plotted for comparison.

As shown in Figs. II.3 and II.4, AAIL-FTMs have high CO_2 permeability and CO_2/N_2 permselectivity for dry gases with low CO_2 concentration at elevated temperature. However, a certain amount of moisture usually exists in real gases. Therefore, the performances under humid conditions should also be checked for practical use. The effect of moisture content on CO_2 permeability and CO_2/N_2 selectivity of the AAIL-FTMs, [Emim][Tf_2N]-SILM, DAPA-FTM and glycine Na-glycerol membrane (Gly-FTM, quoted from the literature[10]) is shown in Fig. II.5. Although the CO_2 permeabilities of DAPA-FTM and Gly-FTM were strongly affected by moisture content in the gas, AAIL-FTMs were only slightly affected. When only a small amount of moisture (5 mol%) was present in the gas, the CO_2 permeabilities of AAIL-FTMs increased; about 1.4 times larger for [P_{4444}][Gly] and about 2 times for [Emim][Gly] than those under dry conditions. The difference in CO_2 permeability of AAIL-FTMs between dry and slightly humid gases would reflect a change in reaction between AAILs and CO_2.[3] When the gas is dry, one mole of [P_{4444}][Gly] or [Emim][Gly] reacts with half a mole of CO_2 to form a complex. On the other hand, when there is a small amount of moisture in the gas, equimolar amounts of [P_{4444}][Gly], CO_2 and H_2O react with one another and bicarbonate would be formed. Another possibility for the increase in CO_2 permeability is a change in viscosity of the AAILs with water absorption. It is reported that the viscosity of AAILs drops when they absorb water.[4]

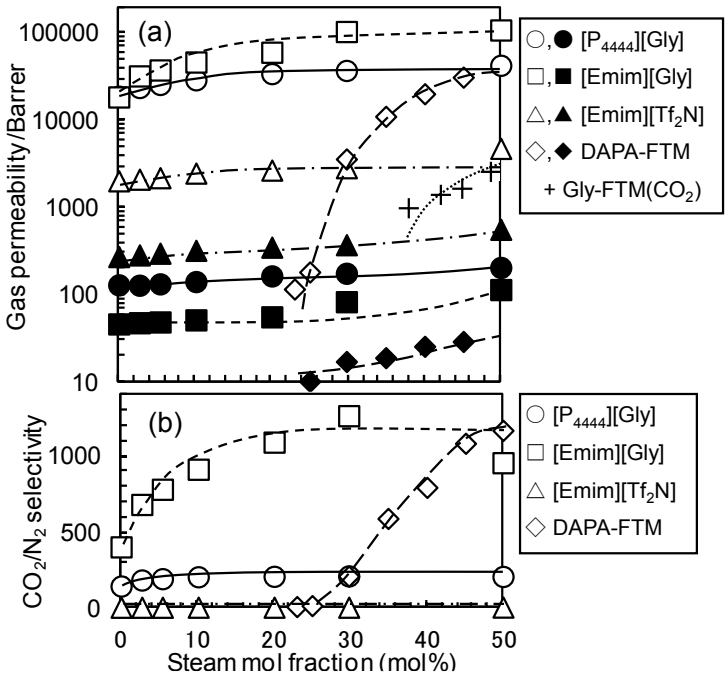

Fig. II.5 Effect of steam mole fraction on (a) CO_2 (open symbols) and N_2 (closed symbols) permeabilities and (b) CO_2/N_2 selectivity of prepared membranes (T= 373.15 K, CO_2 = 2 mol%, N_2: balance, P_F = P_S = 101.3 kPa). The CO_2 permeability of Gly-FTM quoted from literature[10] is also plotted to compare the dependencies of FTMs (T= 296.15±2 K, CO_2 = 0.46 mol%, N_2: balance, P_F = 142.8-153.0 kPa, P_S = 101.3 kPa).

To investigate the contribution of moisture on CO_2 permeation, the water contents of $[P_{4444}][Gly]$ and $[Emim][Tf_2N]$ were measured. Fig. II.6 shows the water content of each IL at 373 K, measured under humid conditions using a thermogravimetry-differential thermal analyzer with a humidity generator (TG-DTA/HUM, Rigaku, Japan). As indicated in Fig. II.6, the water absorption ability of the AAILs was very strong. Even when the steam mole fraction was only 2.5 mol%, the water content in the AAILs was more than 2 wt%. As shown in Fig. II.5, the CO_2 permeability for AAIL-FTMs was mainly influenced at relative humidities below 10%. As reported by Zhang *et al.*, 1 wt% water content is sufficient to change the reactions between CO_2 and $[P_{4444}][Gly]$.[3] Therefore, the major enhancement in CO_2 permeability from 0 to 10% RH is likely to be caused by

a change in the reactions between CO_2 and the AAILs. Comparing the AAILs, the water uptake of [Emim][Gly] is somewhat larger than [P_{4444}][Gly]. This result indicates that the faster CO_2 permeability of [Emim][Gly]-FTM shown in Fig. II.5 would be due to the higher moisture absorbency of [Emim][Gly] than [P_{4444}][Gly].

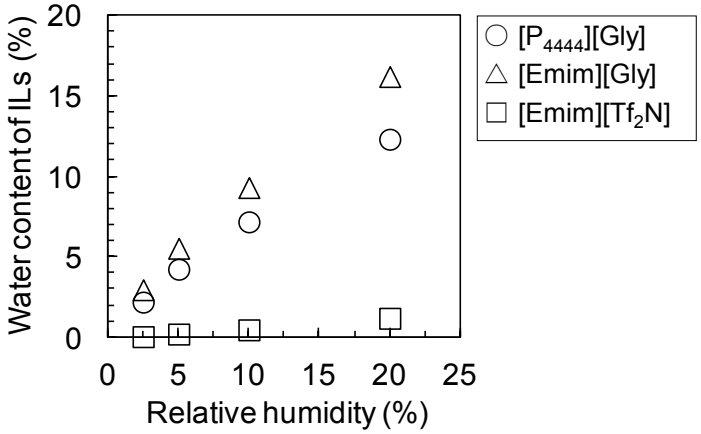

Fig. II.6 Relation between water content of [P_{4444}][Gly], [Emim][Gly] and [Emim][Tf_2N] and RH at 373 K in a N_2/steam environment.

On the other hand, as shown in Fig. II.6, the water content of the AAILs linearly and significantly increased with increasing RH. However, as shown in Fig. II.5, the CO_2 permeability of AAIL-FTMs increased slightly when the RH exceeded 10%. The slight increase in CO_2 permeability above 10% RH would be due to the decrease in viscosity of the AAILs caused by an increase in water content[4] because the ratio of the increase was almost the same as that for N_2 permeability (see Fig. II.5(b)). The degree of CO_2 permeability enhancement above 10% humidity caused by diffusivity is smaller than that below 10% humidity caused by solubility. Therefore, enhancement of the CO_2 absorption capacity of AAILs would be an effective strategy for improving the CO_2 permselectivity as well as CO_2 permeability of AAIL-FTMs. The design of chemical structure of AAILs is flexible.[11,12] Ample opportunities therefore exist for designing

variants with improved physical and chemical properties. Subsequently, I investigated the effect of anion of AAILs on their physicochemical properties and gas permeation properties of the AAIL-FTMs.

II.3.2 Viscosity of AAILs

Fig. II.7 shows the relationship between viscosity of the AAILs and temperature. Among the synthesized tetrabutylphosphonium-type AAILs, the order of viscosities, η(AAILs), from lowest to highest was $\eta([P_{4444}][Ala]) < \eta([P_{4444}][Gly]) < \eta([P_{4444}][Pro]) < \eta([P_{4444}][Ser])$. Although the viscosity values measured in this work were found to be somewhat lower than the reported values, the order was the same.[3,5] The difference in η from the reported values might be due to a difference in the amounts of water retained in the AAILs. It was reported that the viscosity of ionic liquids markedly decreases when a little water is added.[4,13] As shown in Fig. II.7, the viscosity profiles of the synthesized AAILs show hysteresis, whereby the viscosities of the AAILs measured during the heating step were lower than during the cooling step. This would be due to desorption of residual water in each AAIL at elevated temperature. The ratio of the viscosities at 303 K before and after heating was different for each AAIL: $[P_{4444}][Ala]$ (1.36) ≥ $[P_{4444}][Gly]$ (1.35) > $[P_{4444}][Ser]$ (1.30) > $[P_{4444}][Pro]$ (1.19). These differences in the ratios of viscosities would be related to the hygroscopicity, such as water-holding capacity of the AAILs.

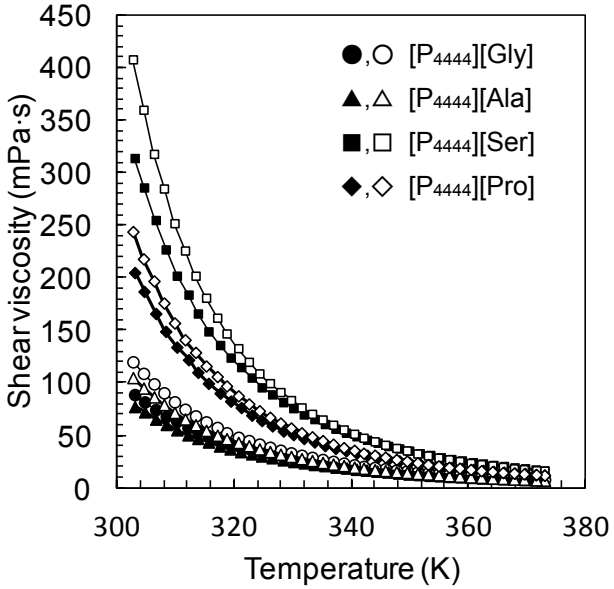

Fig. II.7 Effect of temperature on shear viscosity of AAILs. Closed symbols: heating step, open symbols: cooling step.

II.3.3 Hygroscopicity and water-holding properties of AAILs

The moisture absorption isotherms of the AAILs measured at 373 K are shown in Fig. II.8. As shown in Fig. II.8, the water absorption capacity of the AAILs was very large. Even when the RH was only about 2.5%, the water content in $[P_{4444}][Gly]$ was more than 1 wt%. The order of water content of each AAIL was $[P_{4444}][Gly]$ > $[P_{4444}][Ala]$ > $[P_{4444}][Pro]$ > $[P_{4444}][Ser]$. When AAILs absorb water, their viscosities markedly decrease.[3,4] On the other word, AAILs with larger water absorption capacity should show a more significant difference in viscosity between before and after water desorption. If complete desorption of water had occurred during the viscosity measurement shown in Fig. II.7, the order of the increasing ratio of the viscosities at 303 K before and after heating should correspond to the water absorption capacity. However, the order of the water content was somewhat different from the increasing ratio of the viscosities at 303 K before and after heating. In particular, $[P_{4444}][Pro]$ showed a peculiar result. Although

the water absorption capacity of [P_{4444}][Pro] was higher than [P_{4444}][Ser], the ratio of the viscosity difference was the smallest. This result suggests that the water-holding ability of [P_{4444}][Pro] is higher than the other AAILs.

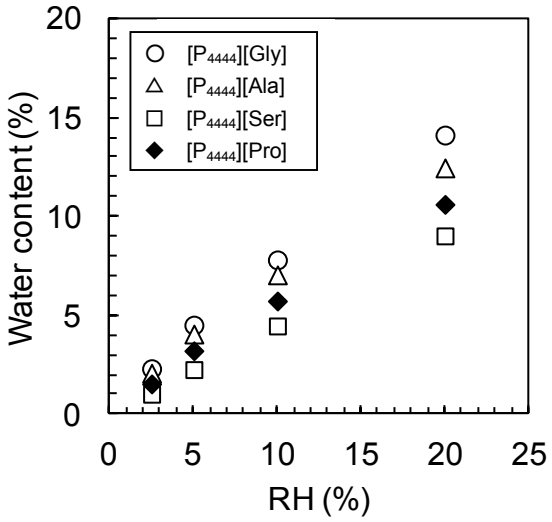

Fig. II.8 Relationship between the water content in each AAIL and RH.

Fig. II.9 show the TG-DTA data used to evaluate the water-holding properties of AAILs. Fig. II.9 is the time course of the weight loss, which was equivalent to the released weight of free water from the AAILs. Fig. II.9 clearly shows that the rate of weight decrease of [P_{4444}][Pro] was slower and its weight loss clearly smaller than the other AAILs. This indicates that free water is strongly adsorbed to [P_{4444}][Pro]. After the experiment of Fig. II.9, the measurement temperature was increased to 473 K at 0.167 K/s to investigate release property of retained water in the AAILs. The DTA and dTG curves for each AAIL were shown in Fig. II.10. As shown in Fig. II.10, only [P_{4444}][Pro] showed a clear endothermic peak and a drastic weight loss around 430 K. From the results, it was confirmed that [P_{4444}][Pro] strongly held water. In addition, it was also

confirmed that amounts of residual water in AAILs after the measurements shown in Fig. II.9 were 0.20, 0.20, 0.18 and 0.32 mg for [P_{4444}][Gly], [P_{4444}][Ala], [P_{4444}][Ser] and [P_{4444}][Pro], respectively. These results suggest that the water-holding ability of [P_{4444}][Pro] was higher than that of the other AAILs. The small ratio of viscosity between before and after heating for [P_{4444}][Pro] shown in Fig. II.7 would be due to its strong water-holding ability, and therefore the water absorbed in [P_{4444}][Pro] was not completely desorbed during the viscosity measurement. As a result, the viscosity change for [P_{4444}][Pro] between the start and the end of measurement would not be very significant.

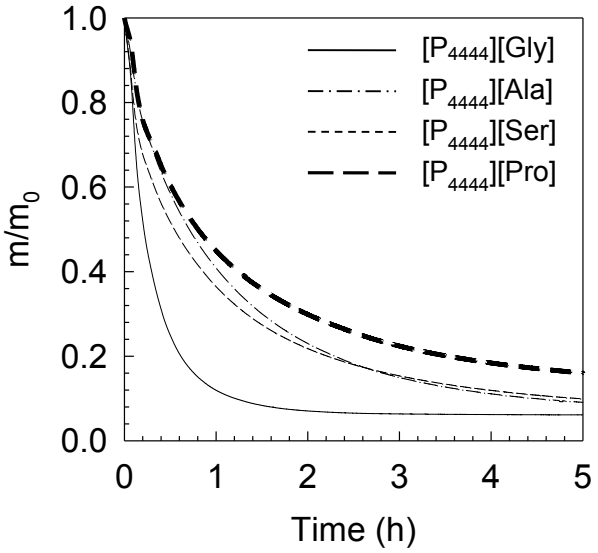

Fig. II.9 Time course of ratio of the released free water from the AAILs. The m_0 means the total amount of water in the AAILs used in this measurement: 3.24 mg for [P_{4444}][Gly], 2.16 mg for [P_{4444}][Ala], 1.80 mg for [P_{4444}][Ser]and 2.01 mg for [P_{4444}][Pro]. The initial weight of AAILs were 20.3 mg for [P_{4444}][Gly], 20.8 mg for [P_{4444}][Ala], 20.4 mg for [P_{4444}][Ser]and 20.5 mg for [P_{4444}][Pro].

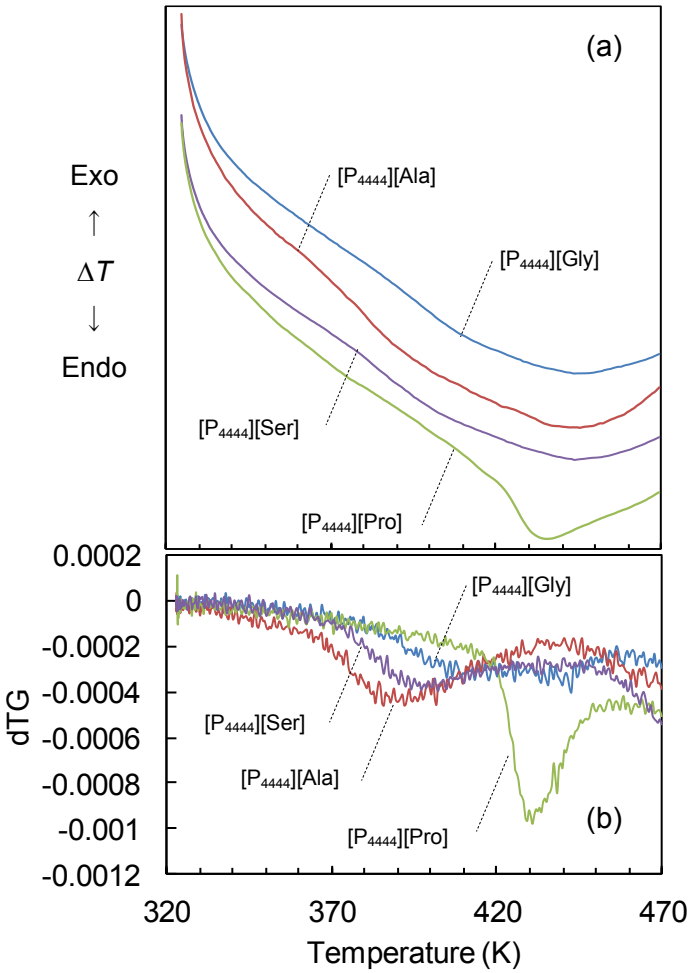

Fig. II.10 DTA (a) and dTG (b) curves of the AAILs after the measurement of water-holding properties.

II.3.4 Effect of anion on gas permeation properties of AAIL-FTMs

The effects of temperature, CO_2 partial pressure and RH on gas permeation properties of the AAIL-FTMs were investigated. The experimental conditions for the investigations on temperature, CO_2 partial pressure and RH are shown in Tables II.1, II.2 and II.3, respectively and the corresponding results are shown in Figs. II.11, II.12 and II.13, respectively. In these figures, the results for a [Emim][Tf_2N]-based supported ionic liquid membrane ([Emim][Tf_2N]-SILM) are also shown for comparison as the gas

permeation properties of a typical SILM. As shown in Fig. II.11, the CO_2 permeabilities for AAIL-FTMs markedly increased with increasing temperature. On the other hand, the permeabilities of N_2 for the AAIL-FTMs increased slightly. Focusing on the results for the [Emim][Tf_2N]-SILM, both CO_2 and N_2 permeabilities increased slightly with temperature. These profiles are typical for the dependence of gas permeation through a SILM with temperature, based on the solution-diffusion mechanism. The slopes of the plots of N_2 permeability for the AAIL-FTMs shown in Fig. II.11 were almost the same as for [Emim][Tf_2N]-SILM. In addition, the magnitude of N_2 permeability for the phosphonium type-AAILs was almost same as the calculated N_2 permeability shown in Fig. II.11(b). The N_2 permeability curves shown in Fig. II.11(b) were calculated based on the Wilke-Chang equation using the viscosity data shown in Fig. II.7 and the Henry's constant for N_2 in [Emim][Tf_2N].[14,15] From these results it was found that the N_2 permeation through AAIL-FTMs is also based on the solution-diffusion mechanism. On the other hand, the marked dependence of CO_2 permeability on temperature in the AAIL-FTMs indicates that AAIL-FTMs permeate CO_2 based on the facilitated transport mechanism. The tendency for facilitated CO_2 permeation is also shown in Fig. II.12. The CO_2 permeability of only the AAIL-FTMs markedly increased with decreasing CO_2 partial pressure. It is well known behavior for FTMs that CO_2 partial pressure significantly influences CO_2 permeability because of carrier saturation with CO_2 in FTMs.[6-8] From the results shown in Figs. II.11 and II.12, there is no doubt that the AAILs facilitated CO_2 permeation.

Table II.1 Experimental conditions of gas permeation test to investigate the temperature dependency

Conditions	Gases		Unit
Temperature		303 – 373 (every 10 K)	K
Pressure	Feed	101.3	kPaA
	Sweep	101.3	kPaA
Pressure difference		0	kPaA
Gas flow rate (dry base)			
Feed	CO_2	20	mL/min
	N_2	180	mL/min
Sweep	He	40	mL/min
Water flow rate	Feed	0	mL/min
	Sweep	0	mL/min

Table II.2 Experimental conditions of gas permeation test to investigate the CO_2 partial pressure dependency

Conditions	Gases		Unit
Temperature		373 (363 K for $[P_{4444}][Ser]$-FTM)	K
Pressure	Feed	101.3	kPaA
	Sweep	101.3	kPaA
Partial pressure difference	CO_2	2.5, 5.0, 10, 25, 50, 75	kPaA
Pressure difference		0	kPaA
Gas flow rate (dry base)			
Feed	Total	200	mL/min
	CO_2	5, 10, 20, 50, 100, 150	mL/min
	N_2	balance	mL/min
Sweep	He	40	mL/min
Water flow rate	Feed	0	mL/min
	Sweep	0	mL/min

Table II.3 Experimental conditions of gas permeation test to investigate the RH dependency

Conditions	Gases		Unit
Temperature		373 (363 K for $[P_{4444}][Ser]$-FTM)	K
Pressure	Feed	101.3	kPaA
	Sweep	101.3	kPaA
Pressure difference		0	kPaA
Gas flow rate (wet base)			
Feed	Total	200	mL/min
	Steam	5.4, 10.9, 20.4, 40.8	mL/min
Gas flow rate (dry base)			
Feed	CO_2	4	mL/min
	N_2	balance	mL/min
Sweep	He	40	mL/min
Water flow rate	Feed	0.004, 0.008, 0.015, 0.03	mL/min
	Sweep	0	mL/min
Relative humidity	Feed	2.7, 5.4, 10.1, 20.0	%

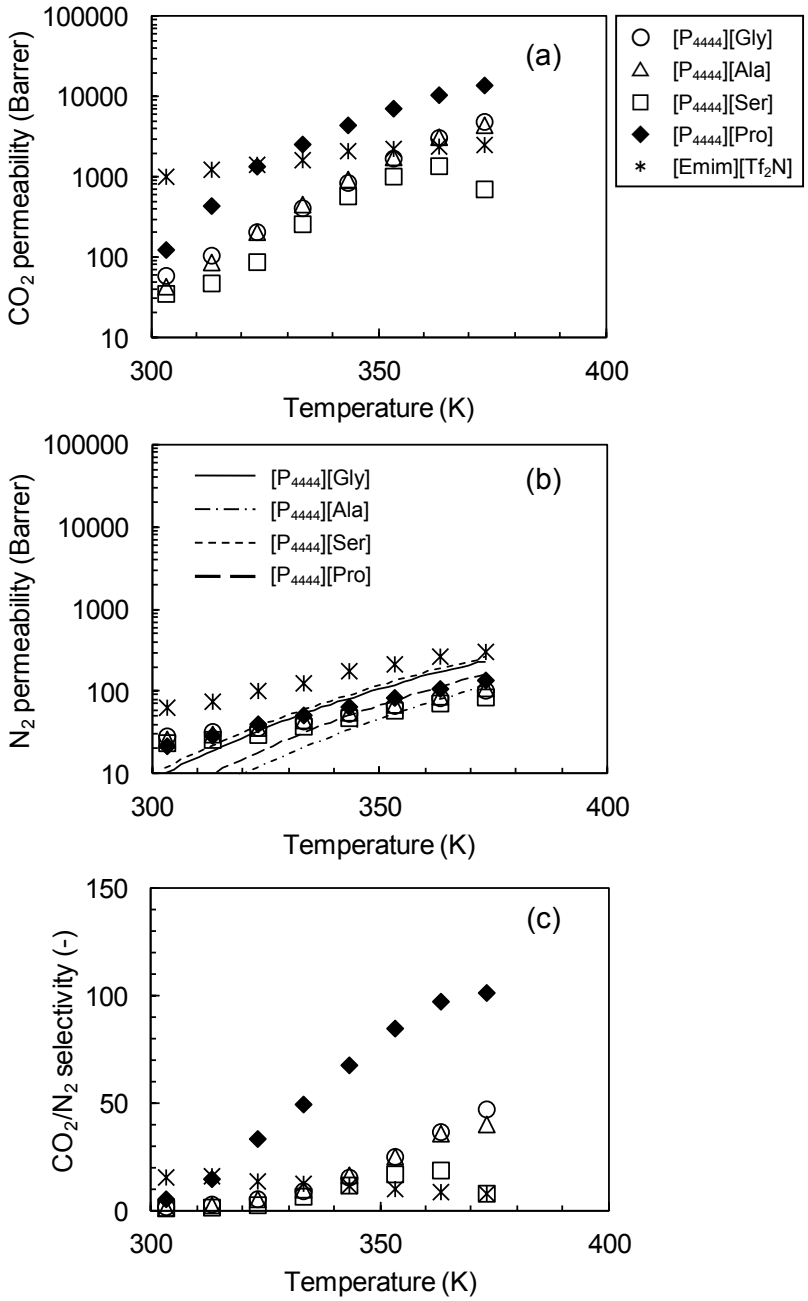

Fig. II.11 Temperature dependences of (a) CO_2 permeability, (b) N_2 permeability and (c) CO_2/N_2 selectivity of [P_{4444}][AA]-FTMs and [Emim][Tf_2N]-SILM (CO_2/N_2 = 10/90 mol/mol, feed-side pressure (P_F) = sweep-side pressure (P_S) = 101.3 kPa, RH = 0%).

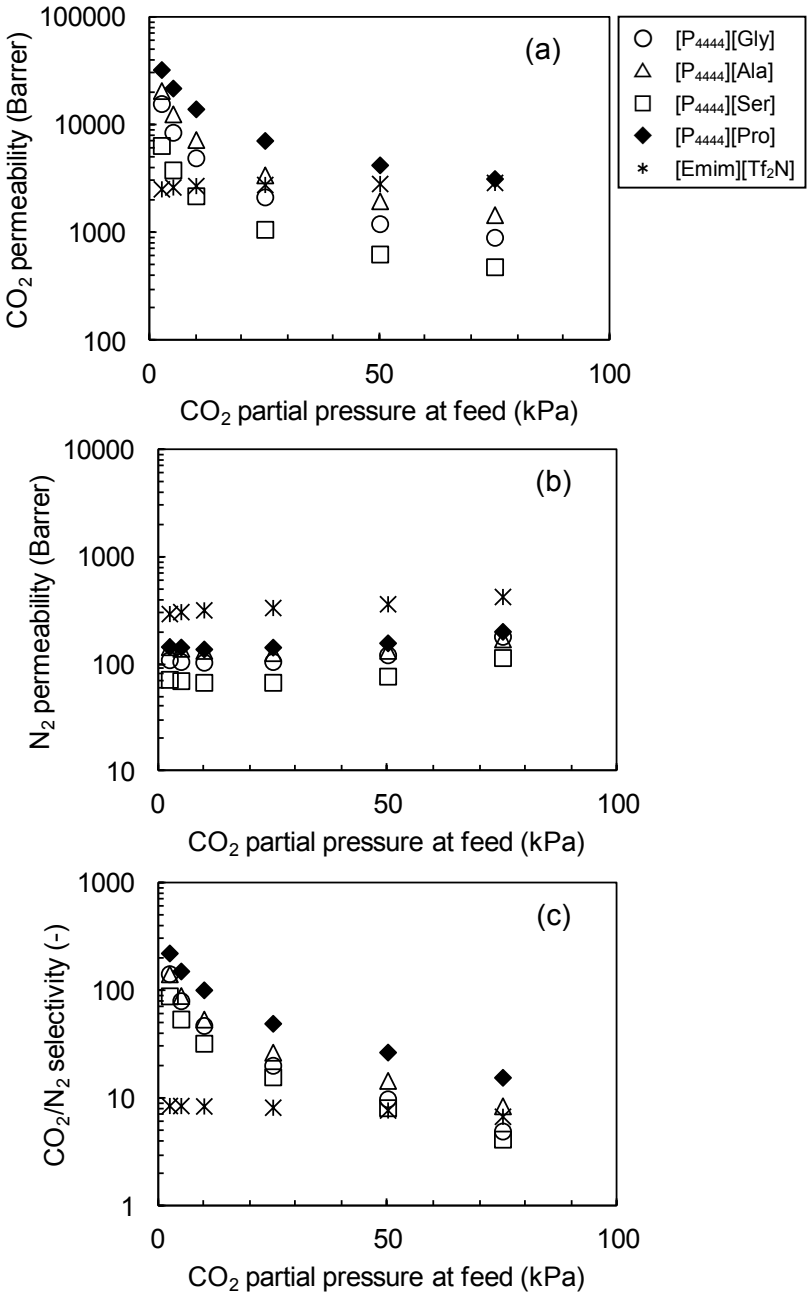

Fig. II.12 CO_2 partial pressure dependences of (a) CO_2 permeability, (b) N_2 permeability and (c) CO_2/N_2 selectivity of $[P_{4444}][AA]$-FTMs and $[Emim][Tf_2N]$-SILM (T = 373.15 K for $[P_{4444}][Gly]$-FTM, $[P_{4444}][Ala]$-FTM, $[P_{4444}][Pro]$-FTM and $[Emim][Tf_2N]$-SILM, T = 363.15 K for $[P_{4444}][Ser]$-FTM, $P_F = P_S$ = 101.3 kPa, RH = 0%).

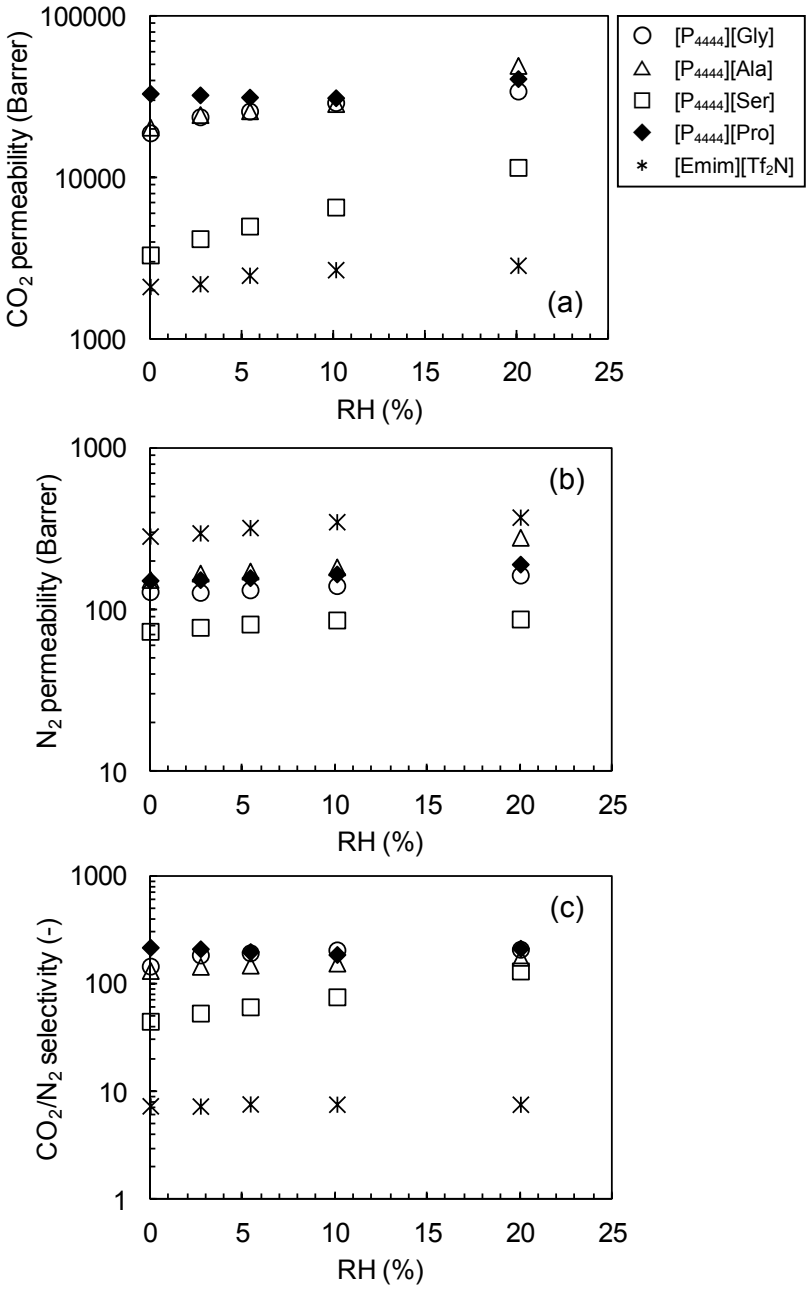

Fig. II.13 Effect of RH on (a) CO_2 permeability, (b) N_2 permeability and (c) CO_2/N_2 selectivity of $[P_{4444}][AA]$-FTMs and $[Emim][Tf_2N]$-SILM (T = 373.15 K for $[P_{4444}][Gly]$-FTM, $[P_{4444}][Ala]$-FTM, $[P_{4444}][Pro]$-FTM and $[Emim][Tf_2N]$-SILM, T = 363.15 K for $[P_{4444}][Ser]$-FTM, CO_2 = 2 mol%, N_2: balance, $P_F = P_S$ = 101.3 kPa).

Focusing on the CO_2 permeability of each AAIL-FTM, it is clearly shown in Figs. II.11 and II.12 that the CO_2 permeability of the $[P_{4444}][Pro]$-FTM was significantly larger than the other AAIL-FTMs. The rapid CO_2 permeability of $[P_{4444}][Pro]$-FTM is a result worthy of consideration. As shown in Fig. II.7, the viscosity of $[P_{4444}][Pro]$ was larger than $[P_{4444}][Gly]$ and $[P_{4444}][Ala]$. These results indicate that the diffusivity of the CO_2-complex in the AAILs is not the main factor determining the CO_2 permeability of the AAIL-FTMs. In addition to the diffusivity of the CO_2-complex, a number of factors contribute to CO_2 permeability. Complexation and decomplexation rates are one of the possible factors. However, chemical reaction rates are generally much faster than diffusion. Therefore, it is hard to believe that the complexation and decomplexation rates determine the overall permeability of CO_2. The CO_2 absorption capacity also affects CO_2 permeability. A large absorption capacity for CO_2 enhances the concentration gradient of the CO_2-complex between the feed side and sweep side of the membrane. If the concentration gradient is large; i.e. the driving force for diffusion is large, the mass transfer rate of the CO_2-complex through the membrane is rapid. Here I investigate the saturation absorption amount of CO_2 in the AAILs. It was reported that the density of the phosphonium type-AAILs were almost equal (about 0.9 cm^3/g).[16] Therefore, if the AAILs impregnated in the membrane react with CO_2 according to the same complexation reaction, it is considered that the concentration of the CO_2-complex near the membrane surface on the feed side, where CO_2 absorption would be saturated, is almost equal for all of the phosphonium type-AAIL-FTMs prepared in this study. However, as reported by Zhang *et al.*, the absorption amount of CO_2 in $[P_{4444}][Gly]$ and $[P_{4444}][Ala]$ was increased when the AAILs had small amounts of water.[3] It is considered that the increase of the absorption amount of CO_2 in AAILs in the presence of water would be due to the

change of the absorption mechanism. Although the absorption mechanism was not fully understood,[3,4] it is suggested that the absorption amount of CO_2 in AAILs would be increased by allowing most AAIL molecules participate to form CO_2-complexes owing to the presence of water. In other words, the possible factor determining the CO_2 permeability of AAILs-FTM would be the water in the AAILs.

According to the increases of driving force of mass transport of CO_2-complexes due to the absorption of water in AAILs, it is expected that the CO_2 permeability through AAIL-FTMs increases by the increase of an absorption amount of water. As shown in Fig. II.9, the water-holding ability of $[P_{4444}][Pro]$ was relatively high. The amount of residual water in $[P_{4444}][Pro]$ after the water release test shown in Fig. II.9 was 0.32 mg, which corresponds to 1.6 wt% of the $[P_{4444}][Pro]$ used in the test. This result suggests that $[P_{4444}][Pro]$-FTM would hold a few percent free water during the gas permeation experiments. On the other hand, more than 90% of the free water in the other AAIL-FTMs investigated in this study was desorbed during the gas permeation tests. The retained free water in the AAILs except for $[P_{4444}][Pro]$ would be less than 1.0wt% of the AALIs. Owing to the difference in the water content between $[P_{4444}][Pro]$ and the other AAILs, the concentration gradient for the CO_2-complex in the $[P_{4444}][Pro]$-FTM between feed and sweep sides would be somewhat larger than the others. As a result, the mass transfer rate of the CO_2-complex through the $[P_{4444}][Pro]$-FTM would be more rapid. As shown in Fig. II.11, the CO_2 permeability of $[P_{4444}][Pro]$-FTM was higher than the others. This observation supports the above consideration.

To confirm the contribution of water to the CO_2 permeability of AAIL-FTMs, the effect of RH on gas permeability was investigated. Fig. II.13 shows the effect of RH on the CO_2 and N_2 permeabilities and the CO_2/N_2 selectivity of the AAIL-FTMs. Focusing on the

CO_2 permeability of [P_{4444}][Pro]-FTM, it is clearly shown that CO_2 permeability depended little on the RH. Because [P_{4444}][Pro] held sufficient water under dry conditions, the additional absorbed water under humid conditions hardly enhance the CO_2 permeability. On the other hand, the CO_2 permeabilities of the AAIL-FTMs, other than for the [P_{4444}][Pro]-FTM, were clearly increased with increasing RH. As shown in Fig. II.8, the AAILs could absorb large amounts of water, even when RH was only 2.5%. The absorbed water from the feed gas would enhance the concentration of CO_2-complex in each AAIL. Therefore, the CO_2 permeability of [P_{4444}][Gly]-FTM, [P_{4444}][Ala]-FTM and [P_{4444}][Ser]-FTM increased with increasing RH. Here, I should consider the effect of water absorption on the viscosity of AAILs because it was also experimentally confirmed that the viscosity of the AAILs drastically decreased by absorbing water.[3,4] The decrease of viscosity causes the increase of molecular diffusivity in AAILs. The enhancement in CO_2 permeability shown in Fig. II.13(a) includes the effect of the decrease in viscosity accompanying the absorption of water. It is necessary to normalize the CO_2 permeability by considering the viscosity effect. Because the effect of the decrease in viscosity should be reflected in N_2 permeability, standardization of CO_2 permeability by N_2 permeability removes the effect of the variation of viscosity. That is to say, CO_2/N_2 selectivity directly shows the effect of the change of reaction mechanism upon the increase of CO_2 permeability. The ratio of CO_2/N_2 selectivity between 20% RH and dry conditions is shown in Table II.4. Although the data contain some experimental error, the increased ratio of CO_2 permeability for [P_{4444}][Gly]-FTM, [P_{4444}][Ala]-FTM and [P_{4444}][Ser]-FTM was more than 1.5. These results also support the consideration regarding the contribution of water to the CO_2 permeability of AAIL-FTMs.

Table II.4 Ratio of CO_2/N_2 selectivity between 20% of RH and dry conditions

	$[P_{4444}][Gly]$	$[P_{4444}][Ala]$	$[P_{4444}][Ser]$	$[P_{4444}][Pro]$	$[Emim][Tf_2N]$
CO_2/N_2 selectivity ratio	1.5	1.6	3.0	1.1	1.0

From the results in this chapter, I suggest the schematic illustration of facilitated CO_2 transport through AAIL-FTMs as shown in Fig. II.14. Therefore, the following recommendations for improving the CO_2 permselectivity and CO_2 permeability of AAIL-FTMs are proposed: (1) design an AAIL with a high CO_2 absorption capacity and (2) design an AAIL with a strong water holding property.

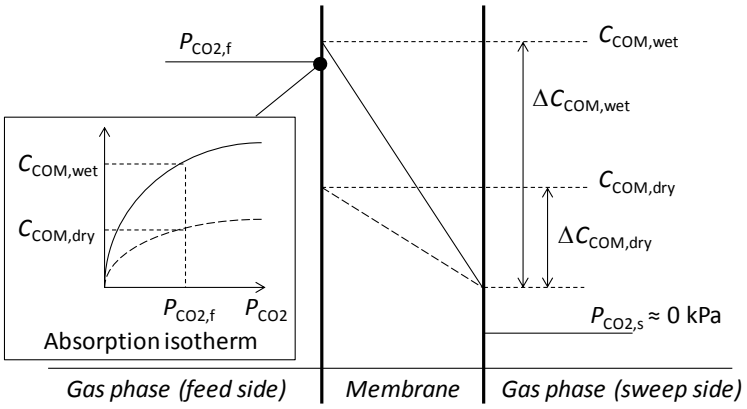

Fig. II.14 Schematic illustration of facilitated CO_2 transport through AAIL-FTMs. P_{CO2} and C_{COM} are the partial pressure of CO_2 and the equilibrium concentration of AAIL-CO_2 complex on P_{CO2}, respectively. The subscripts "f" and "s" denotes the gas phases at the feed and sweep sides of the membrane, respectively; "dry" and "wet" denotes the concentration for dry gas and humid gas, respectively.

II.4 Conclusions

Novel CO_2 selective FTMs containing AAILs were successfully fabricated. All AAIL-FTMs prepared in this study permeated CO_2 based on a facilitated transport mechanism. The AAIL-FTMs showed high CO_2 permselectivity under dry and humid conditions. In

addition, to obtain a guideline for the molecular design of an AAIL suitable to use in an AAIL-FTM for CO_2 separation, a series of tetrabutylphosphonium-type AAILs were synthesized. AAIL-FTMs containing the synthesized AAILs were prepared and the gas permeabilities were evaluated from the physical and physicochemical properties of the AAILs. Among the AAIL-FTMs, $[P_{4444}][Pro]$-FTM showed the best CO_2 permeability and CO_2/N_2 permselectivity under dry conditions. The water-holding ability of $[P_{4444}][Pro]$ was remarkably high among the AAILs investigated in this study. These results suggest that $[P_{4444}][Pro]$ absorbed large amounts of CO_2, based on a 1:1 complex formation mechanism at the feed-side surface of the membrane and that a large concentration for of CO_2-complex was established across the membrane. The large concentration gradient provided a large driving force for the CO_2-complex transport and increased CO_2 permeability. The results provided the following recommendations for the enhancement of the concentration gradient for the CO_2-complex across the membrane to improve the CO_2 permselectivity as well as CO_2 permeability of AAIL-FTMs: (1) design an AAIL with a high CO_2 absorption capacity and (2) design an AAIL with a strong water holding property.

References

1. K. Fukumoto, M. Yoshizawa and H. Ohno, *J. Am. Chem. Soc.*, 2005, **127**, 2398.
2. H. Ohno and K. Fukumoto, *Acc. Chem. Res.*, 2007, **40**, 1122.
3. J. Zhang, S. Zhang, K. Dong, Y. Zhang, Y. Shen and X. Lv, *Chem.- Eur. J.*, 2006, **12**, 4021.
4. B. F. Goodrich, J. C. de la Fuente, B. E. Gurkan, Z. K. Lopez, E. A. Price, Y. Huang and J. F. Brennecke, *J. Phys. Chem. B*, 2011, **115**, 9140.
5. J. Kagimoto, K. Fukumoto and H. Ohno, *Chem. Commun.*, 2006, 2254.
6. M. Teramoto, K. Nakai, N. Ohnishi, Q. Huang, T. Watari and H. Matsuyama, *Ind. Eng. Chem. Res.*, 1996, **35**, 538.
7. H. Matsuyama, M. Teramoto, K. Matsui and Y. Kitamura, *J. Appl. Polym. Sci.*, 2001, **81**, 936.
8. A. S. Kovvali, H. Chen and K. K. Sirkar, *J. Am. Chem. Soc.*, 2000, **122**, 7594.
9. C. Myers, H. Pennline, D. Luebke, J. Ilconich, J. K. Dixon, E. J. Maginn and J. F. Brennecke, *J. Membr. Sci.*, 2008, **322**, 28.
10. H. Chen, A. S. Kovvali and K. K. Sirkar, *Ind. Eng. Chem. Res.*, 2000, **39**, 2447.
11. Y. Zhang, S. Zhang, X. Lu, Q. Zhou, W. Fan and X. P. Zhang, *Chem.- Eur. J.*, 2009, **15**, 3003.
12. Z.-Z. Yang, Y.-N. Zhao and L.-N. He, *RSC Advances*, 2011, **1**, 545.
13. K. R. Seddon, A. Stark and M.-J. Torres, *Pure Appl. Chem.*, 2000, **72**, 2275.
14. C. R. Wilke and P. Chang, *Am. Inst. Chem. Eng. J.*, 1955, **1**, 264.
15. A. Finotello, J. E. Bara, D. Camper and R. D. Noble, *Ind. Eng. Chem. Res.*, 2008, **47**, 3453.
16. J. Kagimoto, S. Taguchi, K. Fukumoto and H. Ohno, *J. Mol. Liq.*, 2010, **153**, 133.

Chapter III

Fundamental investigation of the factors controlling the CO_2 permeability of facilitated transport membranes containing amine-functionalized task-specific ionic liquids

III.1 Introduction

The present AAIL-FTMs have two disadvantages. One is their low CO_2 permeabilities at low temperature under dry conditions, and the other is their low permeabilities at high CO_2 partial pressures. In this work, I have focused on improving the permeability at a low temperature under dry conditions.

The gas permeability through FTMs can usually be defined as a product of diffusion coefficient (which represents the speed of diffusion) and the transmembrane concentration gradient (the driving force for diffusion) of the complex formed by chemical reaction between the absorbed gases and carrier compound in the membrane. For AAIL-FTMs, I do not know which parameter is dominant for CO_2 permeation. If the diffusion coefficient of the CO_2 complex significantly affects CO_2 permeation, then choosing a low-viscosity AAIL would improve the CO_2 permeability. Conversely, if the transmembrane concentration gradient is the dominant factor, an AAIL with high CO_2 capacity is a better choice to improve the CO_2 permeability.

In this chapter, I first evaluated the effects of the diffusion coefficient on the CO_2 permeability of AAIL-FTMs, using three types of AAILs containing different glycinate

anions. The viscosities of the ILs before and after CO_2 absorption were measured and compared with the CO_2 permeabilities of the corresponding AAIL-FTMs. To further reduce the viscosity of the IL after CO_2 absorption, an aTSIL with a tailored chemical structure was synthesized. The CO_2 permeability of the FTM containing this aTSIL was evaluated experimentally and by model calculations. From these calculations, I propose guidelines for fabricating FTMs with better CO_2 permeability over a wide temperature range.

III.2 Experimental

III.2.1 Materials

Tetrabutylphosphonium hydroxide ([P_{4444}][OH], 40 wt% in water), N-methylglycine (Bioxtra grade), 2-cyanopyrrole (96%), acetonitrile (> 99.9%), and anion exchange resin (OH type) were purchased from Sigma-Aldrich Co. (St. Louis, MO, USA). Glycine and N,N-dimethylglycine (> 98.0%) were purchased from Tokyo Chemical Industry Co. (Tokyo, Japan). Methanol (99.8%) was purchased from Wako Pure Chemicals Industry Ltd. (Osaka, Japan). All reagents were used as received. CO_2 and N_2 gases of 99.9% purity were used for gas permeation tests. A hydrophilic polytetrafluoroethylene (PTFE) microporous membrane with an average pore size of 0.1 μm and a film thickness of 37.5 μm was purchased from Sumitomo Electric Industries Ltd. (Osaka, Japan) and used as a support for the supported ionic liquid membranes.

Tetrabutylphosphonium-type AAILs with a series of glycinate anions (tetrabutylphosphonium glycinate ([P_{4444}][Gly]), tetrabutylphosphonium N-methylglycinate ([P_{4444}][mGly]), and tetrabutylphosphonium N,N-dimethylglycinate ([P_{4444}][dmGly])) were synthesized following a neutralization procedure reported

previously.[1] An aqueous solution of tetrabutylphosphonium hydroxide ([P_{4444}][OH]) was added to a slight excess of an equimolar amino acid aqueous solution to prepare [P_{4444}][AA] salts, with water as a byproduct. The product was dried in vacuo for 24 h at 313 K. Subsequently, an appropriate amount of acetonitrile/methanol mixture or ethanol was added to precipitate and remove unreacted amino acids. The filtrate was evaporated to remove solvents. The reaction ratios were 99.9, 98.3, and 99.9% for [P_{4444}][Gly], [P_{4444}][mGly], and [P_{4444}][dmGly], respectively. The structures of the resulting [P_{4444}][AA]s were confirmed by ^{1}H-NMR spectroscopy (Bruker Avance 500, Bruker Bio Spin) and FT-IR (ALPHA FT-IR Spectrometer, Bruker Optics) measurements, as shown in the appendix.

Tetrabutylphosphonium 2-cyanopyrrolide ([P_{4444}][2-CNpyr]), proposed in this research as an appropriate aTSIL, was also synthesized by a neutralization procedure.[2] A 1.1 molar equivalent of 2-cyanopyrrole was added to the [P_{4444}][OH] aqueous solution and stirred for 24 h at room temperature. The solution was evaporated to remove water. The structure of the resulting [P_{4444}][2-CNpyr] was confirmed by ^{1}H-NMR spectroscopy and FT-IR measurements. The data are also shown in the appendix. The chemical structures of each IL are shown in Fig. III.1.

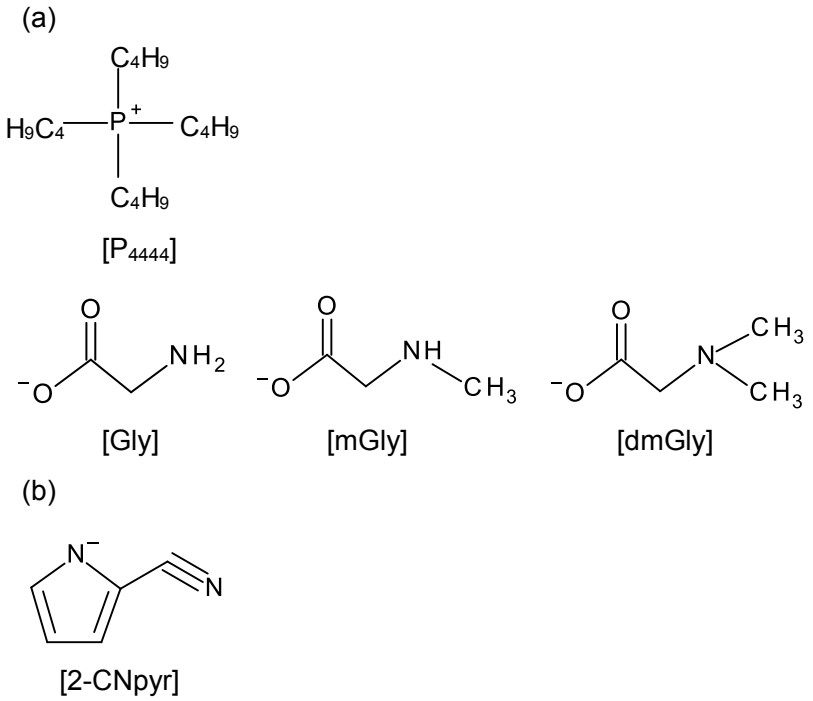

Fig. III.1 Chemical structure of aTSILs used in this study. (a) AAILs ([P_{4444}][X]; X=glycinate, methylglycinate, or dimethylglycinate) and (b) [P_{4444}][2-CNpyr].

III.2.2 Membrane preparation including IL

The membranes containing ILs were prepared as follows. A hydrophilic PTFE microporous membrane was immersed into the synthesized ILs ([P_{4444}][Gly], [P_{4444}][mGly], [P_{4444}][dmGly] or [P_{4444}][2-CNpyr]) and immediately placed under vacuum for 1 h to completely exchange the air in the PTFE membrane for IL. The IL-impregnated PTFE membrane was taken out and excess IL was wiped off the surface. The thickness of IL-based membranes investigated in this study depends on the thickness of the support membrane because IL-based membranes were prepared by ionic liquid impregnation process. Therefore, thinner IL-based membranes could be fabricated by using a thinner support.

III.2.3 Characterization of the ILs before and after CO_2 absorption

The viscosities of the ILs before and after CO_2 absorption were measured with an Electro-Magnetically Spinning Sphere Viscometer (EMS-1000W; Kyoto Electronics Manufacturing Co., Ltd., Kyoto, Japan), using a metallic sphere at a constant rotating speed of 1000 rpm. The CO_2-saturated ILs for viscosity measurements were prepared by bubbling CO_2 into the ILs at room temperature. The viscosity was measured from 303 to 373 K.

FT-IR spectra (Nicolet iS5vFT-IR; Thermo Scientific Inc.) of the CO_2-saturated ILs were measured to confirm the formation of hydrogen bonds between the CO_2 complexes. The FT-IR spectra were measured in a glove box (NDGF080; Nagano Electric Co., Ltd., Osaka, Japan) under a CO_2 environment to measure the changes with time of the spectra of ILs during CO_2 absorption. Because CO_2 saturation during IR measurements was slow, the FT-IR spectra of the CO_2-saturated ILs were measured separately in a glove box filled with CO_2.

III.2.4 Gas permeation test

Gas permeation tests were carried out with a similar procedure described in II.2.3.

III.2.5 CO_2 absorption test

The apparatus used to measure CO_2 absorption isotherms is illustrated in Fig. III.2. The equipment consisted of stainless steel tubes, and reference and sample cells. The volume of each cell, including connecting tubes, was measured by filling them with CO_2. The weights of the cells before and after filling with CO_2 were measured and the volumes of the cells determined by mass. To begin the absorption experiments, about 1.5 g of IL

was added to the sample cell. The temperature of the system was controlled by a water bath (T-105B; Thomas Kagaku Co., Ltd., Tokyo, Japan) to ± 0.1 K. The absorption experiment was carried out according to the following process. The reference and sample cells were evacuated and the valve separating the two cells then closed. The reference cell was pressurized to charge a known amount of CO_2, and the temperature allowed to equilibrate. After the CO_2 was charged, the stirrer was turned on and the IL was then constantly stirred throughout the experiment. The CO_2 absorption was started when the valve connecting the two cells was opened, and the feed CO_2 in the reference cell was transferred into the sample cell to come into contact with the IL. The pressure drop from absorption of CO_2 by the IL was measured with a digital pressure gauge (Model AM-756 digital manometer; GE Sensing & Inspection Technologies Co., Ltd., Tokyo, Japan). The pressure was monitored until it remained constant for more than 2 h. Equilibration was usually attained within 12 h. After equilibration had been attained, the final pressure was measured and the amount of CO_2 absorbed was determined from the observed pressure change.

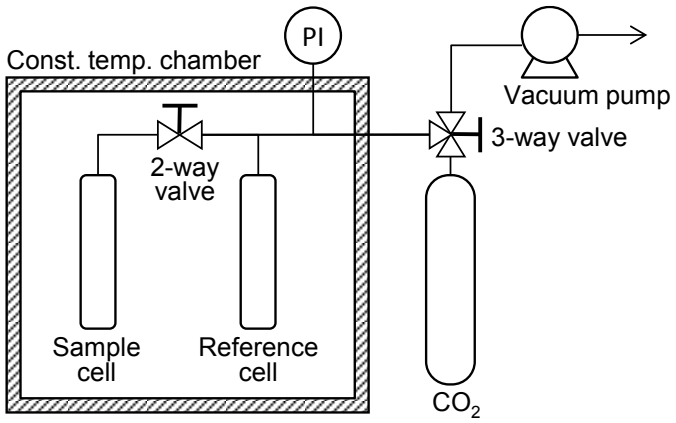

Fig. III.2 Schematic of apparatus used for gas absorption tests.

III.3 Results and discussion

III.3.1 Effect of temperature on viscosity of AAILs

Fig. III.3 shows the effect of temperature on the viscosities of AAILs before and after CO_2 absorption. It has been reported that the viscosity of ILs is well described by the modified Vogel-Fulcher-Tammann (VFT) equation:[3-5]

$$\eta = AT^{0.5} \exp\left(\frac{k}{T - T_0}\right) \quad \text{(III.1)}$$

where A, k, and T_0 are fitting parameters and T (K) is temperature. Those fitting parameters are listed in Table III.1. Within a wide temperature range, the modified VFT equation is suitable for estimating not only the viscosities of the pure ILs, but also the viscosities of two-component liquids, regardless of composition. The viscosities predicted by the modified VFT equation are shown in Fig. III.3, along with the experimental data. As shown in Fig. III.3 a and b, the viscosities of $[P_{4444}][Gly]$, $[P_{4444}][mGly]$, and $[P_{4444}][dmGly]$ increased with CO_2 absorption. Importantly, as shown in Fig. III.3(b), the viscosities of the CO_2-saturated $[P_{4444}][Gly]$ and $[P_{4444}][mGly]$ drastically increased at low temperature. The calculated viscosity of $[P_{4444}][mGly]$ after CO_2 absorption was higher than the others at low temperature. In fact, the viscosity of CO_2-saturated $[P_{4444}][mGly]$ was out of the measurable range of the viscometer. On the contrary, the increase in viscosity of CO_2-saturated $[P_{4444}][dmGly]$ was lower than for the other ILs. This different tendency indicates that there may be differences in CO_2 absorption mechanisms between $[P_{4444}][dmGly]$ and the other ILs. In general, primary and secondary amines absorb CO_2 by chemical reaction. On the other hand, tertiary amines cannot react with CO_2 under dry conditions, such as those used for the viscosity measurements in this study.[6] Thus, CO_2 must have been only physically dissolved in $[P_{4444}][dmGly]$. Therefore, the chemical structure of $[P_{4444}][dmGly]$ was not changed

before and after CO_2 absorption. Conversely, $[P_{4444}][Gly]$ and $[P_{4444}][mGly]$ changed their chemical structure after CO_2 absorption, and formed CO_2 complexes. It has been reported that AAIL-CO_2 complexes form hydrogen bond networks.[7,8] This suggests that the significant increase in the viscosity of $[P_{4444}][Gly]$ and $[P_{4444}][mGly]$ upon CO_2 absorption is because of hydrogen bonding.

Table III.1 Fit parameters for VFT equation

	Before CO_2 absorption			After CO_2 absorption		
	A	*k*	T_0	*A*	*k*	T_0
$[P_{4444}][Gly]$	0.0450	600	203	0.135	530	252
$[P_{4444}][mGly]$	0.0245	725	200	0.00550	800	248
$[P_{4444}][dmGly]$	0.0260	735	194	0.0150	900	206
$[P_{4444}][2\text{-}CNpyr]$	0.0120	680	208	0.0170	647	216

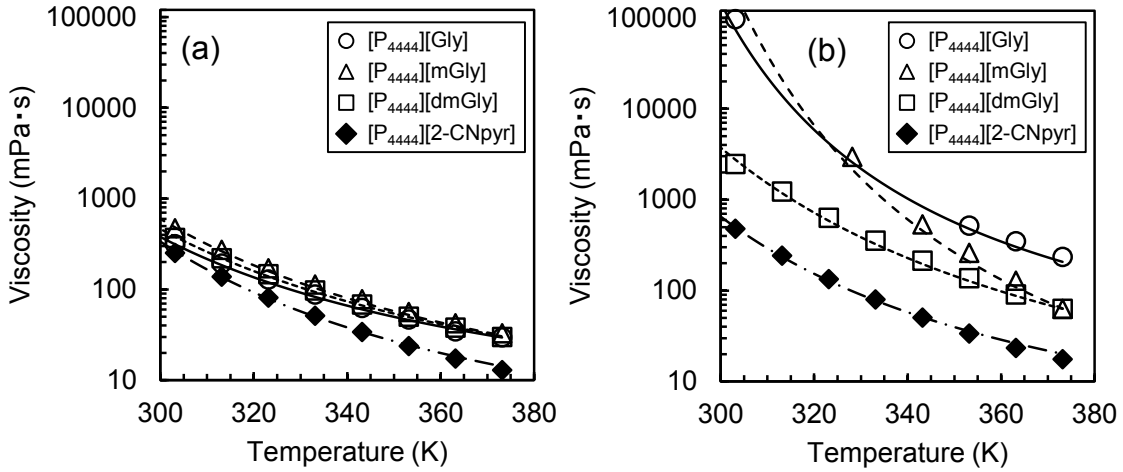

Fig. III.3 Effect of temperature on viscosity of the aTSILs. (a) before CO_2 absorption and (b) after CO_2 absorption. The points and lines show experimental data and results calculated according to the modified VFT model, respectively.

To confirm the hydrogen-bond formation in AAILs after CO_2 absorption, the chemical structure change of the AAILs with CO_2 absorption was measured using FT-IR. Fig. III.4 shows the FT-IR spectra of $[P_{4444}][Gly]$ as a function of CO_2 absorption time, and those of $[P_{4444}][mGly]$ and $[P_{4444}][dmGly]$ before and after complete CO_2 absorption. As shown in Fig. III.4(a), at $t = 0$ s (before CO_2 absorption), a sharp peak derived from an amino group was observed at 1590 cm^{-1}. With CO_2 absorption, the sharp peak at 1590 cm^{-1} decreased in intensity as the amino group in $[P_{4444}][Gly]$ reacted with CO_2 and formed a CO_2 complex, and new peak derived from a carboxyl group appeared at 1737 cm^{-1}. Comparing the spectra of $[P_{4444}][Gly]$ before and after CO_2 absorption, the peak at 1590 cm^{-1} shifted to a higher wave number at 1605 cm^{-1}. This blue shift is attributed to hydrogen bonding interactions.[9-11] As shown in Fig. III.4(b), $[P_{4444}][mGly]$ also chemically absorbed CO_2 and formed hydrogen bonds between the AAIL-CO_2 complexes; the FT-IR spectra of $[P_{4444}][mGly]$ showed similar behavior to the spectra of $[P_{4444}][Gly]$. On the other hand, as shown in Fig. III.5(c), the FT-IR spectrum of $[P_{4444}][dmGly]$ did not change with CO_2 absorption. This means that no chemical reaction between $[P_{4444}][dmGly]$ and CO_2 occurred. As shown in Fig. III.3, the viscosities of $[P_{4444}][Gly]$ and $[P_{4444}][mGly]$ after CO_2 absorption drastically decreased with increasing temperature. This temperature dependence results from hydrogen bond breakage with heating.

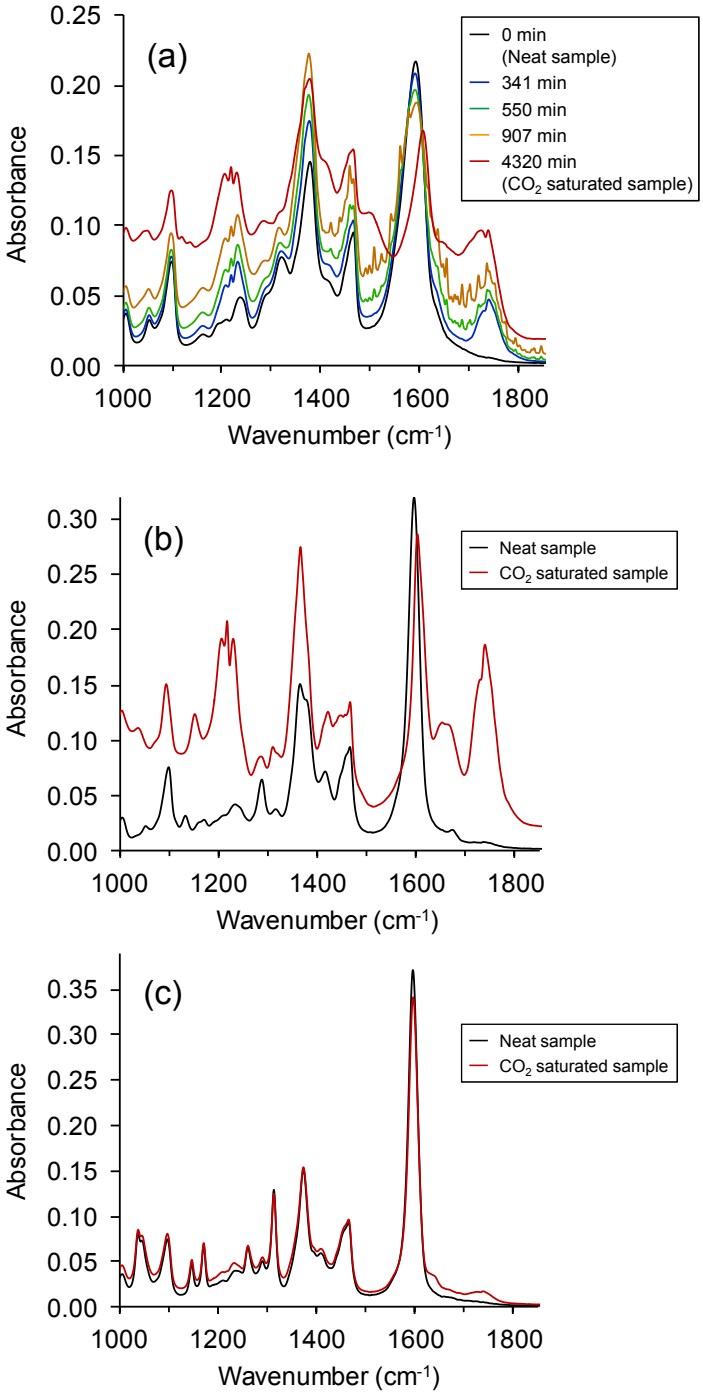

Fig. III.4 FT-IR spectra of the AAILs and their CO_2 complexes. (a) FT-IR spectra recorded as a function of time during CO_2 absorption of $[P_{4444}][Gly]$, (b) FT-IR spectra of $[P_{4444}][mGly]$ before and after CO_2 absorption and (c) FT-IR spectra of $[P_{4444}][dmGly]$ before and after CO_2 absorption.

III.3.2 Gas permeation properties of AAIL-based membranes

The effect of temperature on the CO_2 permeability of AAIL-based membranes was investigated. The experimental conditions are shown in Table III.2. All experiments were done under dry conditions. The permeation results are shown in Fig. III.5. The CO_2 permeabilities of three AAIL-based membranes increased with increasing temperature. However, the temperature dependences of the CO_2 permeability were different. In $[P_{4444}][Gly]$- and $[P_{4444}][mGly]$-based membranes, the CO_2 permeability strongly depended on temperature, while the CO_2 permeability of the $[P_{4444}][dmGly]$-based membrane showed weak dependence. The CO_2 permeabilities of $[P_{4444}][Gly]$ and $[P_{4444}][mGly]$ crossed at about 323 K, which was also the crossing point of their viscosity curves (Fig. III.3). In other words, the temperature dependence of the CO_2 permeabilities of the membranes was essentially the inverse of that of the viscosities of the corresponding AAILs. The results shown in Figs. III.3 and III.5 strongly suggest that the CO_2 permeability of AAIL-based membranes was mostly controlled by the viscosity of the AAIL used to make the CO_2-separation membrane. However, the CO_2 permeabilities of $[P_{4444}][Gly]$- and $[P_{4444}][mGly]$-based membranes were higher than that of the $[P_{4444}][dmGly]$-based membrane at high temperature, although the viscosities of $[P_{4444}][Gly]$ and $[P_{4444}][mGly]$ were higher than that of $[P_{4444}][dmGly]$ at these temperatures. This can probably be attributed to the low transmembrane concentration gradient of dissolved CO_2, which is the driving force of CO_2 transport, in the $[P_{4444}][dmGly]$-based membrane, because CO_2 only dissolves physically into $[P_{4444}][dmGly]$, without chemical reaction.

Table III.2 Experimental conditions for temperature-dependent gas permeation tests

Conditions		
Temperature		303 – 373 K (every 10 K)
Pressure	Feed	101.3 kPa
	Sweep	101.3 kPa
Pressure difference		0 kPa
Gas flow rate (dry base)		
Feed	CO_2	20 cm^3/min
	N_2	180 cm^3/min
Sweep	He	40 cm^3/min

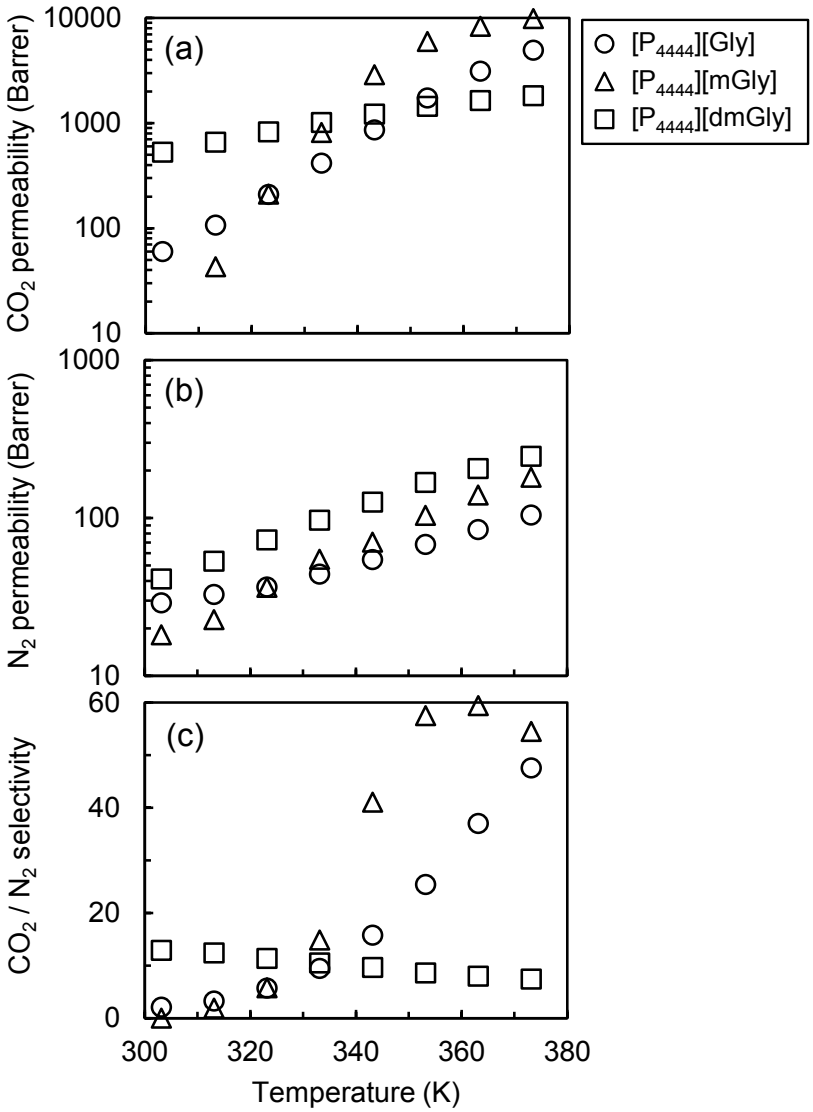

Fig. III.5 Effect of temperature on (a) CO_2 permeabilities, (b) N_2 permeabilities and (c) CO_2/N_2 selectivities of [P_{4444}][Gly]-, [P_{4444}][mGly]-, and [P_{4444}][dmGly]-based FTMs.

To confirm the CO_2 permeation mechanism of the AAIL-based membranes, the effect of CO_2 partial pressure on gas permeability and selectivity were investigated. It is well known for FTMs that CO_2 partial pressure markedly influences CO_2 permeability. The behavior reflects carrier saturation with CO_2 in FTMs. The experimental conditions and corresponding results for the investigations on CO_2 partial pressure are shown in Table III.3 and Fig. III.6. As shown in Fig. III.6, the CO_2 permeabilities of $[P_{4444}][Gly]$- and $[P_{4444}][mGly]$-based membranes decreased with increasing the CO_2 partial pressure. On the other hand, the CO_2 permeabilities of $[P_{4444}][dmGly]$-based membrane kept constant regardless of the CO_2 partial pressure. From the results, it can be said that the CO_2 permeation mechanisms were facilitated transport for $[P_{4444}][Gly]$- and $[P_{4444}][mGly]$-based membranes and solution-diffusion for $[P_{4444}][dmGly]$-based membranes.

Table III.3 Experimental conditions of gas permeation test to investigate the CO_2 partial pressure dependency

Conditions	Gases	
Temperature		373 K and 303 K (only $[P_{4444}][2\text{-}CNpyr]$-based membrane)
Pressure	Feed	101.3 kPa
	Sweep	101.3 kPa
Partial pressure difference	CO_2	2.5, 5.0, 10, 25, 50, 75 kPa
Pressure difference		0 kPa
Gas flow rate (dry base)		
Feed	Total	200 cm^3/min
	CO_2	5, 10, 20, 50, 100, 150 cm^3/min
	N_2	Balance
Sweep	He	40 cm^3/min
Water flow rate	Feed	0 cm^3/min
	Sweep	0 cm^3/min

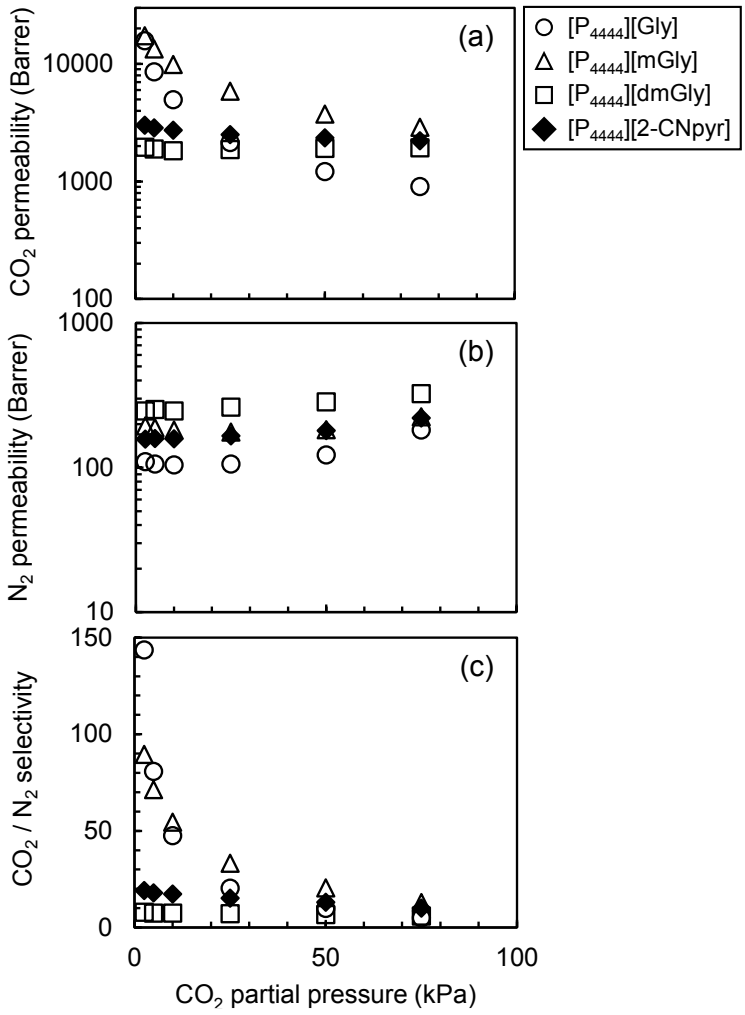

Fig. III.6 CO_2 partial pressure dependences of (a) CO_2 permeability, (b) N_2 permeability, (c) CO_2/N_2 selectivity for $[P_{4444}][Gly]$-, $[P_{4444}][mGly]$-, $[P_{4444}][dmGly]$-, and $[P_{4444}][2\text{-}CNpyr]$-based membranes at 373 K.

III.3.3 Comparison of FTMs based on $[P_{4444}][2\text{-}CNpyr]$ and $[P_{4444}][Gly]$

The results above imply that an IL that chemically reacts with CO_2 but barely forms hydrogen bonds between the CO_2 complexes would be likely to achieve higher performance. If an IL has no protons available for donation, then hydrogen bonds should be insignificant. In fact, as reported by Gurkan *et al.*,[2] an IL with 2-cyanopyrrolide (which has no proton donor) as its anion can chemically absorb CO_2 without any increase in viscosity. This led me to expect that a membrane based on such an IL would show

improved CO_2 permeability. Therefore, I synthesized [P_{4444}][2-CNpyr], made the corresponding FTM, and examined its CO_2 permeability.

First, the viscosity of [P_{4444}][2-CNpyr] after CO_2 absorption was investigated. The temperature dependences of [P_{4444}][2-CNpyr] viscosity before and after CO_2 absorption are also shown in Fig. III.3. Comparing Figs. III.3(a) and III.3(b), the viscosity of [P_{4444}][2-CNpyr] barely changes with CO_2 absorption, indicating that the CO_2 complex of [P_{4444}][2-CNpyr] does not hydrogen bond, because [P_{4444}][2-CNpyr] has no proton donor. In addition, as shown in Fig. III.3(b), the viscosity of CO_2-saturated [P_{4444}][2-CNpyr] was much lower than that of CO_2-saturated [P_{4444}][Gly]. This suggests that the diffusion coefficient of the CO_2 complex in the [P_{4444}][2-CNpyr]-based membrane would be quite high, and that the prepared membrane should show high performance, because the low viscosity of [P_{4444}][2-CNpyr] would be maintained despite CO_2 absorption.

Fig. III.7 shows the CO_2 permeability of a [P_{4444}][2-CNpyr]-based membrane. The experiment was carried out under dry conditions. As expected, the CO_2 permeability of the [P_{4444}][2-CNpyr]-based membrane was much higher than that of the [P_{4444}][Gly]-based membrane, particularly at lower temperatures. Thus, I improved the CO_2 permeability of the membrane at low temperatures under dry conditions using an aTSIL, which does not form CO_2 complexes that can hydrogen bond. However, above 363 K, the CO_2 permeability of the [P_{4444}][2-CNpyr]-based membrane was lower than that of the [P_{4444}][Gly]-based membrane. This is probably because of the lower amount of CO_2 absorbed by [P_{4444}][2-CNpyr]. To compare the CO_2 permeation mechanism through the [P_{4444}][2-CNpyr]-based membrane between high and low temperature, the effect of CO_2 partial pressure on gas permeability and selectivity were investigated. The experimental conditions and corresponding results for the investigations on CO_2 partial pressure are

shown in Table III.3 and Fig. III.6 and III.8. As shown in Fig. III.6, the CO_2 permeabilities of $[P_{4444}][2\text{-CNpyr}]$-based membrane kept constant regardless of the CO_2 partial pressure at 373 K. On the other hand, as shown in Fig. III.8, the CO_2 permeabilities decreased with increasing the CO_2 partial pressure at 303 K. From the results, it can be said that the CO_2 permeation mechanisms of $[P_{4444}][2\text{-CNpyr}]$-based membrane were facilitated transport at high temperature and solution-diffusion at low temperature.

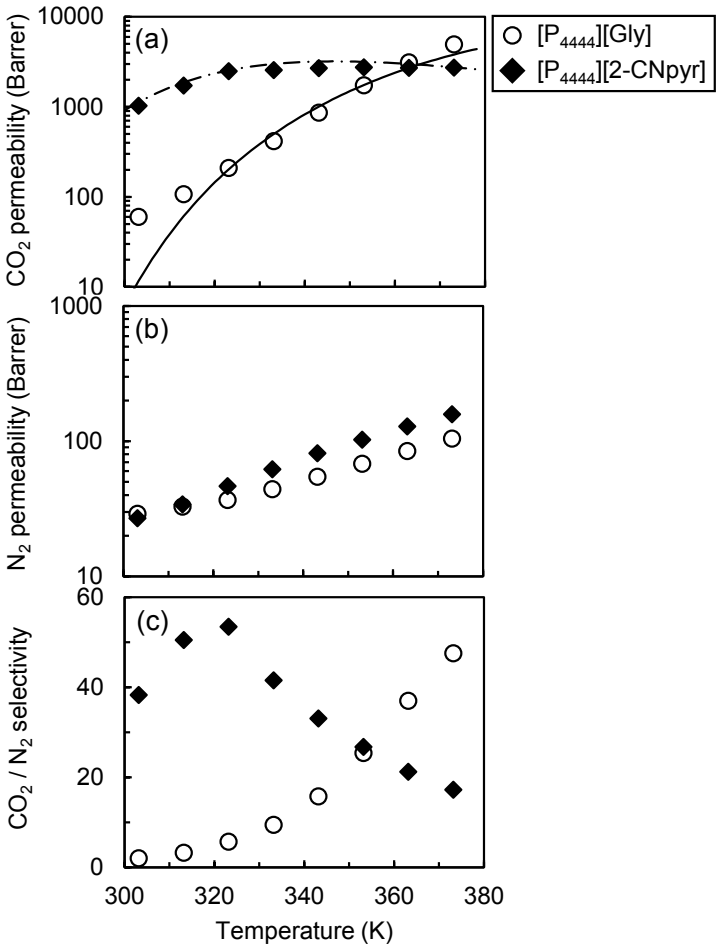

Fig. III.7 Temperature dependence of (a) CO_2 permeabilities, (b) N_2 permeabilities and (c) CO_2/N_2 selectivities of $[P_{4444}][Gly]$- and $[P_{4444}][2\text{-CNpyr}]$-based FTMs. The points and lines show the experimental data and results calculated according to the CO_2 permeation model proposed in this study, respectively.

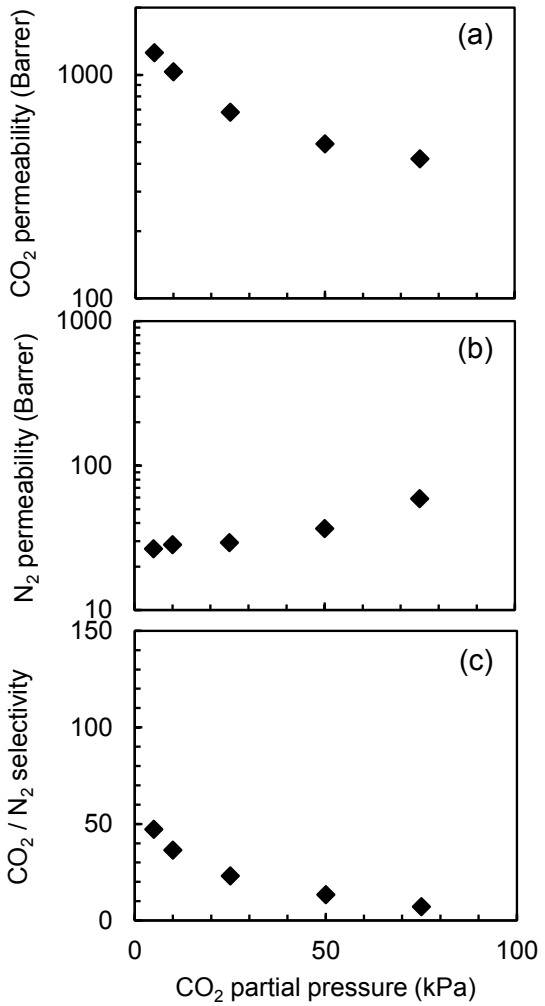

Fig. III.8 CO_2 partial pressure dependences of (a) CO_2 permeability, (b) N_2 permeability, (c) CO_2/N_2 selectivity for $[P_{4444}][2\text{-CNpyr}]$-based membrane at 303 K.

The CO_2 separation performances of the IL-based membranes prepared in this study can be compared with current ionic liquid-based membranes along with the Robeson's upper bound for dense polymer membranes.[12] The upper bound plot is shown in Fig. III.9.

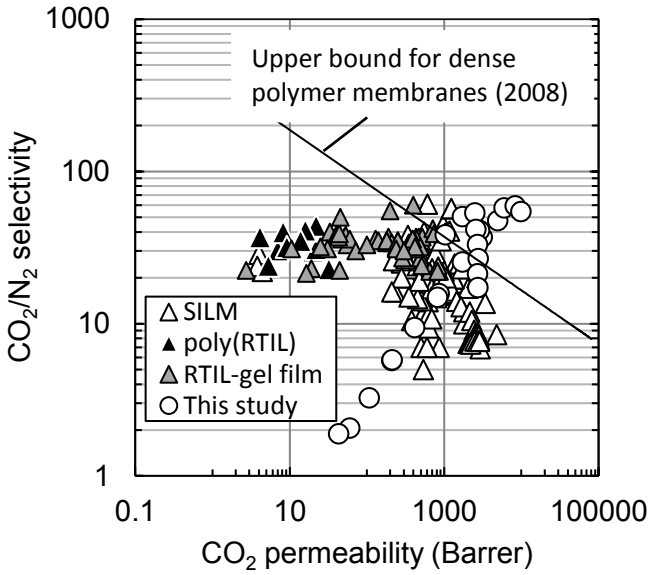

Fig. III.9 Comparison of gas separation performance for various ionic liquid-based membranes.

In general, gas permeation through a membrane can be described by the product of the concentration gradient of the gas dissolved in the membrane and the diffusion coefficient.[13] Even in the FTM, permeation can be described by multiplying the concentration gradient of the complex by the diffusion coefficient (when the reaction between CO_2 and carrier is fast and equilibrium is established in the membrane). The flux (J) and permeability (R) for CO_2 permeation in the FTM are:

$$J_{CO2} = \frac{\varepsilon}{\tau}\frac{D_{com}}{\delta}\left(C_{com,f} - C_{com,s}\right) \quad \text{(III.2)}$$

$$R_{CO2} = \frac{\varepsilon}{\tau} D_{com}\frac{C_{com,f} - C_{com,s}}{P_{com,f} - P_{com,s}} \quad \text{(III.3)}$$

where ε (-), τ (-), and δ (m) are the porosity, tortuosity, and thickness of the membrane, respectively. D_{com} (m^2/s) is the molecular diffusion coefficient of the CO_2 complex in the IL. $C_{com,f}$ (mol/m^3) and $C_{com,s}$ (mol/m^3) are the concentrations of CO_2 complex near the surface of the membrane at the feed and permeate sides, respectively. The saturation of the CO_2 permeability of the $[P_{4444}][2\text{-CNpyr}]$-based membrane shown in Fig. III.7 is a

result of the decrease in concentration of CO_2 complex with increasing temperature.

To investigate the temperature dependences further, the CO_2 absorption isotherms of $[P_{4444}][Gly]$ and $[P_{4444}][2\text{-}CNpyr]$ were measured at 313, 323, 333, and 343 K, and are shown in Fig. III.10. The amount of CO_2 absorbed by $[P_{4444}][2\text{-}CNpyr]$ was lower than that by $[P_{4444}][Gly]$ at every temperature. To evaluate the CO_2 permeability through the aTSIL-based membranes, I must estimate the amount of CO_2 absorbed in the aTSILs. Therefore, a theoretical model to describe the CO_2 absorption isotherms is required. Goodrich et al.[14] proposed a model for CO_2 absorption in an AAIL such as trihexyl(tetradecyl)phosphonium glycinate ($[P_{66614}][Gly]$). In their model, the equilibrium relationship of the complex-formation reaction between the amine group and CO_2 was described as a two-step consecutive reaction, where the CO_2 reacts with one anion to form a carbamic acid (the 1:1 complex-formation mechanism) followed by further reaction with another anion to make a carbamate (the 1:2 complex-formation mechanism). Conversely, some papers have reported that either the 1:1 or 1:2 complex-formation mechanism was dominant. However, there has been no agreement on the reaction model between CO_2 and amine-functionalized ILs.[1,15-17] In this study, I followed the two-step consecutive reaction model proposed by Goodrich *et al.*[14] and derived a theoretical CO_2 absorption model. I assumed that the physically dissolved CO_2 reacts with aTSILs near the surface of the aTSIL phase. Physical dissolution and chemical reactions between aTSILs and CO_2 would occur simultaneously. The physical dissolution, carbamic acid formation, and carbamate formation equilibria are described by eqs III.4, III.5, and III.6, respectively.

$$CO_2(g) \leftrightarrow CO_2(IL), \qquad H_{CO2} \tag{III.4}$$

$$TSIL + CO_2(IL) \leftrightarrow com1, \qquad K_{com} \tag{III.5}$$

$$com1 + TSIL \leftrightarrow com2, \qquad K_{com2} \tag{III.6}$$

where com1 and com2 denote the carbamic acid and carbamate, respectively. H_{CO2} is the Henry's constant (mol/(m^3·kPa)), and K_{com1} (mol/m^3)$^{-1}$ and K_{com2} (mol/m^3)$^{-1}$ are the equilibrium constants corresponding to eqs III.5 and III.6, respectively. These can be expressed by the following equations:

$$C_{CO2} = H_{CO2} p_{CO2} \tag{III.7}$$

$$K_{com1} = \frac{C_{com1}}{C_{TSIL} C_{CO2}} \tag{III.8}$$

$$K_{com2} = \frac{C_{com2}}{C_{com1} C_{TSIL}} \tag{III.9}$$

where C_{TSIL} (mol/m^3) is the equilibrium concentration of free aTSIL. It can be expressed with the initial aTSIL concentration in the system, $C_{TSIL,0}$, and the concentrations of com1 and com2 in the following mass balance:

$$C_{TSIL,0} = C_{TSIL} + C_{com1} + 2C_{com2} \tag{III.10}$$

In addition, the mass balance of CO_2 in the aTSIL can be written as follows:

$$C_{CO2,total} = C_{CO2} + C_{com1} + C_{com2} \tag{III.11}$$

Therefore, by substituting eqs III.7–III.9 into eq III.11, $C_{CO2,total}$ can be expressed as follows:

$$C_{CO2,total} = H_{CO2} p_{CO2} \left(1 + K_{com1} C_{TSIL} + K_{com1} K_{com2} C_{TSIL}^{\ 2}\right) \tag{III.12}$$

where C_{TSIL} is described from eqs III.7 to III.10 as follows:

$$C_{TSIL} = \frac{-\left(1 + K_{com1} H_{CO2} p_{CO2}\right) + \sqrt{\left(1 + K_{com1} H_{CO2} p_{CO2}\right)^2 + 8 K_{com1} K_{com2} H_{CO2} p_{CO2} C_{TSIL,0}}}{4 K_{com1} K_{com2} H_{CO2} p_{CO2}} \tag{III.13}$$

For the 2-cyanopyrrole aTSIL, it was reported that the complex-formation reaction

was a one-step reaction to form a 1:1 complex.[13] Therefore, it can be regarded that com2 is zero in eqs III.9-III.11. Substituting eqs III.7, III.8, and III.10 into eq III.11 gives the $C_{CO2,total}$ for [P_{4444}][2-CNpyr]:

$$C_{CO2,total} = \frac{H_{CO2} p_{CO2} \left(K_{com1} C_{TSIL,0} + K_{com1} H_{CO2} p_{CO2} + 1\right)}{K_{com1} H_{CO2} p_{CO2} + 1} \quad \text{(III.14)}$$

For [P_{4444}][Gly] and [P_{4444}][2-CNpyr], the values of H_{CO2}, K_{com1}, and K_{com2} were determined, and a good correlation was found between the lines calculated from eqs III.12 and III.14 and the experimental absorption isotherms (Figs. III.10(a) and (b) for [P_{4444}][Gly] and [P_{4444}][2-CNpyr], respectively). In this work, to predict the amount of CO_2 absorbed at various temperatures, the entropies (ΔS_{CO2}, for physical absorption, and ΔS_{com1} and ΔS_{com2}, for the com1 and com2 complex-formation reactions) and enthalpies (ΔH_{CO2}, for physical absorption, and ΔH_{com1} and ΔH_{com2} for the com1 and com2 complex-formation reactions) were determined from the following van't Hoff relationships:

$$\ln H_{CO2} = -\frac{\Delta H_{CO2}}{RT} + \frac{\Delta S_{CO2}}{R} \quad \text{(III.15)}$$

$$\ln K_{comi} = -\frac{\Delta H_{comi}}{RT} + \frac{\Delta S_{comi}}{R} \quad ; \text{i} = 1 \text{ or } 2 \quad \text{(III.16)}$$

To determine each ΔS and ΔH, H_{CO2}, K_{com1}, and K_{com2} were determined for different temperatures. The plots based on eqs III.15 and III.16 for [P_{4444}][Gly] and [P_{4444}][2-CNpyr] are linear, as shown in Figs. III.10(c) and (d), respectively. The ΔS and ΔH values were determined from the intercept and slope, respectively, and are listed in Table III.4.

Table III.4 Thermodynamic constants for CO_2 absorption by [P_{4444}][Gly] and [P_{4444}][2-CNpyr]

	dissolution		com1 formation		com2 formation	
	ΔH_{CO2} kJ/mol	ΔS_{CO2} J/(K·mol)	ΔH_{com1} kJ/mol	ΔS_{com1} J/(K·mol)	ΔH_{com2} kJ/mol	ΔS_{com2} J/(K·mol)
[P_{4444}][Gly]	-11.2	-108.5	-45.7	-61.6	-23.3	-54.1
[P_{4444}][2-CNpyr]	-10.7	-106.7	-33.8	-56.2	-	-

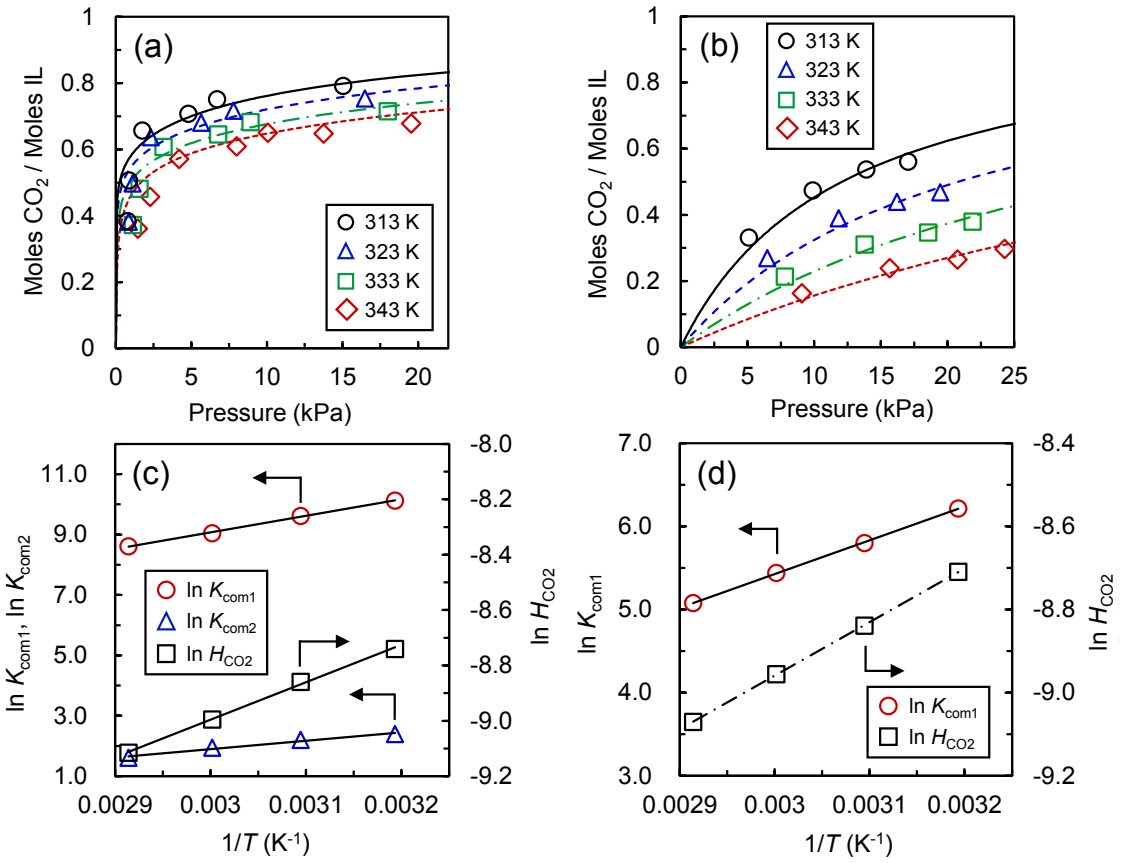

Fig. III.10 CO_2 absorption equilibrium relationships of [P_{4444}][Gly] and [P_{4444}][2-CNpyr]. Panels (a) and (b) are the absorption isotherms for CO_2 in [P_{4444}][Gly] and [P_{4444}][2-CNpyr], respectively, at various temperatures. Panel (c) is a van't Hoff plot of the Henry constant for CO_2 dissolution and the equilibrium constants of the 1:1 and 1:2 complex-formation reactions for [P_{4444}][Gly] and (d) is a van't Hoff plot of the Henry constant for CO_2 dissolution and the equilibrium constant of the 1:1 complex-formation reaction for [P_{4444}][2-CNpyr].

Using the thermodynamic parameters summarized in Table III.4, eqs III.15 and III.16, and either eq III.12 or III.14, I calculated the equilibrium amounts of CO_2 absorbed at various temperatures by [P_{4444}][Gly] and [P_{4444}][2-CNpyr] at a CO_2 partial pressure of 10 kPa; the results are graphed in Fig. III.11. The calculated amount of CO_2 absorbed, shown in Fig. III.11, corresponds to $C_{com,f}$ in eq III.2, which is the concentration of CO_2 complex near the surface of the membrane at the feed side. In my experiment, the

CO_2 partial pressure at the permeate side can be assumed to be zero because the gases permeating through the membrane were continuously swept. Thus, $C_{com,s}$ can also be considered as zero, assuming that intramembrane diffusion is the rate-determining step. Therefore, the transmembrane concentration gradient of the CO_2 complex, $\Delta C_{com} = C_{com,f} - C_{com,s}$, can simply be expressed by $C_{com,f}$; predicted values of which are shown in Fig. III.11 for various temperatures.

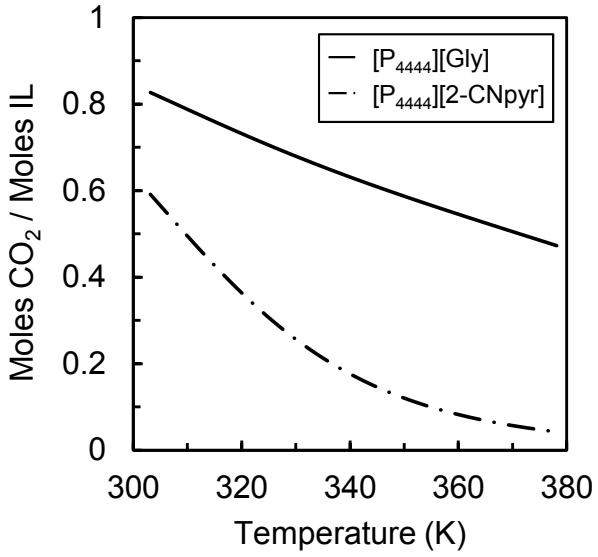

Fig. III.11 Temperature dependence of the equilibrium amount of CO_2 absorbed by $[P_{4444}][Gly]$ and $[P_{4444}][2\text{-CNpyr}]$ at P_{CO2} = 10 kPa.

Conversely, as shown in eqs III.2 and III.3, the flux and the permeability of CO_2 through the membrane are related to the product of the diffusion coefficient of CO_2 and the transmembrane concentration gradient of the CO_2 complex. Therefore, the relationship between the diffusion coefficient and temperature is also necessary to predict the CO_2 permeability through the membrane. As shown in Fig. III.3, the effect of temperature on the viscosity of CO_2-saturated ILs could be expressed by the modified VFT model. The relationship between the molecular diffusion coefficient and viscosity

can be estimated by the following Wilke-Chang equation.[18]

$$D_{\mathrm{com}} = 7.4\times10^{-12}\frac{\sqrt{\psi_{\mathrm{IL}}M_{\mathrm{IL}}}}{\eta V_{\mathrm{com}}^{\ 0.6}}T \qquad \text{(III.17)}$$

where the subscripts "IL" and "com" denote the IL used and the complex between the anion and CO_2, respectively. ψ_{IL} (-) and M_{IL} (g/mol) are the association constant and molecular weight of the ionic liquid, respectively. V_{com} (cm^3/mol) is the molecular volume of the complex between the anion and CO_2. In my calculation of the molecular diffusion coefficient, the value of ψ_{IL} was 2 (-), while V_{com} was 108 cm^3/mol or 152 cm^3/mol for $[P_{4444}][Gly]$ or $[P_{4444}][2\text{-CNpyr}]$, respectively. The calculated values of D_{com} versus T are shown in Fig. III.12.

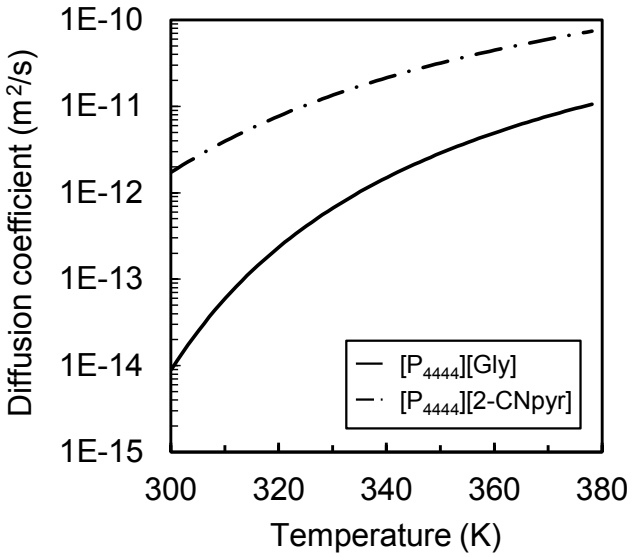

Fig. III.12 Temperature dependence of the molecular diffusion coefficients of the CO_2 complex in $[P_{4444}][Gly]$ and $[P_{4444}][2\text{-CNpyr}]$.

By substituting eq III.12 or III.14 and eq III.17 into eq III.3, the temperature dependence of the CO_2 permeability for both $[P_{4444}][Gly]$-based FTM and $[P_{4444}][2\text{-CNpyr}]$-based FTM could be calculated. The values of porosity, ε (-) and tortuosity, τ (-)

used for the calculations were 0.5 and 1.2, respectively. The calculated CO_2 permeability values for various temperatures are shown in Fig. III.7. As shown in Fig. III.7, the calculated results agreed with the experimental data for FTMs containing $[P_{4444}][Gly]$ or $[P_{4444}][2\text{-}CNpyr]$. The CO_2 permeabilities of the FTMs containing $[P_{4444}][Gly]$ and $[P_{4444}][2\text{-}CNpyr]$ are almost the same at an elevated temperature around 363 K. However, as shown in Fig. III.11, the calculated amount of CO_2 absorbed by $[P_{4444}][2\text{-}CNpyr]$ was 5–10 times smaller than that for $[P_{4444}][Gly]$. Conversely, as shown in Fig. III.4(b), the viscosity of CO_2-saturated $[P_{4444}][2\text{-}CNpyr]$ was 5–10 times smaller than that of CO_2-saturated $[P_{4444}][Gly]$. The combination of the smaller amount absorbed, and the smaller viscosity (i.e., larger diffusion coefficient), meant that the CO_2 permeability of the $[P_{4444}][2\text{-}CNpyr]$-based FTM was similar to that of the $[P_{4444}][Gly]$-based FTM. That is to say, even if only less than 10% of the total content of the aTSIL in the membrane is effectively available for CO_2 absorption, higher CO_2 permeability would be achieved for the aTSIL with lower viscosity after CO_2 absorption. This also applies to the CO_2 permeability at lower temperature. As shown in Fig. III.7, if I consider the CO_2 permeability around room temperature, the $[P_{4444}][2\text{-}CNpyr]$-based FTM shows better performance than the $[P_{4444}][Gly]$-based FTM. The higher CO_2 permeability of $[P_{4444}][2\text{-}CNpyr]$-based FTM is owing to the lower viscosity of the CO_2 complex of $[P_{4444}][2\text{-}CNpyr]$. However, the CO_2 permeability of $[P_{4444}][2\text{-}CNpyr]$-based FTM around room temperature is insufficient and further improvement is desirable. As shown in Fig. III.9, about 60% of the total $[P_{4444}][2\text{-}CNpyr]$ complexes CO_2 at 303 K. If I can increase the CO_2-absorption capacity so that all the $[P_{4444}][2\text{-}CNpyr]$ forms 1:1 complex with CO_2, which is the maximum CO_2 absorption capacity, the CO_2 permeability would be enhanced by a factor of 1.7 at the most compared with the CO_2 permeability of the present $[P_{4444}][2\text{-}CNpyr]$-

based FTM. Conversely, if I can reduce the viscosity of the aTSIL to one-tenth of the present [P_{4444}][2-CNpyr], the CO_2 permeability would be enhanced by a factor of 10. Therefore, designing an aTSIL with lower viscosity than [P_{4444}][2-CNpyr] is an effective way to improve the CO_2 permeability of the aTSIL-FTM at relatively low temperatures as well as elevated temperature.

The major factors controlling the CO_2 permeability of the aTSIL-FTMs appear to be the viscosity of the CO_2 complex and the amount of CO_2 absorbed. The most significant factor is the viscosity of the CO_2 complex. Consequently, I propose the following three design guidelines for an aTSIL that could be used to create a FTM with high CO_2 permeability over a wide temperature range: 1) the aTSIL has somewhat higher CO_2 absorption ability than that of 2-cyanopyrrolide, 2) the aTSIL does not change its viscosity with CO_2 absorption, and 3) the aTSIL has lower viscosity than that of [P_{4444}][2-CNpyr]. ILs with pyrrolide-based anions are preferred candidates. The first guideline could be met by introducing electron-donating groups to the pyrrole ring. As demonstrated in this paper, selecting an amine compound that produces a CO_2 complex without proton donors will ensure that the second guideline is met. Meeting the third guideline requires careful design of the cation component of the IL.

III.4 Conclusions

Three types of AAILs containing various glycinate anions, and an aTSIL with a chemical structure tailored for use in a CO_2-separation membrane were synthesized. The AAILs that can chemically react with CO_2, such as [P_{4444}][Gly] and [P_{4444}][mGly], showed drastically increased viscosity with CO_2 absorption. FT-IR implied that this increase in the viscosity was because of formation of hydrogen bonds between the CO_2 complexes.

The temperature dependence of the CO_2 permeability of the AAIL-FTMs was the opposite of that of the viscosity of the AAILs after CO_2 absorption. The CO_2 permeability at a low temperature under dry conditions was improved by changing the IL to $[P_{4444}][2\text{-CNpyr}]$, which forms CO_2 complexes that do not readily hydrogen bond. This means that decreasing the viscosity of the CO_2 complex can significantly increase the CO_2 permeability of AAIL-FTMs. Furthermore, the results calculated using my proposed CO_2-permeation model explained well the temperature dependences of the CO_2 permeabilities for FTMs containing $[P_{4444}][Gly]$ or $[P_{4444}][2\text{-CNpyr}]$. I recommended the following to fabricate a FTM with high CO_2 permeability over a wide temperature range: the aTSIL has moderately high CO_2 absorption ability, and has lower viscosity that does not change with CO_2 absorption.

References

1. J. Zhang, S. Zhang, K. Dong, Y. Zhang, Y. Shen and X. Lv, *Chem. Eur. J.*, 2006, **12**, 4021.
2. B. Gurkan, B. F. Goodrich, E. M. Mindrup, L. E. Ficke, M. Massel, S. Seo, T. P. Senftle, H. Wu, M. F. Glaser, J. K. Shah, E. J. Maginn, J. F. Brennecke and W. F. Schneider, *J. Phys. Chem. Lett.*, 2010, **1**, 3494.
3. B. F. Goodrich, J. C. Fuente, B. E. Gurkan, D. J. Zadigian, E. A. Price, Y. Huang and J. F. Brennecke, *Ind. Eng. Chem. Res.*, 2011, **50**, 111.
4. G. S. Fulcher, *Am. Ceram. Soc. J.*, 1925, **8**, 339.
5. H. Rodriguez and J. F. Brennecke, *J. Chem. Eng. Data*, 2006, **51**, 2145.
6. J. Benitez-Garcia, G. Ruiz-Ibanez, H. A. Al-Ghawas and O. C. Sandall, *Chem. Eng. Sci.*, 1991, **46**, 2927.
7. K. E. Gutowski and E. J. Maginn, *J. Am.Chem. Soc.*, 2008, **130**, 14690.
8. H. Gao, Y. Zhang, H. Wang, J. Liu and J. Chen, *J. Phys. Chem. A*, 2010, **114**, 10243.
9. R. Tamaki, K. Naka and Y. Chujo, *Polym. J.*, 1998, **30**, 60.
10. J. Joseph and E. D. Jemmis, *J. Am. Chem. Soc.*, 2007, **129**, 4620.
11. K. S. Rutkowski, W. A. Herrebout, S. M. Melikova, B. J. van der Veken and A. A. Koll, *Chem. Phys.*, 2008, **354**, 71.
12. P. Scovazzo, *J. Membr. Sci.*, 2009, **343**, 199.
13. W. S. W. Ho and K. K. Sirkar, Eds. *Membrane Handbook*; Kluwer Academic Publishers: Boston, 1992.
14. B. F. Goodrich, J. C. Fuente, B. E. Gurkan, Z. K. Lopez, E. A. Price, Y. Huang and J. F. Brennecke, *J. Phys. Chem. B*, 2011, **115**, 9140.
15. B. E. Gurkan, J. C. Fuente, E. M. Mindrup, L. E. Ficke, B. F. Goodrich, E. A. Price,

W. F. Schneider and J. F. Brennecke, *J. Am. Chem. Soc.*, 2010, **132**, 2116.

16. L. M. Galan Sanchez, G. W. Meindersma and A. B. Haan, *Chem. Eng. J.*, 2011, **166**, 1104.
17. J. Ma, Z. Zhou, F. Zhang, C. Fang, Y. Wu, Z. Zhang and A. Li, *Environ. Sci. Technol.*, 2011, **45**, 10627.
18. C. R. Wilke, P. Chang, *Am. Inst. Chem. Eng. J.*, 1955, **1**, 264.

Chapter IV

Improvements in the CO_2 permeation selectivities of amino acid ionic liquid-based facilitated transport membranes by controlling their gas absorption properties

IV.1 Introduction

In this study, I have attempted to improve the CO_2 selectivity of FTMs by reducing their N_2 permeabilities. Two methods are available for decreasing the N_2 permeability of FTMs to improve their CO_2 selectivity, including (1) a reduction in the N_2 amount in a solvent of the FTM; and (2) reducing the diffusion coefficient of the FTM. The second of these two methods is the least preferable because its implementation would also lead to a decrease in the CO_2 permeability. In contrast, the amounts of CO_2 and N_2 absorbed in the solvent in the FTM can only be independently varied in the FTM. CO_2 is absorbed in the solvent in the FTM via a chemical reaction, and the amount of CO_2 absorbed is mostly dependent on the amount of CO_2 carrier included in the FTM. In other words, CO_2 absorption is not so influenced by a molecular structure of the solvent. In contrast, N_2 is absorbed in the solvent without a chemical reaction. The amount of N_2 absorbed in the solvent depends on a molecular structure of the solvent, such as molar volume.

The N_2 absorption properties of RTILs have recently been investigated by many researchers.[1-4] Camper *et al.*[1] proposed that the amount of N_2 absorbed in a RTIL is strongly dependent on its molar volume. This molar volume of RTILs can be easily

changed by changing the size of their cation or anion. Therefore, if an RTIL was used as the solvent for a FTM, the N_2 permeability of the membrane could be reduced by controlling the cation and/or anion sizes of the RTILs.

In this chapter, I have proposed a methodology for improvement of the CO_2 selectivity of AAIL-FTMs by reducing N_2 permeability. AAILs with a series of cation size were synthesized and the effects of the cation size on the amount of gas absorption in the AAIL and gas permeability of the AAIL-FTM were systematically investigated both experimentally and theoretically.

IV.2 Experimental

IV.2.1 Materials

Tetrabutylphosphonium hydroxide ($[P_{4444}][OH]$, 40 wt% in water), trihexyl(tetradecyl)phosphonium bromide ($[P_{66614}][Br]$, ≧ 95%), acetonitrile (> 99.9%) and anion exchange resin (OH type) were purchased from Sigma Aldrich (St. Louis, MO, USA). Glycine was purchased from Tokyo Chemical Industry Co. (Tokyo, Japan). Methanol (99.8%) was purchased from Wako Pure Chemicals Industry Ltd. (Osaka, Japan). Triethyl(pentyl)phosphonium bromide ($[P_{2225}][Br]$, 50 wt% in water) was purchased from Nippon Chemical Industrial Co., Ltd. (Tokyo, Japan). All of the reagents were used as received. CO_2 and N_2 gases of 99.9% purity were used for the gas permeation tests. A hydrophilic polytetrafluoroethylene (PTFE) microporous membrane with an average pore size of 0.1 μm and a film thickness of 37.5 μm was purchased from Sumitomo Electric Industries Ltd. (Osaka, Japan) and used as a support for the AAIL-based membranes.

Tetrabutylphosphonium glycinate ($[P_{4444}][Gly]$) was synthesized according to a

previously reported neutralization procedure.[5] An aqueous solution of $[P_{4444}][OH]$ (50.0 g) was added to an aqueous solution of glycine containing 1.05 molar equivalent of the appropriate glycine to prepare the $[P_{4444}][AA]$ salts. The product was collected by filtration and dried in vacuo for 12 h at 313 K. The material was then added to a mixture of acetonitrile/methanol to allow for any unreacted glycine to be removed by sequential crystallization and filtration, and the resulting filtrate was collected and evaporated to remove solvents. The reaction ratio of $[P_{4444}][Gly]$ was 99.9%.

Trihexyl(tetradecyl)phosphonium glycinate ($[P_{66614}][Gly]$) was synthesized using a previously reported anion exchange and neutralization procedure.[6] $[P_{66614}][Br]$ (40.0 g) was dissolved in methanol (80.0 g), and the resulting solution was treated with a basic anion exchange resin (142.0 g) to form $[P_{66614}][OH]$. The mixture was then filtered before being treated with the appropriate glycine (1.1 molar equivalents) and stirred for 24 h at room temperature. Cold acetonitrile was added to the mixture to precipitate any unreacted glycine, which was removed by filtration, and the resulting filtrate was evaporated to remove solvents. The reaction ratio of $[P_{66614}][Gly]$ was 91.2%.

Triethyl(pentyl)phosphonium glycinate ($[P_{2225}][Gly]$) was synthesized by similar procedure to $[P_{66614}][Gly]$ except the source solution. A commercial aqueous solution of $[P_{2225}][Br]$ (50.0 g) was used as the source solution and treated with a basic anion exchange resin (190.0 g). The reaction ratio of $[P_{2225}][Gly]$ was 91.9%.

The structures of the resulting $[P_{66614}][Gly]$, $[P_{4444}][Gly]$ and $[P_{2225}][Gly]$ products were confirmed by ^{1}H-NMR and FT-IR analyses, as shown in the appendix. The chemical structures of the different AAILs are shown in Fig. IV.1.

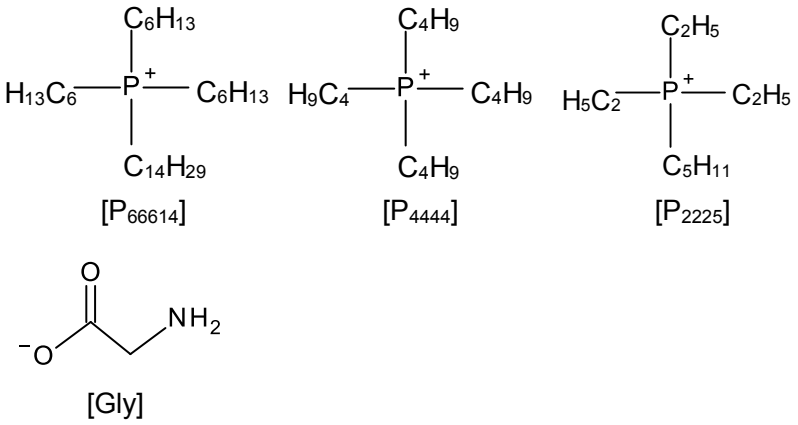

Fig. IV.1 Chemical structures of the AAILs used in this study ([Px][Gly]; X=tetrabutyl, trihexyl(tetradexyl) and triethyl(pentyl)).

IV.2.2 Measurement of AAILs properties

The viscosities of the AAILs were measured before and after CO_2 absorption with an ElectroMagnetically Spinning Sphere Viscometer (EMS-1000W, Kyoto Electronics Manufacturing Co., Ltd., Kyoto, Japan), using a metallic sphere at a constant rotating speed of 1000 rpm. The CO_2 saturated AAILs for the viscosity measurements were prepared by bubbling CO_2 through the AAILs at room temperature. The viscosities were measured at temperatures in the range of 303 to 373 K.

The densities of the AAILs were measured using a density/specific gravity meter (DA-650, Kyoto Electronics Manufacturing Co., Ltd.). The densities were measured at temperatures in the range of 303 to 363 K.

IV.2.3 Absorption of N_2 in AAILs

The apparatus used to measure N_2 absorption isotherms is illustrated in Fig. IV.2. The temperature of the system was controlled by a water bath (T-105B, Thomas Kagaku Co., Ltd., Tokyo, Japan) at constant temperature with an accuracy of ±0.1 K. The equipment consisted of stainless steel tubes, and reference and sample cells. The

volumes of both the reference and sample cells were determined by the following experiments. The reference cell was pressurized to the desired pressure with N_2 and the sample cell was evacuated by closing the valve separating the two cells. The experiments basically consisted of measuring the pressure drop when the valve was opened. The measurements were conducted with and without a stainless ball, which acted as a known volume, placed in the sample cell. Using the measurements from these experiments, it was possible to generate two equations with two unknowns:

$$P_1 V_{\text{ref}} = P_2 \left(V_{\text{ref}} + V_{\text{sam}} \right) \tag{IV.1}$$

$$P_1' V_{\text{ref}} = P_2' \left\{ V_{\text{ref}} + \left(V_{\text{sam}} - V_{\text{ball}} \right) \right\} \tag{IV.2}$$

where P_1 (or P_1') (Pa) and P_2 (or P_2') (Pa) are the pressure before and after opening the valve. V_{ref} (m^3) and V_{sam} (m^3) are the reference and sample cell volumes. V_{ball} (m^3) is a known volume of the stainless ball. These equations were subsequently solved for both the reference and sample cell volumes of the apparatus.

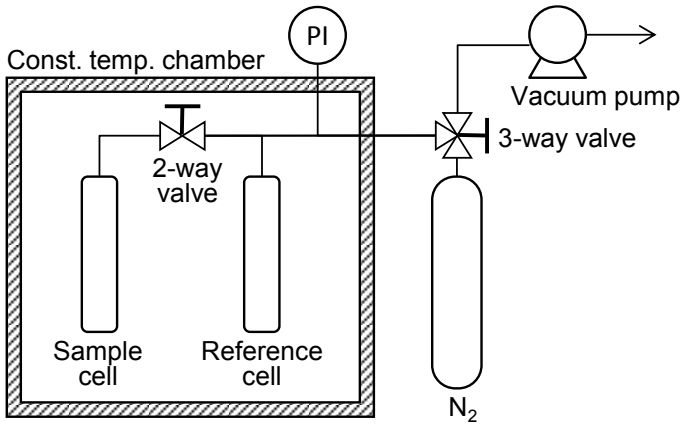

Fig. IV.2 Schematic diagram of the apparatus used for the gas absorption tests.

To begin the absorption experiments, AAIL (5.0 g) was added to the sample cell, and the experiments were conducted according to the following procedure. The reference and

sample cells were evacuated and the valve separating the two cells was then closed. The reference cell was pressurized with a known amount of N_2 and the temperature was kept constant. After the N_2 was charged, the stirrer was turned on and the AAIL was stirred at a constant rate throughout the experiment. The N_2 absorption was started when the valve connecting the two cells was opened. Once the valve was opened, the N_2 in the reference cell was transferred into the sample cell, bringing the N_2 into contact with the AAIL. This mixing led to a drop in the pressure which was caused by the absorption of N_2 in the AAIL. The pressure was measured by a digital pressure gauge (MODEL AM-756 digital manometer, GE Sensing & Inspection Technologies CO., Ltd., Tokyo, Japan). The pressure was monitored until it became constant for more than 1 h, with equilibration generally being achieved within 30 min. After the system reached equilibrium, the final pressure was measured and the amount of N_2 absorption was determined from the observed pressure change.

IV.2.4 Preparation of AAIL-FTMs

The AAIL-based membranes were prepared as follows. A hydrophilic PTFE microporous membrane was immersed into the synthesized AAILs (i.e., $[P_{66614}][Gly]$, $[P_{4444}][Gly]$ and $[P_{2225}][Gly]$) and immediately decompressed for 1 h to allow for the air in the PTFE membrane to be completely exchanged with ionic liquid. The ionic liquid impregnated in the PTFE membrane was taken out and the excess ionic liquid was wiped from the surface.

IV.2.5 Gas permeability measurements

A diagram of the experimental setup is shown in Fig. IV.3. Gas permeability

measurements were carried out with a similar procedure described in II.2.3, except that no water was added.

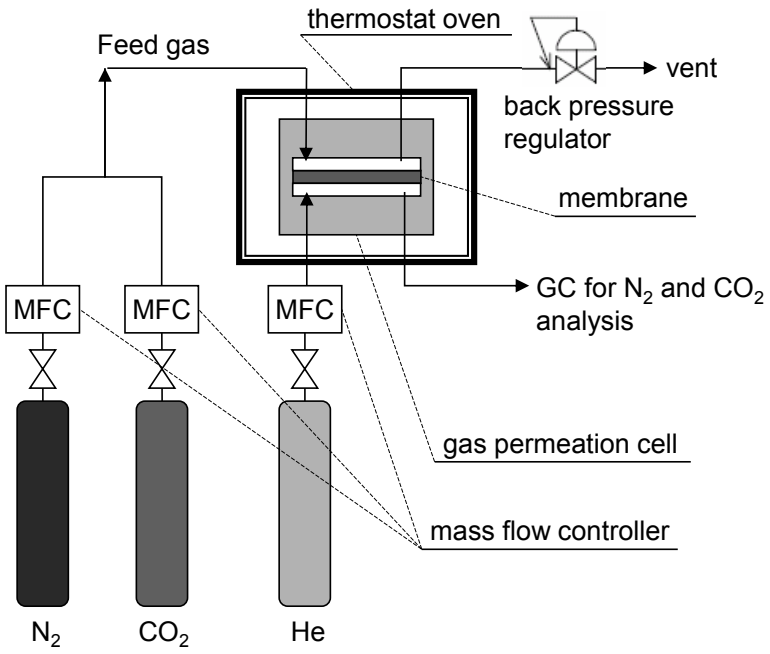

Fig. IV.3 Schematic diagram of the apparatus used for the gas permeation tests.

IV.3 Results and discussion

IV.3.1 Viscosity measurement of AAILs

In solution-diffusion model, gas permeation through a membrane can be described by multiplying the concentration gradient of the gas in the membrane by the diffusion coefficient.[7] The flux of gas permeation, J, can then be expressed as follows:

$$J = \frac{\varepsilon}{\tau}\frac{D}{\delta}\left(C_{\mathrm{f}} - C_{\mathrm{p}}\right) \qquad \text{(IV.3)}$$

where ε (-), τ (-) and δ (m) are the porosity, tortuosity and thickness of the support membrane, respectively, D (m^2/s) is the molecular diffusion coefficient of the solute in the membrane, and C_f (mol/m^3) and C_p (mol/m^3) are the concentrations of the gas near the surface of the membrane at the feed and permeate sides, respectively. In this study, I

wanted to focus on the effect of the amount of gas absorption. Thus, it was necessary to select a preferred set of experimental conditions which would have a relatively small effect on the diffusion coefficient of the gas permeability of the AAIL-FTM. It has been reported that the viscosities of AAILs increase significantly with CO_2 absorption.[7] It is also well known that the diffusion coefficient is strongly dependent on the viscosity. The viscosities of the AAILs synthesized in this study were therefore measured and investigated before and after CO_2 absorption to establish experimental conditions that were capable of revealing small differences in the viscosities among three synthesized AAILs. Fig. IV.4 shows the effect of temperature on the viscosities of the AAILs before and after CO_2 absorption. It has been reported that the viscosities of ILs can be adequately described by the modified Vogel-Fulcher-Tammann (VFT) equation:[8,9]

$$\eta = AT^{0.5} \exp\left(\frac{k}{T - T_0}\right) \tag{IV.4}$$

where A, k and T_0 are fitting parameters and T (K) is the temperature. The fitting parameters were obtained for three AAILs based on the data shown in Fig. IV.4 and are listed in Table IV.1. Within a wide temperature range, the modified VFT equation can be used to estimate not only the viscosities of the pure ILs but also the viscosities of two-component liquids, regardless of their composition. The predicted viscosities obtained using the modified VFT equation are shown in Fig. IV.4 together with the experimental data. As shown in Fig. IV.4, the viscosities of $[P_{66614}][Gly]$, $[P_{4444}][Gly]$ and $[P_{2225}][Gly]$ increased with CO_2 absorption, and these increases were attributed to the formation of hydrogen bonding networks between the AAIL-CO_2 complexes.[10,11] Following the CO_2 absorption, the viscosities of the different AAILs were reduced significantly with increasing temperature because the hydrogen bonding networks were being broken by

heating. It is also noteworthy that the viscosities of the AAILs after CO_2 absorption showed almost the same value at 373 K, which indicated that the effect of the diffusion coefficient on the gas permeability was relatively small for three AAILs at 373 K. Based on these results, my work towards improving the N_2 barrier properties by controlling the amount of N_2 absorbed in the AAILs was investigated at 373 K.

Table IV.1 Fitting parameters for the VFT equation

	Before CO_2 absorption			After CO_2 absorption		
	A	k	T_0	A	k	T_0
$[P_{66614}][Gly]$	0.0245	725	200	0.00550	800	248
$[P_{4444}][Gly]$	0.0450	600	203	0.135	530	252
$[P_{2225}][Gly]$	0.0120	680	208	0.0170	647	216

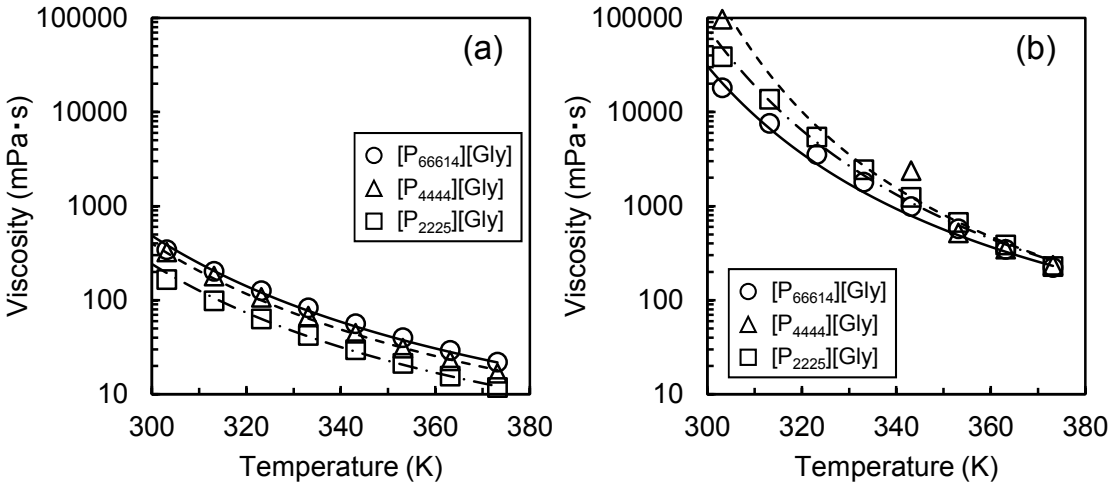

Fig. IV.4 Effect of temperature on the viscosity of the AAILs. (a) before CO_2 absorption and (b) after CO_2 absorption. The points and lines show experimental data and results calculated according to the modified VFT model, respectively.

IV.3.2 Density and molar volume of AAILs

It has been reported that the amount of N_2 absorbed in an RTIL is predominantly dependent on its molar volume if the temperature is kept constant.[1-4] It is therefore necessary to measure the molar volume at 373 K to predict the amount of N_2 absorbed

at 373 K. The molar volume can be calculated by multiplying the molecular weight by the reciprocal of density. In this study, the densities of the AAILs at 373 K were estimated using the linear relationship between the density and the temperature. Fig. IV.5(a) shows the effect of temperature on the density. As shown in Fig. IV.5(a), the densities of the AAILs were of the order $[P_{2225}][Gly]$ > $[P_{4444}][Gly]$ > $[P_{66614}][Gly]$ at all of the temperatures studied. The densities of the AAILs became higher as the size of the cation decreased. This result is reasonable because the amount of molecule per unit volume increases as the size of the molecule decreases. From the results shown in Fig. IV.5(a), I was able to establish a linear relationship between the density of the AAILs and the temperature. The molar volumes of the AAILs were then calculated using the molar weight and density values. Fig. IV.5(b) shows the effect of temperature on the molar volume of the AAILs. As shown in Fig. IV.5(b), the molar volumes were of the order $[P_{66614}][Gly]$ > $[P_{4444}][Gly]$ > $[P_{2225}][Gly]$ at all of the temperatures studied, including 373 K, and it was assumed that the order of the N_2 absorption amounts would be $[P_{66614}][Gly]$ > $[P_{4444}][Gly]$ > $[P_{2225}][Gly]$ at 373 K.

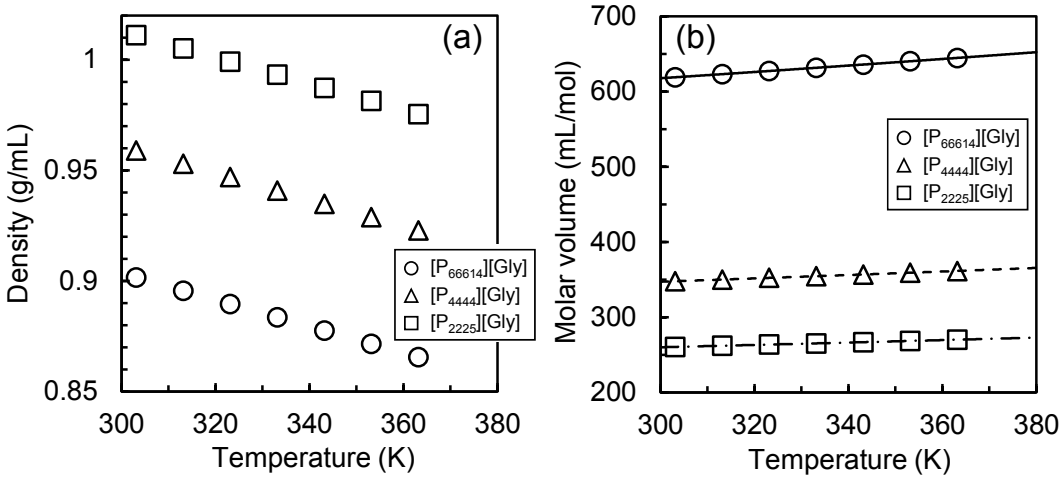

Fig. IV.5 Effect of temperature on the properties of the AAILs. (a) density and (b) molar volume.

Based on these results, it appears plausible to suggest that the molar volume of an AAIL can be successfully controlled according to the size of the cation used in the AAIL. It therefore follows naturally that the N_2 absorption amount could also be controlled in the same way.

IV.3.3 N_2 absorption test

Fig. IV.6 shows the experimental for the N_2 absorption isotherms of the different AAILs. In general, the physical dissolution can be described according to the following equation:

$$C_{N2} = H_{N2} p_{N2} \quad \text{(IV.5)}$$

where H_{N2} is the Henry's constant (mol/(m^3·kPa)), and C_{N2} and p_{N2} are the concentration of N_2 in the AAIL and the partial pressure of N_2, respectively. The H_{N2} values were determined for each AAIL to demonstrate a good correlation between the lines calculated according to eq IV.5 and the experimental absorption isotherms. The calculated Henry's constants are listed in Table IV.2. As shown in Fig. IV.6, the AAILs absorbed different amount of N_2 in the order $[P_{66614}][Gly] > [P_{4444}][Gly] > [P_{2225}][Gly]$ at every temperature. This order was the same as that obtained for the molar volumes of the AAILs, as shown in Fig. IV.5(b). In this study, it was not possible to conduct an N_2 absorption test at 373 K because of the limitations of my experimental apparatus, and the N_2 absorption isotherm at 373 K was therefore theoretically predicted. To predict the amount of N_2 physically absorbed at 373 K, the thermodynamic constants of the entropy for the physical absorption (ΔS_{N2}) and the enthalpy for the physical absorption (ΔH_{N2}) were determined using the following van't Hoff relationships:

$$\ln H_{N2} = -\frac{\Delta H_{N2}}{RT} + \frac{\Delta S_{N2}}{R} \quad \text{(IV.6)}$$

Table IV.2 Henry's constant for the AAILs

	Henry's constant (mol/(m^3 kPa))				
	313 K	323 K	333 K	343 K	373 K
[P_{66614}][Gly]	0.31	0.25	0.20	0.17	0.10[a]
[P_{4444}][Gly]	0.29	0.22	0.17	0.14	0.074[a]
[P_{2225}][Gly]	0.27	0.20	0.15	0.12	0.060[a]

[a]Caluculated parameters from eq IV.6.

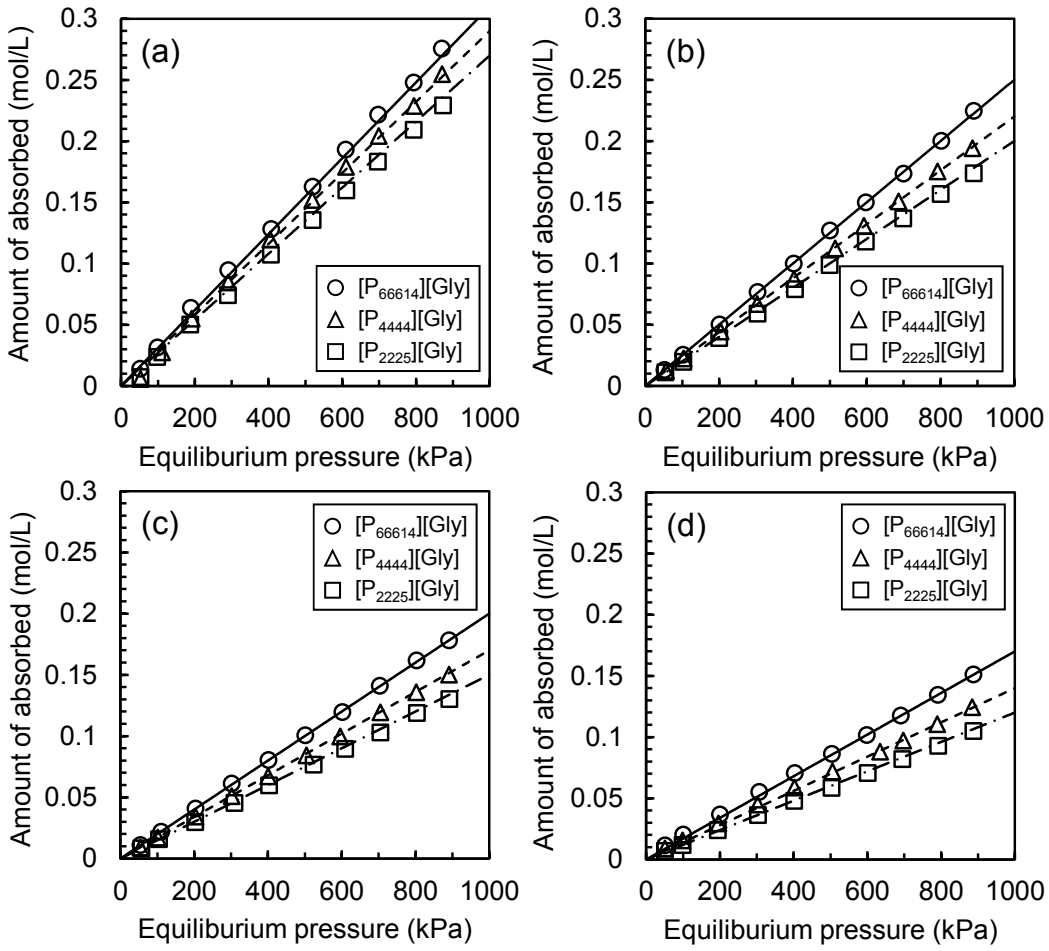

Fig. IV.6 N_2 absorption isotherms of the AAILs at (a) 313 K, (b) 323 K, (c) 333 K and (d) 343 K.

The plots based on eq IV.6 for $[P_{66614}][Gly]$, $[P_{4444}][Gly]$ and $[P_{2225}][Gly]$ are shown in Fig. IV.7. As shown in Fig. IV.7, all of these plots showed linear relationships. The ΔS_{N2} and ΔH_{N2} values were determined from the intercept and slope, respectively, and are listed in Table IV.3. The N_2 absorption isotherms of $[P_{66614}][Gly]$, $[P_{4444}][Gly]$ and $[P_{2225}][Gly]$ at 373 K were calculated using the thermodynamic parameters summarized in Table IV.3. In addition, the calculated Henry's constants for all three of the AAILs at 373 K are shown in Table IV.2. Fig. IV.8 shows the calculated isotherms for all three of the AAILs at 373 K. As was the case at the other temperatures, the amount of N_2 absorbed in the AAILs also decreased as the size of the cation decreased at 373 K. From these results, it is plausible to suggest that the N_2 absorption amount can be successfully controlled by controlling the size of the cation. It was envisaged that a CO_2 separation membrane with high N_2 barrier properties could be fabricated using an AAIL with a small cation such as $[P_{2225}][Gly]$.

Table IV.3 Thermodynamic constants the N_2 absorption into the AAILs

	ΔH_{N2} kJ/mol	ΔS_{N2} J/(K·mol)
$[P_{66614}][Gly]$	-18.1	-125.0
$[P_{4444}][Gly]$	-21.8	-137.6
$[P_{2225}][Gly]$	-24.3	-146.1

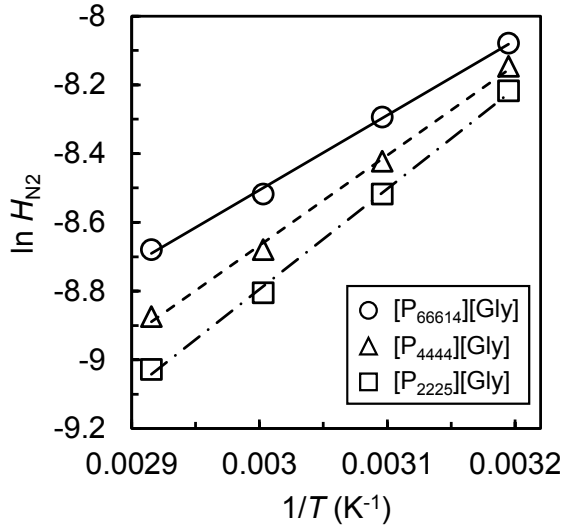

Fig. IV.7 van't Hoff plots of the Henry constants for N_2 absorption.

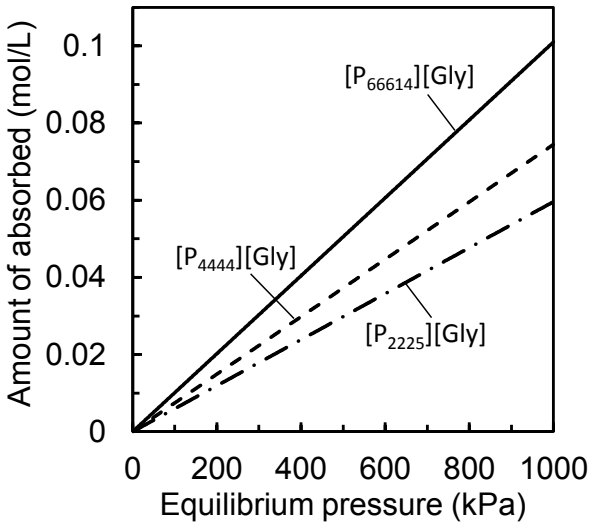

Fig. IV.8 Calculated N_2 absorption isotherms of the AAILs at 373 K.

IV.3.4 Gas permeation properties of AAIL-FTMs

The effect of CO_2 partial pressure on the gas permeation properties of the AAIL-FTMs was investigated. The experimental conditions for the gas permeation test are shown in Table IV.4 and the corresponding results are shown in Fig. IV.9. As shown in Fig. IV.9(a), the order of the N_2 permeability for the tree AAIL-FTMs was [P_{66614}][Gly] > [P_{4444}][Gly] > [P_{2225}][Gly]. This order was identical to that observed for the amount of N_2 absorbed in

each AAIL (Fig. IV.8). In contrast, as shown in Fig. IV.9(b), the CO_2 permeabilities for the three AAIL-FTMs were of the order $[P_{2225}][Gly] > [P_{4444}][Gly] > [P_{66614}][Gly]$. This increase in the CO_2 permeability with decreasing cation size in the AAILs was attributed to increases in the CO_2 absorption amount, because this amount would increase as the number of amine groups per unit volume increased. Consequently, the $[P_{2225}][Gly]$-FTM showed better CO_2/N_2 selectivity, as shown in Fig. IV.9(c).

Table IV.4 Experimental conditions for the gas permeation test

Conditions		
Temperature		373 K
Pressure	Feed	101.3 kPa
	Sweep	101.3 kPa
Partial pressure difference	CO_2	2.5, 5.0, 10, 25, 35, 50 kPa
Pressure difference		0 kPa
Gas flow rate (dry base)		
Feed	Total	200 mL/min
	CO_2	5, 10, 20, 50, 70, 100 mL/min
	N_2	balance
Sweep	He	40 mL/min

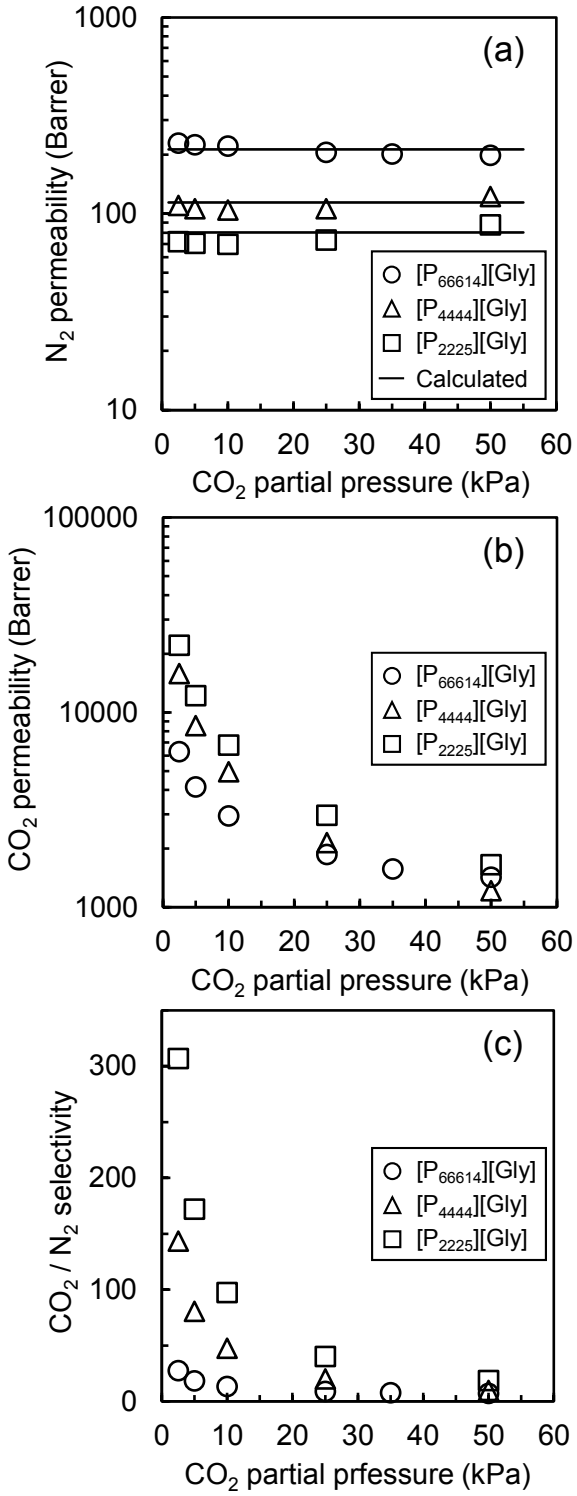

Fig. IV.9 Effect of CO_2 partial pressure on gas permeation properties of the AAIL-FTMs. (a) N_2 permeability, (b) CO_2 permeability and (c) CO_2/N_2 selectivity.

Instead of focusing on the dependence of the CO_2 partial pressure on the CO_2 permeability, the CO_2 permeability of the AAIL-FTMs underwent significant reduction with increasing CO_2 partial pressure. This trend was attributed to the carrier in the FTM becoming saturated with CO_2.[12] In contrast, no discernible changes were noted in the N_2 permeability of the AAIL-FTMs following increases in the CO_2 partial pressure because the permeation mechanism is the solution-diffusion mechanism. In conclusion, it was suggested that the CO_2 separation performances of the AAIL-FTMs could be improved by controlling the molar volumes of the AAILs, which contribute to both the N_2 barrier property and CO_2 permeability of the FTMs.

Finally, the N_2 permeation behaviors through all three of the AAIL-FTMs were investigated using theoretical considerations. According to eq IV.3, the diffusion coefficient and transmembrane concentration gradient would be required to predict the N_2 permeability through the membrane. The concentration of dissolved N_2 can be determined using Henry's law (eq IV.5). Therefore, by substituting eq IV.5 into eq IV.3, the flux and permeability of N_2 through an AAIL-FTM can be expressed according to eqs IV.7 and IV.8, respectively.

$$J_{N2} = \frac{\varepsilon}{\tau}\frac{D}{\delta}H_{N2}\left(p_{N2,f} - p_{N2,p}\right) \quad \text{(IV.7)}$$

$$R_{N2} = D_{eff}H_{N2} \quad \text{(IV.8)}$$

where the subscripts "f" and "p" denote the feed and permeate sides, respectively, and D_{eff} is the effective diffusion coefficient, which takes into account the effects of porosity and tortuosity.

$$D_{eff} = \frac{\varepsilon}{\tau}D \quad \text{(IV.9)}$$

A general form for the effective diffusion coefficients of the RTILs has been given as

follows:[13-16]

$$D_{\mathrm{eff}} = B\frac{V_{\mathrm{IL}}^{\mathrm{a}}}{\eta_{\mathrm{IL}}^{\mathrm{b}} V_{\mathrm{I}}^{\mathrm{c}}} \qquad \text{(IV.10)}$$

where B, a, b and c are the fitting parameters, η_{IL} is the viscosity of the RTIL, V_{IL} is the molar volume of the IL (cm^3/mol), and V_{I} is the molar volume of the gas dissolved in the IL. By substituting eq IV.10 into eq IV.8, it was possible to calculate the N_2 permeabilities for different CO_2 partial pressures when B, a, b and c are obtained. The calculated lines are shown in Fig. IV.9(a). In the calculation, the values of B, a, b and c were 2.3×10^{-9} (-), 0.5, 0.5 and 0.5 for all AAILs, respectively. V_{I} was 31.2 cm^3/mol as the molar volume of N_2. The calculated effective diffusion coefficients are listed in Table IV.5. The difference of the effective diffusion coefficients was caused from the differences of the molar volume and the viscosity of the AAILs with different cation size. However, it can be considered that the effect of viscosity was much smaller than the effect of molar volume under the experimental condition of the gas permeation tests because the viscosities of each AAIL at 373 K were almost same as shown in Fig. IV.4. Therefore, the molar volume of the AAILs mainly affected the difference of the effective diffusion coefficient among the AAIL-FTMs. As shown in Fig. IV.9(a), the calculated results for the N_2 permeabilities of the AAIL-FTMs were in good agreement with the experimental data. The ratio of Henry's constants and that of diffusion coefficients for each AAIL were calculated to confirm each contribution of solubility change and diffusivity change to the N_2 permeability change. The calculated ratio of the Henry's constants and the effective diffusion coefficients for each AAIL were listed in Table IV.6. As shown in Table IV.6, the decrease of the solubility with the decrease of AAIL size was almost same as that of effective diffusion coefficient. This means that the decrease of both solubility and effective diffusion coefficient with

decreasing the AAIL size brought about the N_2 permeability decrease. Concerning them, the decrease of the diffusion coefficient is not preferable for improvement of the selectivity because the decrease of the N_2 diffusion coefficient also cause the decrease of the CO_2 diffusion coefficient. In contrast, the N_2 solubility of the AAILs can be separately controlled from their CO_2 solubility because N_2 is dissolved physically, while CO_2 is dissolved chemically. With this in mind, the decrease of the N_2 permeability with controlling the gas solubility which easily controlled by designing the cation size in the AAILs is preferable methodology for improving the selectivity of the AAIL-FTMs.

Table IV.5 Calculated effective diffusion coefficients for the AAILs at 373 K

	$[P_{66614}][Gly]$	$[P_{4444}][Gly]$	$[P_{2225}][Gly]$
D_{eff} (m^2/s)	7.04×10^{-10}	5.12×10^{-10}	4.50×10^{-10}

Table IV.6 Calculated ratio of Henry's constants and effective diffusion coefficients for the AAILs

	i=$[P_{2225}][Gly]$ j=$[P_{4444}][Gly]$	i=$[P_{2225}][Gly]$ j=$[P_{66614}][Gly]$
$H_{N2,i}/H_{N2,j}$	0.81	0.60
$D_{eff,i}/D_{eff,j}$	0.88	0.64

IV.4 Conclusions

AAILs with containing a series of cations of different sizes were synthesized and the effects of the cation size on their gas absorption and gas permeation properties were systematically investigated. Their physical properties, including viscosity, density and molar volume were also determined. The use of an AAIL with a small cation could lead to a reduction in the N_2 permeability, whereas the CO_2 permeability kept at high value. Among three AAILs used in this study, $[P_{2225}][Gly]$-FTM showed the best N_2 barrier property and CO_2/N_2 selectivity at high temperature. The amount of N_2 absorbed in

[P_{2225}][Gly] was remarkably small compared to the other AAILs investigated in this study because the [P_{2225}][Gly] had the smallest molar volume. In addition, the effective N_2 diffusivity was also smallest in the case of [P_{2225}][Gly]. These two factors brought about the low N_2 permeability and high CO_2 selectivity. As mentioned above, I showed that the AAIL-FTMs with both high N_2 barrier and high CO_2 permeation properties could be fabricated by decreasing the size of the cation in the AAILs.

References

1. D. Camper, J. Bara, C. Koval and R. Noble, *Ind. Eng. Chem. Res.*, 2006, **45**, 6279.
2. D. Camper, C. Becker, C. Koval and R. Noble, *Ind. Eng. Chem. Res.*, 2005, **44**, 1928.
3. D. Camper, P. Scovazzo, C. Koval and R. Noble, *Ind. Eng. Chem. Res.*, 2004, **43**, 3049.
4. P. Scovazzo, D. Camper, J. Kieft, J. Poshusta, C. Koval and R. Noble, *Ind. Eng. Chem. Res.*, 2004, **43**, 6855.
5. J. Zhang, S. Zhang, K. Dong, Y. Zhang, Y. Shen and X. Lv, *Chem. Eur. J.*, 2006, **12**, 4021.
6. B. F. Goodrich, J. C. de la Fuente, B. E. Gurkan, Z. K. Lopez, E. A. Price, Y. Huang and J. F. Brennecke, *J. Phys. Chem. B*, 2011, **115**, 9140.
7. W. S. W. Ho and K. K. Sirkar, Eds. Membrane Handbook; Kluwer Academic Publishers: Boston, 1992.
8. B. F. Goodrich, J. C. de la Fuente, B. E. Gurkan, D. J. Zadigian, E. A. Price, Y. Huang and J. F. Brennecke, *Ind. Eng. Chem. Res.*, 2011, **50**, 111.
9. H. Rodriguez and J. F. Brennecke, *J. Chem. Eng. Data*, 2006, **51**, 2145.
10. K. E. Gutowski and E. J. Maginn, *J. Am.Chem. Soc.*, 2008, **130**, 14690.
11. H. Gao, Y. Zhang, H. Wang, J. Liu and J. Chen, *J. Phys. Chem. A*, 2010, **114**, 10243.
12. M. Teramoto, K. Nakai, N. Ohnishi, Q. Huang, T. Watari and H. Matsuyama, *Ind. Eng. Chem. Res.*, 1996, **35**, 538.
13. D. Morgan, L. Ferguson and P. Scovazzo, *Ind. Eng. Chem. Res.*, 2005, **44**, 4815.
14. L. Ferguson and P. Scovazzo, *Ind. Eng. Chem. Res.*, 2007, **46**, 1369.
15. P. Scovazzo, *J. Membr. Sci.*, 2009, **343**, 199.
16. S. M. Mahurin, J. S. Lee, G. A. Baker, H. Luo and S. Dai, *J. Membr. Sci.*, 2010, **353**, 177.

Chapter V

An amino acid ionic liquid-based facilitated transport membrane with excellent CO_2 permeation properties under humid and/or elevated temperature conditions

V.1 Introduction

The viscosity of AAILs is drastically increased through the formation of an intermolecular hydrogen bond network among AAIL-CO_2 complexes with CO_2 absorption.[1,2] Therefore, the viscosity of the AAILs was the dominant factor for CO_2 permeation properties of AAIL-FTMs under dry conditions at room temperature. On the other hand, the intermolecular hydrogen bonding interaction becomes weak under humid and/or elevated temperature conditions because the hydrogen bonds are broken by heat or by forming other hydrogen bonds between water and the complex through addition of water. Therefore, under humid and/or elevated temperature conditions, the marked increase in viscosity of the AAIL-CO_2 complex can be prevented. Thus, it is presumed that the diffusion coefficient of the complex in AAIL-FTMs is increased under humid and/or elevated temperature conditions. In other words, the gas absorption properties of AAILs would play a dominant role in the CO_2 separation properties under these conditions. In this study, I designed a novel AAIL with suitable gas absorption properties of high CO_2 but low N_2 absorbability.

I attempted to introduce an amino group into both the cation and anion of the AAIL

as a strategy to increase the number of amino groups per ionic liquid molecule. It was reported that the amount of CO_2 absorbed in dual-AAILs, which have two amino groups, the cation and the anion, was increased two-fold over that in an AAIL with only one amino group present in the anion.[3] On the other hand, regarding the N_2 absorbability, it has been demonstrated that the amount of gas physically absorbed in RTILs strongly depends on their free volume or molar volume. [4-6] In chapter IV, the amount of N_2 absorbed in AAILs was successfully controlled by controlling the cation size, which directly affects molar volume. I therefore attempted to decrease the amount of N_2 absorbed in AAILs by combining cation and anion groups of smaller size.

I synthesized a novel dual-AAIL, constructed using small cation and anion groups on the basis of the above guideline and investigated the gas absorption and permeation properties of an AAIL-FTM.

V.2 Experimental

V.2.1 Materials

Glycinate was chosen as the anion part of the AAILs because it is the smallest amino acid. Tetrabutylammonium glycinate ($[N_{4444}][Gly]$) was chosen and synthesized as a basic AAIL, tetramethylammonium glycinate ($[N_{1111}][Gly]$) as a small AAIL with low N_2 absorbability, and 1,1,1-trimethylhydrazinium glycinate ($[aN_{111}][Gly]$) as a small dual-AAIL with high CO_2 and low N_2 absorbabilities. The chemical structures of these AAILs are shown in Fig. V.1.

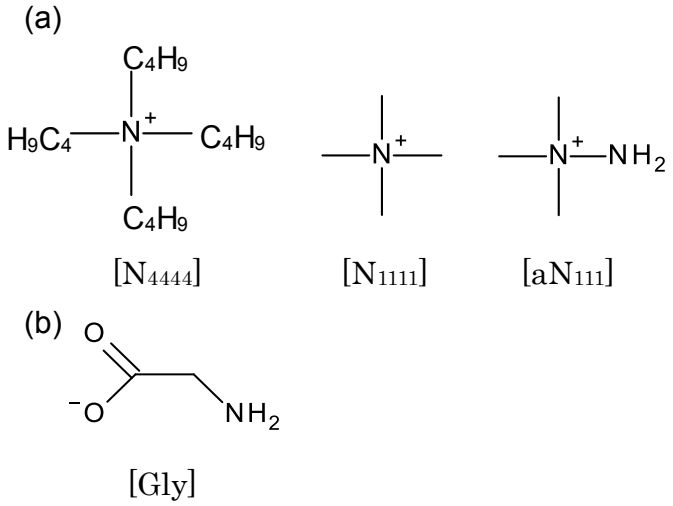

Fig. V.1 Chemical structure of the AAILs used in this study. (a) Cation (tetrabutylammonium [N_{4444}], tetramethylammonium [N_{1111}], and 1,1,1-trimethylhydrazinium [aN_{111}]). (b) anion (glycinate).

Tetrabutylammonium hydroxide ([N_{4444}][OH], 40 wt% in water), tetramethylammonium hydroxide ([N_{1111}][OH], 25 wt% in water), 1,1,1-trimethylhydrazinium iodide ([aN_{111}][I], ≧ 97%), acetonitrile (> 99.9%) and anion exchange resin (OH type) were purchased from Sigma Aldrich (St. Louis, MO, USA). Glycine was purchased from Tokyo Chemical Industry Co. (Tokyo, Japan). Methanol (99.8%) and ethanol (99.5%) were purchased from Wako Pure Chemicals Industry Ltd. (Osaka, Japan). All reagents were used as received.

[N_{4444}][Gly] was synthesized according to a previously described neutralization procedure.[7] An aqueous solution of [N_{4444}][OH] (100.0 g) was added dropwise to an aqueous solution of glycine containing 1.05 molar equivalent of the appropriate glycine. The mixture was stirred for 24 h at room temperature. The water was then evaporated at 333 K. The residual liquid was combined with 100 mL of ethanol to allow for unreacted glycine to be removed by sequential crystallization and filtration, and the resulting filtrate was collected and evaporated to remove solvents. The reaction ratio of

$[N_{4444}][Gly]$ was 95.4%.

$[N_{1111}][Gly]$ was synthesized using a similar procedure to that used for $[N_{4444}][Gly]$ except for the source solution, for which a commercial aqueous solution of $[N_{1111}][OH]$ (80.0 g) was used. The reaction ratio of $[N_{1111}][Gly]$ was 99.9%.

$[aN_{111}][Gly]$ was synthesized using a previously described anion exchange and neutralization procedure.[8] $[aN_{111}][I]$ (16.2 g) was dissolved in Milli-Q water (200.0 g), and the resulting solution was treated with a basic anion exchange resin (121.8 g) to form $[aN_{111}][OH]$. The mixture was then filtered, before reaction with the appropriate glycine (1.05 molar equivalents), with which it was stirred for 24 h at room temperature. Water was then evaporated at 333 K and ethanol was added to the solution to precipitate unreacted glycine, which was removed by filtration, and the resulting filtrate was evaporated to remove solvents. The reaction ratio of $[aN_{111}][Gly]$ was 98.2%.

The structures of the resulting $[N_{4444}][Gly]$, $[N_{1111}][Gly]$ and $[aN_{111}][Gly]$ products were confirmed by ^{1}H-NMR (Bruker Advance 500, Bruker BioSpin, Kanagawa, Japan) and FT-IR (ALPHA FT-IR Spectrometer, Bruker Optics, Tokyo, Japan) analyses, as shown in the appendix. It was confirmed that the target peaks were observed for all AAILs, and thus $[N_{4444}][Gly]$, $[N_{1111}][Gly]$ and $[aN_{111}][Gly]$ were successfully synthesized. CO_2 and N_2 gases of 99.9% purity were used for gas permeation tests. A hydrophilic polytetrafluoroethylene (PTFE) microporous membrane with an average pore size of 0.1 μm and a film thickness of 37.5 μm was purchased from Sumitomo Electric Industries Ltd. (Osaka, Japan) and used as a support for the AAIL-based membranes.

V.2.2 Physicochemical properties of the AAILs

V.2.2.1 Density and viscosity measurements

Samples for density and viscosity measurements were prepared by drying the synthesized AAILs for 12 h at 343 K. The densities of the AAILs were measured using a density/specific gravity meter (DA-650, Kyoto Electronics Manufacturing Co., Ltd., Kyoto, Japan). The densities were measured at temperatures in the range 303 to 363 K. The viscosities of the AAILs were measured with an electro-magnetically spinning sphere viscometer (EMS-1000W, Kyoto Electronics Manufacturing Co., Ltd.), using a metallic sphere at a constant rotation speed of 1000 rpm. The measurements were carried out at temperatures in the range 303 to 373 K. Water content in AAILs was controlled by adding Milli-Q water to the dried AAILs.

V.2.2.2 Gas absorption

The apparatus used to measure the gas absorption isotherms is illustrated in Fig. V.2. The volumes of both the reference and sample cells were determined by a similar procedure described in IV.2.3.

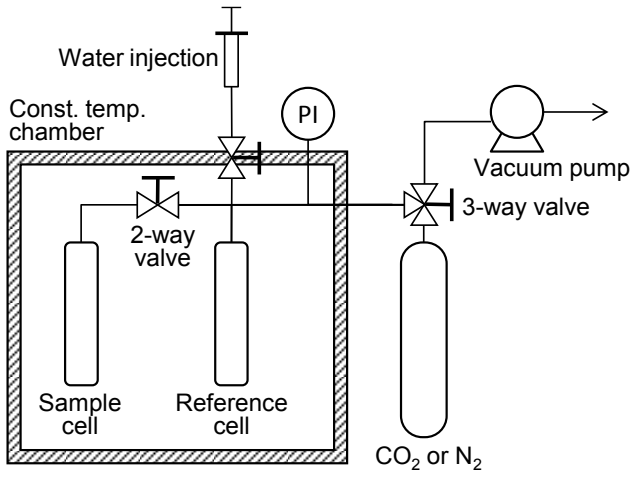

Fig. V.2 Schematic of the apparatus used for gas absorption tests.

In this study, CO_2 and N_2 absorption tests were carried out under different conditions. Each test was conducted according to the following procedures.

CO_2 absorption test

The CO_2 absorption test was carried out at 343 K at 100% relative humidity (RH). Initially, AAIL (1.5 g) was added to the sample cell. The reference and sample cells were evacuated and the valve separating the two cells was then closed. A known amount of water which was enough to achieve 100% RH was added into the reference cell. The pressure was monitored until it became constant. I confirmed that the pressure increase was equal to the saturated water vapor pressure. The valve separating the two cells was then opened to allow contact between the water vapor and the AAIL. After the AAIL fully absorbed the water vapor, the valve was closed. The remained amount of water in the reference cell was calculated from the amount of added water and the saturated water vapor pressure, and the actual volume of the cells excluding water was recalculated. The reference cell was then pressurized to the desired pressure by introducing CO_2 from a CO_2 cylinder. After the CO_2 was charged, the stirrer was turned on and the AAIL was stirred at a constant rate throughout the experiment. The CO_2 absorption was started when the valve connecting the two cells was opened. Once the valve was opened, the CO_2 in the reference cell was transferred into the sample cell, bringing the CO_2 into contact with the AAIL. This mixing led to a drop in the pressure, caused by the absorption of CO_2 in the AAIL. The pressure was monitored until it remained constant for more than 1 h, with equilibration generally being achieved within 3 h. After the system reached equilibrium, the final pressure was measured and the amount of CO_2 absorption was determined from the observed pressure change.

N_2 absorption test

In this study, I focused on the CO_2 permeation properties of AAIL-FTMs under high temperature and/or humid conditions. Therefore, it was preferable to measure the gas absorption properties under humid conditions. However, under humid conditions, water and nitrogen co-existed in the system. Because the N_2 absorbability in the AAILs was quite small, the pressure drop by N_2 absorption would also be very small. Therefore, the relative pressure fluctuation caused by water evaporation and condensation cannot be neglected. That is, I cannot measure the amount of N_2 absorbed correctly under humid conditions. Hence, the N_2 absorption tests were carried out under dry conditions.

The N_2 absorption test was carried out at 343 K. AAIL (7.0 g) was added to the sample cell and the N_2 absorption test was carried out by similar procedure to that used for the CO_2 absorption test, except that no water was added.

V.2.3 Molecular dynamics simulation for evaluation of absorbability under humid conditions

Owing to the experimental limitation described above, I could not investigate the N_2 absorbability of each AAIL under humid conditions. However, it is important to know the N_2 absorbability under humid conditions to evaluate my proposed guideline for the structure of AAILs with superior N_2 barrier properties. It was reported that the amount of N_2 physically absorbed in RTILs correlated well with the free volume of ionic liquids.[5,6] Thus, I calculated the fractional free volume (FFV) based on a molecular dynamics (MD) simulation and investigated the amount of N_2 absorbed in AAILs under humid conditions. The relationship between the amount of N_2 absorbed and the FFV of the AAILs was presumed by using the relationship under dry conditions.

The structures were built using Material Studio version 6.1.[9] Quantum chemistry calculations were performed with the Gaussian 09 program.[10] Vibrational analysis on all calculated structures revealed a lack of imaginary frequencies, confirming the presence of true minima on the potential energy surface. The electrostatic potential surface was generated by the Merz-Kollman method at a HF/6-31G(d) level of theory as usual for Amber-like force fields, followed by a multi-configurationally two-stage relaxed electrostatic potential (RESP) fitting. The software code R. E. D. IV was used for the RESP fitting.[11] I used the Amber force field to determine the intra- and intermolecular force constants for the cation and anion groups of the ionic liquids.[12]

Simulation Details

I generated initial configurations of the ionic liquid with the Packmol program.[13] All simulations reported here were performed with the Gromacs 4.5 simulation program.[14] The simulated systems are composed of 384 ion pairs. Under humid conditions, I added 384 water molecules to the ionic mixture using Packmol. The configurations were then optimized by Gromacs, using an energy minimization routine. The MD simulations were performed at 300 K for the neat ionic liquid, to reproduce the experimental density and validate the model. Production simulations were carried out using the isothermal-isobaric (NPT) ensemble for 25 ns. Temperature and pressure were controlled with coupling times of 5 and 1 ps, using the velocity-scaling[15] and Berendsen methods,[16] respectively. Equations of motion were integrated with the leapfrog algorithm with a time step of 2.0 fs. The full electrostatic interactions were accounted for using the particle mesh Ewald (PME) summation.[17] Coulomb and van der Waals cutoffs of 1.2 nm were used. Periodic boundary conditions in all directions were used to mimic the bulk behavior. Bond lengths were constrained with the LINCS algorithm. After the simulation, the

physical properties were characterized using Gromacs analysis tools, and the structures were visualized by visual molecular dynamics (VMD).[18] A similar procedure was followed for ionic liquid-water mixtures.

Binding Energy Calculation

To investigate the strength of interaction between cation-anion groups in the gas and solvent phases, density functional theory (DFT) calculations were carried out. DFT calculation was carried out using B3LYP functional and 6-31+G(d,p) basis set, using the Gaussian 09 program.[10] Different possible orientations of cation-anion group interactions were considered and the minimum energy conformation was selected for single-point energy calculation. Frequency calculation was performed to make sure ionic pairs were indeed at minimum energy. Starting with an optimized geometry, single-point energy calculations were carried out using 6-311+G(3df,2p) basis set and M05-2X functional routine. Previous studies demonstrated that the DFT method is suitable for calculation of ILs using the method described above.[19,20] Solvent effects were mimicked using the SMD solvation model.[21]

Free Volume Calculation

The equilibrated structures obtained after molecular dynamics were selected for FFV calculations. The FFV was calculated using the following method:[22]

$$FFV = \frac{V_{\mathrm{m}} - V_{\mathrm{vdW}}}{V_{\mathrm{m}}} \qquad \text{(V.1)}$$

where V_{vdW} is the van der Waals volume of the molecule and V_{m} is the molar volume. The van der Waals radii due to the Bondi were used for this calculation and were calculated using the Material Studio program.[9,23]

V.2.4 Gas permeability measurement

Gas permeability measurements were carried out with a similar procedure described in II.2.3.

V.3 Results and discussion

V.3.1 Density and molar volume of AAILs

It was reported that the amount of N_2 absorbed in an RTIL depends strongly on the molar volume as well as the free volume of the RTIL if the temperature is kept constant.[4-6] I indicated that the molar volume of ionic liquids can be decreased by decreasing their cation group size in chapter IV. To evaluate the effect of molecular size of the AAILs on their N_2 absorbability, their molar volumes were investigated in this study. The molar volume can be calculated by multiplying the molecular weight by the reciprocal of density. In this study, the densities of the AAILs at various temperatures were measured and their molar volumes were calculated from the densities. Fig. V.3(a) shows the effect of temperature on the density of the AAILs. As shown in Fig. V.3(a), the densities of the AAILs indicated a linear relationship to temperature and were in the order: $[aN_{111}][Gly]$ > $[N_{1111}][Gly]$ > $[N_{4444}][Gly]$. The molar volumes of the AAILs are shown in Fig. V.3(b). $[N_{4444}][Gly]$, with a large cation group, showed the highest molar volume at all temperatures. The molar volumes of $[N_{1111}][Gly]$ and $[aN_{111}][Gly]$ showed similar values because the sizes of $[N_{1111}]^+$ and $[aN_{111}]^+$ are similar. From the results, it can be predicted that the amount of N_2 absorbed in the AAILs synthesized in this study would be in the order $[N_{4444}][Gly]$ > $[N_{1111}][Gly]$ ≒ $[aN_{111}][Gly]$ at all temperatures.

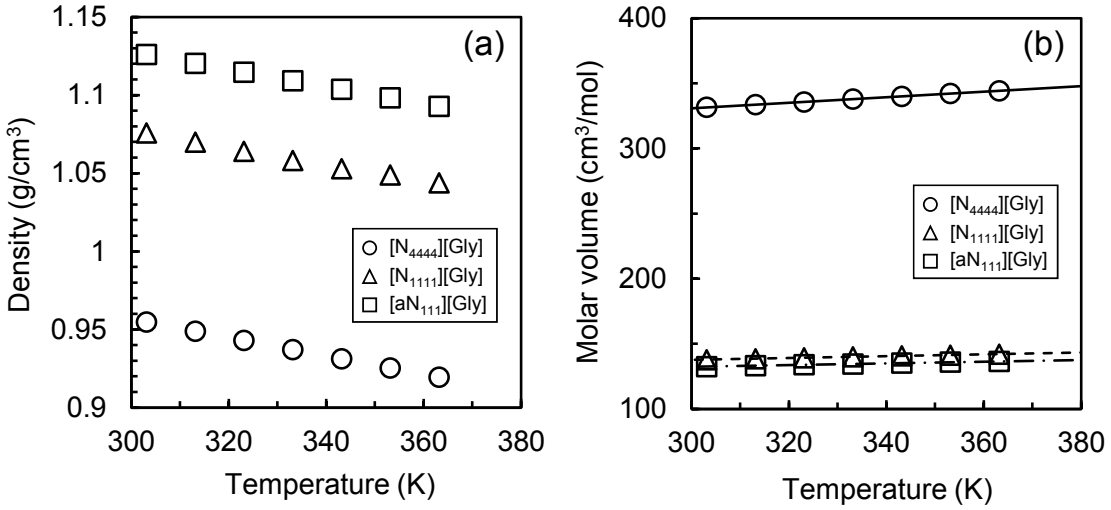

Fig. V.3 Effect of temperature on the density and molar volume of the AAILs synthesized in this study. (a) density and (b) molar volume.

V.3.2 Gas absorption test

V.3.2.1 N_2 absorption

In the case of applying the AAILs to CO_2 separation membranes, CO_2, N_2 and water vapor exist around the AAILs. It is therefore reasonable to measure the amount of gas absorbed by the AAILs under such conditions, to enable discussion of the CO_2 and N_2 permeation properties of the AAIL-FTMs from the gas absorbabilities. However, I cannot accurately measure the amount of N_2 absorbed in the AAILs under such conditions, as described above. In this study, therefore, I calculated the FFV of the AAILs by MD simulation and discussed the amount of N_2 absorption in light of the computational results.

The FFVs and densities of the AAILs calculated from MD simulation are listed in Table V.1. First, to check the validity of the computational results, the densities before CO_2 absorption calculated from the simulation under dry conditions were compared with the experimental results. Comparing the calculated results shown in Table V.1 and the

experimental results shown in Fig. V.3(a), the densities of the neat AAILs at 300 K showed almost the same values. Thus, it was confirmed that the computational results calculated in this study were reasonable.

Table V.1 FFV and density of AAILs from molecular dynamics simulation at 300 K

	Before CO_2 absorption under dry condition		After CO_2 absorption under humid condition	
	FFV (SD)	ρ (g/cm^3)	FFV (SD)	ρ (g/cm^3)
[N_{4444}][Gly]	0.19 (0.0058)	0.905	0.16 (0.012)	1.022
[N_{1111}][Gly]	0.12 (0.010)	1.058	0.050 (0.0058)	1.311
[aN_{111}][Gly]	0.12 (0.010)	1.123	0.070 (0.010)	1.403

SD means standard deviation.

Subsequently, I considered the FFVs of the AAILs shown in Table V.1. Regarding the FFV before CO_2 absorption under dry conditions, the FFV of [N_{4444}][Gly] was the highest value, about 1.6 times larger than the FFVs of [N_{1111}][Gly] and [aN_{111}][Gly]. In the case of [N_{1111}][Gly] and [aN_{111}][Gly], the FFVs were closely similar. To investigate the relationship between the FFV and the amount of N_2 absorbed, the computational results of the FFVs were compared with the experimentally obtained amounts of N_2 absored. It was reported that FFVs showed a good relationship with the molar amount of N_2 absorbed per unit volume of the RTILs.[5] Therefore, I described the units of the amount of N_2 absorbed in the AAILs as "mol-N_2 / dm^3-AAIL". As shown in Fig. V.4(a), the amount of N_2 absorption by [N_{4444}][Gly] was the highest, at about 1.9 times higher than the other AAILs. The amounts absorbed by [N_{1111}][Gly] and [aN_{111}][Gly] were closely similar. These tendencies were almost the same as those of the FFV under dry conditions. From these results, it was confirmed that the amounts of N_2 absorbed were strongly correlated with the FFV of the AAILs. The trend of N_2 absorption amounts could be qualitatively predicted from the FFVs of the AAILs. The correlation between FFV and amounts of N_2

absorbed would also be applicable under humid conditions. The amounts of N_2 absorbed in $[N_{4444}][Gly]$, $[N_{1111}][Gly]$ and $[aN_{111}][Gly]$ after CO_2 absorption under humid conditions were successively investigated on the basis of the FFVs under dry conditions. As shown in Table V.1, the FFVs of AAIL-CO_2 complexes formed after CO_2 absorption under humid conditions were in the order $[N_{4444}][Gly] > [aN_{111}][Gly] \fallingdotseq [N_{1111}][Gly]$. Hence, the amounts of N_2 absorbed under humid conditions would be in the order $[N_{4444}][Gly] > [aN_{111}][Gly] \fallingdotseq [N_{1111}][Gly]$. From these results, it was confirmed that the amount of N_2 absorbed can be successfully reduced by decreasing the size of the AAILs.

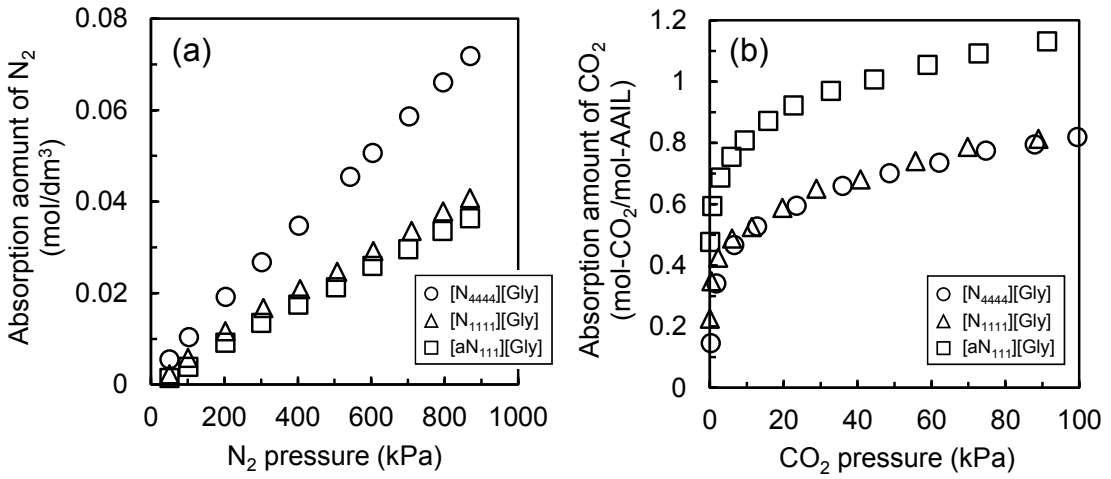

Fig. V.4 Gas absorption isotherms of $[N_{4444}][Gly]$, $[N_{1111}][Gly]$ and $[aN_{111}][Gly]$ at 343 K. (a) N_2 absorption under dry conditions and (b) CO_2 absorption under humid conditions at 100% RH.

V.3.2.2 CO_2 absorption

Fig. V.4(b) shows the amount of CO_2 absorbed in $[N_{4444}][Gly]$, $[N_{1111}][Gly]$ and $[aN_{111}][Gly]$ at 100% RH. In this study, I attempted to increase the amount of CO_2 absorbed in AAILs by increasing the number of amino groups per AAIL molecule. The CO_2 is absorbed by AAILs through chemical reaction with an amino group in the AAILs.

This means that the molar amount of CO_2 absorbed would be proportional to the number of amino groups in the AAILs. In short, the effect of an increase in amino groups on the amount of CO_2 absorbed can be easily evaluated by measuring the molar amount of CO_2 absorbed per unit mole of the AAILs. Therefore, I described the units for the amount of CO_2 absorbed in the AAILs as "mol-CO_2 / mol-AAIL".

As shown in Fig. V.4(b), [aN_{111}][Gly] exhibited the highest CO_2 absorption, while [N_{4444}][Gly] and [N_{1111}][Gly] absorptions were approximately equal to one another. In addition, the amount of CO_2 absorbed in [aN_{111}][Gly] was twice that in [N_{4444}][Gly] and [N_{1111}][Gly]. [aN_{111}][Gly] is a "dual-AAIL", which has two amino groups per molecule, compared with one the amine group of [N_{4444}][Gly] and [N_{1111}][Gly]. Thus, the amount of CO_2 absorbed by [aN_{111}][Gly] was twice that adsorbed by [N_{4444}][Gly] and [N_{1111}][Gly]. Based on the above results, [aN_{111}][Gly] has suitable gas absorption properties for application as a carrier in a CO_2 separation membrane, and it can be expected that [aN_{111}][Gly]-FTM would show excellent CO_2 permeation properties.

V.3.3 Gas permeation properties of AAIL-FTMs

Gas permeation performances of AAIL-FTMs were tested under humid conditions and/or elevated temperature. Under such conditions, the hydrogen bond networks between AAIL-CO_2 complexes are only loosely formed i.e. the viscosities of the AAILs after CO_2 absorption were relatively low. In other words, the gas absorption properties under such conditions play the key role in determining the CO_2 separation properties of the AAIL-FTMs. Therefore, the CO_2 separation performance of the FTMs containing the AAILs, which were designed to possess desirable gas absorption properties, would be maximized under humid and/or elevated temperature conditions. I investigated the

dependence of AAIL-FTM gas permeation properties on temperature under humid conditions and on RH at high temperature. These experimental conditions are shown in Tables V.2 and V.3 and the corresponding results are shown in Figs. V.5 and V.6.

Table V.2 Experimental conditions for temperature-dependent gas permeation tests

Conditions		
Temperature		303 - 373 K (every 10 K)
Pressure	Feed	101.3 kPa
	Sweep	101.3 kPa
Partial pressure difference	CO_2	1 kPa
Pressure difference		0 kPa
Gas flow rate (dry base)		
Feed	Total	200 cm^3/min
	CO_2	2 cm^3/min
	N_2	Balance
Sweep	He	40 cm^3/min
Relative humidity		50%

Table V.3 Experimental conditions for RH-dependent gas permeation tests

Conditions		
Temperature		373 K
Pressure	Feed	101.3 kPa
	Sweep	101.3 kPa
Partial pressure difference	CO_2	1 kPa
Pressure difference		0 kPa
Gas flow rate (dry base)		
Feed	Total	200 cm^3/min
	CO_2	2 cm^3/min
	N_2	Balance
Sweep	He	40 cm^3/min
Relative humidity		0, 2.7, 10 – 90% (every 10%)

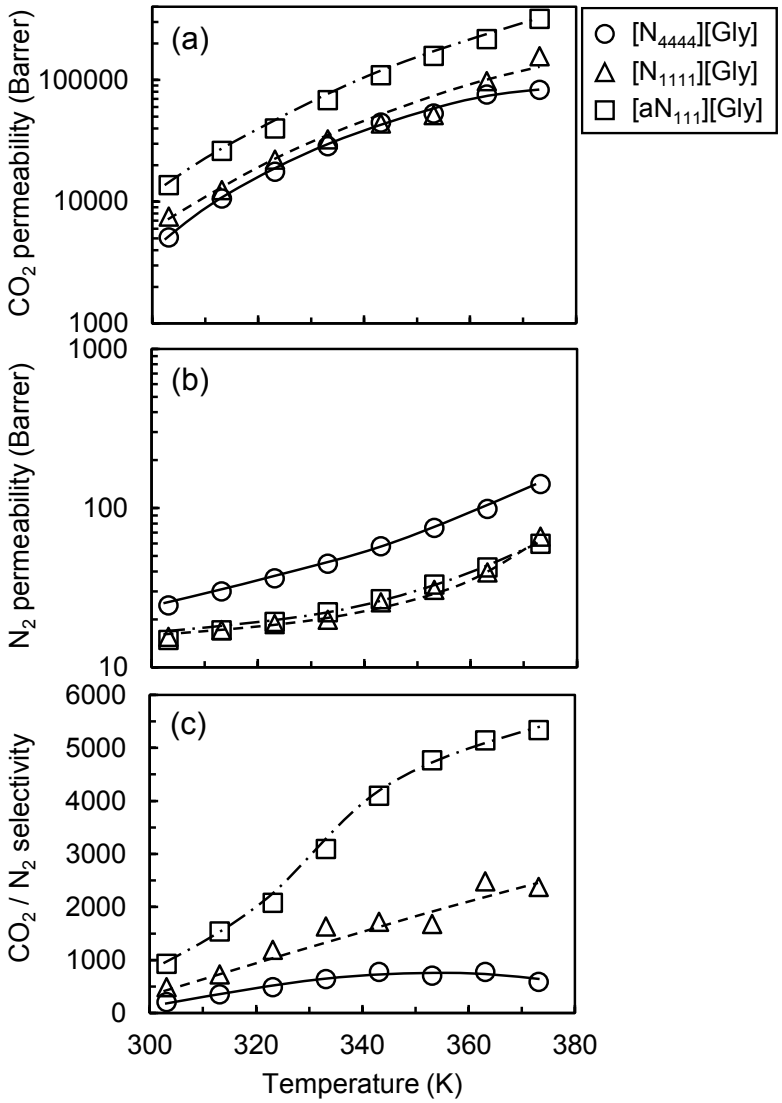

Fig. V.5 Effect of temperature on gas permeation properties of the AAIL-FTMs under humid conditions (RH = 50%). (a) CO_2 permeability, (b) N_2 permeability and (c) CO_2/N_2 selectivity.

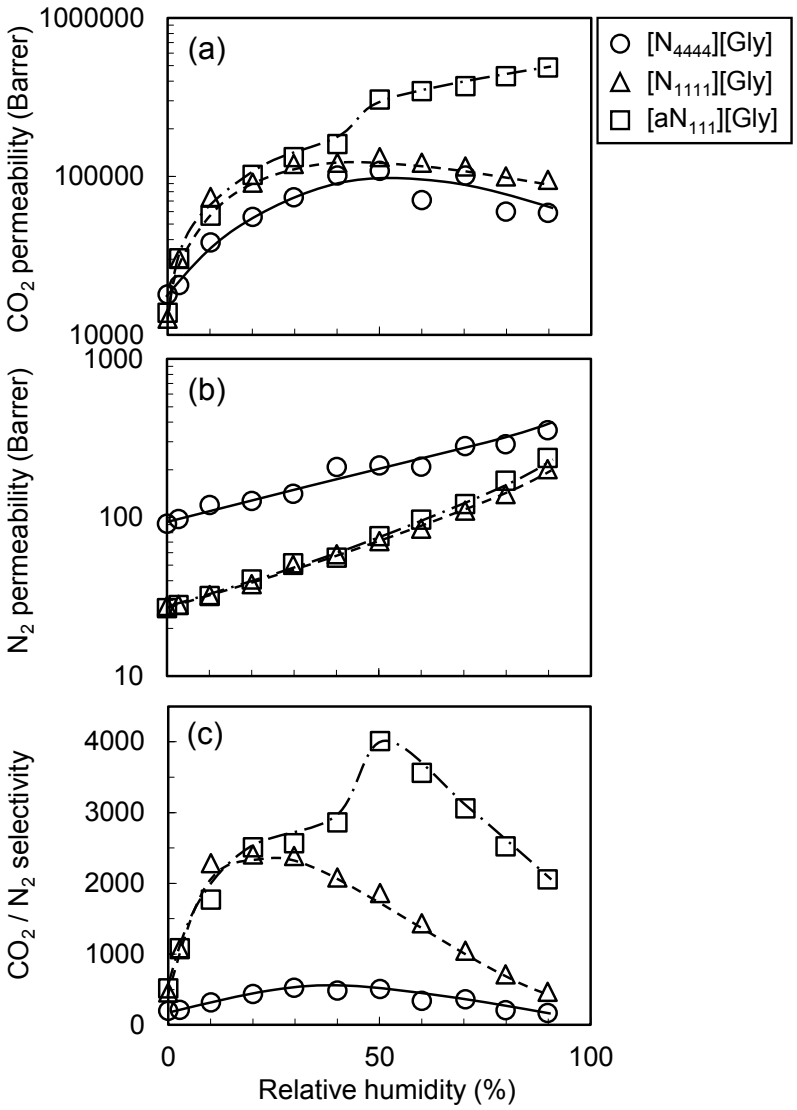

Fig. V.6 Effect of RH on gas permeation properties of the AAIL-FTMs at 373 K. (a) CO_2 permeability, (b) N_2 permeability and (c) CO_2/N_2 selectivity.

V.3.3.1 Effect of temperature on gas permeation properties

As shown in Fig. V.5(a), [aN_{111}][Gly]-FTM exhibited the highest CO_2 permeability at all temperatures, with values exceeding 10,000 Barrer, which are two-fold higher than those of [N_{4444}][Gly]- and [N_{1111}][Gly]-FTMs. This behavior originated from the higher CO_2 absorption capacity of [aN_{111}][Gly]-FTM. The gas permeability of non-porous membranes can generally be described by multiplying the concentration gradient of the

gas in the membrane by the diffusion coefficient. Therefore, the gas flux, J, and permeability, R, of the AAIL-FTMs are described as follows:[24]

$$J = \frac{\varepsilon}{\tau}\frac{D}{\delta}\left(C_{\mathrm{f}} - C_{\mathrm{s}}\right) \tag{V.2}$$

$$R = \frac{\varepsilon}{\tau}D\frac{C_{\mathrm{f}} - C_{\mathrm{s}}}{P_{\mathrm{f}} - P_{\mathrm{s}}} \tag{V.3}$$

where ε (-), τ (-), and δ (m) are the porosity, tortuosity, and thickness of the membrane, respectively; D (m^2/s) is the molecular diffusion coefficient of the gas in the AAIL; C_f and C_s (mol/m^3) are the concentrations of the gas species in the AAIL at the feed and permeate sides of the membrane, respectively; and P_f and P_s (Pa) are the pressures of the gas at the feed and permeate sides, respectively. In my experiment, the gas partial pressure and concentration at the permeate side can be assumed to be zero because the gases permeating the membrane were continuously swept; i.e. P_s and C_s are zero. Therefore, the transmembrane concentration gradient of the solute, $\Delta C = C_f - C_s$, can simply be expressed by C_f which corresponds to the equilibrium absorption amount shown in Fig. V.4. Thus, the transmembrane concentration gradients as driving force for gas permeation of the AAIL-FTMs were determined by the amount of gas absorbed in the AAILs. As mentioned before, the two-fold higher CO_2 permeability of [aN_{111}][Gly]-FTM over that of [N_{4444}][Gly]-FTM and [N_{1111}][Gly]-FTM, shown in Fig. V.5(b), was caused by double the amount of CO_2 being absorbed in [aN_{111}][Gly] compared with in [N_{4444}][Gly] and [N_{1111}][Gly], shown in Fig. V.4(b).

On the other hand, according to Fig. V.5(b), the N_2 permeabilities of [N_{1111}][Gly]- and [aN_{111}][Gly]-FTMs were almost the same at all temperatures, and lower than in [N_{4444}][Gly]-FTM. The reason for this is clear and is similar to that discussed above. The results of the N_2 permeabilities are in good agreement with the FFVs of the AAIL-CO_2

complexes presented in Table V.1. From the results, it can be concluded that the N_2 barrier property of the AAIL-FTMs was successfully enhanced by using a small AAIL species. In particular, [aN_{111}][Gly]-FTM displayed an extremely high CO_2 permeability and N_2 barrier behavior, leading to a CO_2/N_2 selectivity of over 1,000 over a wide temperature range, as shown in Fig. V.5(c).

Regarding the dependence of gas permeabilities shown in Fig. V.5 on temperature, both CO_2 and N_2 permeabilities increased monotonically with temperature. As noted above, the gas permeability of the AAIL-FTMs was determined by the molecular diffusion coefficient and the gas absorption. In addition, the molecular diffusion coefficient can be described by the following Wilke-Chang equation:[25]

$$D = 7.4\times10^{-12}\frac{\sqrt{\psi M}}{\eta V^{0.6}}T \qquad \text{(V.4)}$$

where ψ (-) and M (g/mol) are the association constant and molecular weight of the AAIL, respectively; and η (mPa·s) and V (m^3/mol) are the viscosity of the AAIL and the molecular volume of the solute in the membrane, respectively. Generally, it is well known that the viscosity of a RTIL decreases with increasing temperature. According to the results of the viscosity measurement for [N_{4444}][Gly], [N_{1111}][Gly] and [aN_{111}][Gly] (Fig. V.7), the viscosities of all AAILs decreased with increasing temperature. Thus, it can be suggested that the increase in CO_2 and N_2 permeabilities with temperature were caused by enhancement of the molecular diffusion coefficient, resulting from the decrease in viscosity of the AAILs.

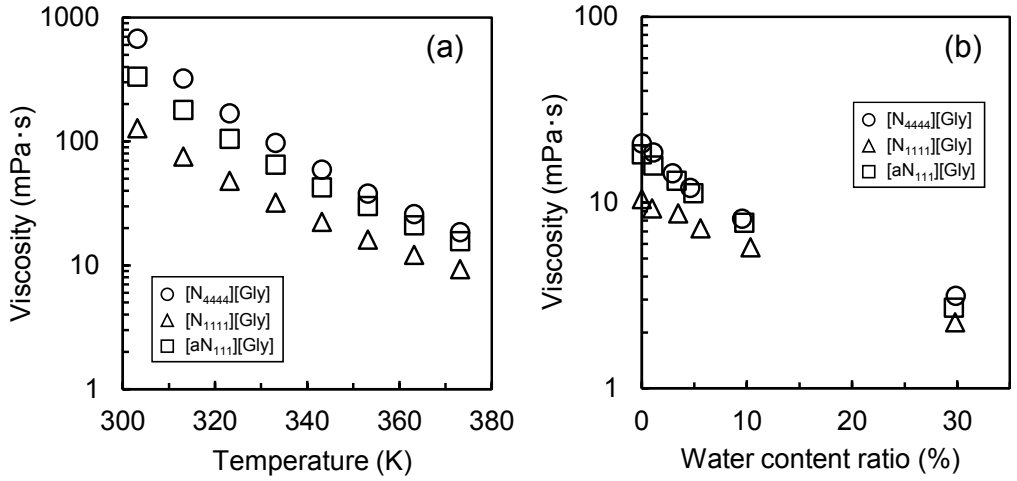

Fig. V.7 Effect of (a) temperature and (b) water content ratio on viscosity of [N_{4444}][Gly], [N_{1111}][Gly] and [aN_{111}][Gly].

V.3.3.2 Effect of RH on gas permeation properties

The effect of RH on the CO_2 permeation properties of the AAIL-FTMs is shown in Fig. V.6. All FTMs displayed a high CO_2 permeability, exceeding 10,000 Barrer at all relative humidities. In particular, [aN_{111}][Gly]-FTM exhibited a CO_2/N_2 selectivity of over 1,000 over a wide RH range, as shown in Fig. V.6(c). CO_2 permeabilities increased with increasing RH and then reached a constant value, as shown in Fig. V.6(a). Note that the CO_2 permeability of [aN_{111}][Gly]-FTM increased again above 50% RH. This phenomenon was observed only in the case of [aN_{111}][Gly]-FTM. Therefore, I can conclude that this phenomenon might be caused by chemical reaction between an amino acid sidechain in the cation group of [aN_{111}][Gly] and CO_2. The effect of RH on the CO_2 reactivity of [aN_{111}][Gly] is revealed by evaluating the difference between the amounts of CO_2 absorbed under dry and humid conditions in the CO_2 absorption tests. However, it is quite difficult to measure CO_2 absorption under dry conditions because the viscosity of the AAILs markedly increases with CO_2 absorption. I therefore investigated the effect of RH on the reactivities of the AAILs with CO_2 by using DFT studies. Regarding

[aN_{111}][Gly], the formation of three types of [aN_{111}][Gly]-CO_2 complexes would be possible: 1) COM_C, which could be formed via the reaction between CO_2 and the amino group available in the cation of [aN_{111}][Gly] (Fig. V.8(a)), 2); COM_A, which could be formed via the reaction between CO_2 and an amino group present in the anion of [aN_{111}][Gly] (Fig. V.8(b)), 3); and COM_{CA}, which could be formed via the reaction between CO_2 and the amino groups in both the cation and anion of [aN_{111}][Gly] (Fig. V.8(c)). The binding energies of these complexes under dry and humid conditions were calculated by using DFT studies and I discussed the structure of the complex under each condition on the basis of the structural stability predicted from the binding energy. The binding energies of three complexes under dry and humid conditions are listed in Table V.4, which shows that the binding energies under both dry and humid conditions were in the order COM_C < COM_{CA} < COM_A. In general, it is well known that a structure with smaller binding energy is more stable. Therefore, the stabilities of the complexes were in the order COM_C > COM_{CA} > COM_A under dry and humid conditions. Based on above explanations, the binding energies of COM_A and COM_{CA} were significantly different from that of COM_C under dry conditions. The binding energy difference between COM_C and COM_A was -36.48 kcal/mol and that between COM_C and COM_{CA} was -16.87 kcal/mol. In contrast, the binding energy of COM_{CA} was similar to that of COM_C and much smaller than that of COM_A under humid conditions. The binding energy difference between COM_C and COM_{CA} under humid conditions was only -3.71 kcal/mol. From the results, it seems that the COM_C would be preferentially formed under dry conditions, while COM_C and COM_{CA} would co-exist under humid conditions. The amount of CO_2 absorbed in [aN_{111}][Gly] increased to form COM_{CA} above 50% RH, which led to the second increase in CO_2 permeability. Thus, the second increase in CO_2 permeability of [aN_{111}][Gly]-FTM above

50% RH shown in Fig. V.6(a) was caused by changing the mechanism of complex formation with increasing RH.

Table V.4 Binding energy of $[aN_{111}][Gly]$-CO_2 complexes

Complex	Dry condition ΔE (kcal/mol)	Humid condition ΔE (kcal/mol)
COM_C	-130.54	-16.00
COM_A	-94.06	-1.05
COM_{CA}	-113.67	-12.29

(a)

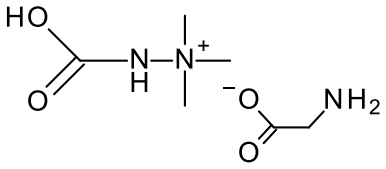

(b)

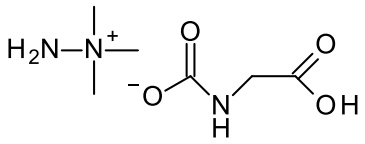

(c)

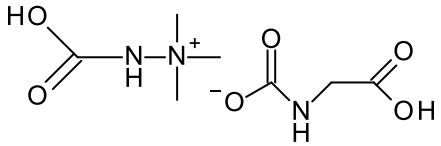

Fig. V.8 The structure of (a) COM_C, (b) COM_A and (c) COM_{CA}.

On the other hand, as shown in Fig. V.6(b), the N_2 permeabilities of the AAIL-FTMs monotonically increased with RH. This is because the viscosities of each AAIL decreased with increasing water content ratio in the AAILs, as shown in Fig. V.7. Comparing each

AAIL-FTM, the N_2 permeabilities of [N_{1111}][Gly]- and [aN_{111}][Gly]-FTMs were similar at every RH and lower than that of [N_{4444}][Gly]-FTM. The difference in N_2 permeabilities was caused by a difference in the amount of N_2 absorbed as a result of the FFVs of the AAILs.

V.3.3.3 Comparison of gas separation performance with various membranes

Finally, I compared the CO_2 separation performance of [aN_{111}][Gly]-FTM fabricated in this study with several CO_2 separation membranes reported in previous work. Fig. V.9 shows the CO_2 separation performance of the [aN_{111}][Gly]-FTM, dense polymeric membranes and other conventional FTMs.[26-37] As shown in Fig. V.9, the CO_2 separation performances of the polymeric membranes were almost all below the upper bound presented by Robeson[29] in 2008 and were insufficient for practical use. Conventional FTMs showed much higher performance than polymeric membranes. However, they exhibited excellent performance only over a narrow range of preferred experimental conditions. On the other hand, [aN_{111}][Gly]-FTM fabricated in this study, showed much higher CO_2 permeability and CO_2/N_2 selectivity than the conventional FTMs, which were observed over wide temperature and RH ranges. In addition, the CO_2 separation performance of [aN_{111}][Gly]-FTM was over 300,000 Barrer of CO_2 permeability and a CO_2/N_2 selectivity of over 5,000 under optimum conditions. Thus, I conclude that [aN_{111}][Gly]-FTM is a promising CO_2 separation membrane, with excellent CO_2 permeability and CO_2/N_2 selectivity, that can be applied in numerous practical applications.

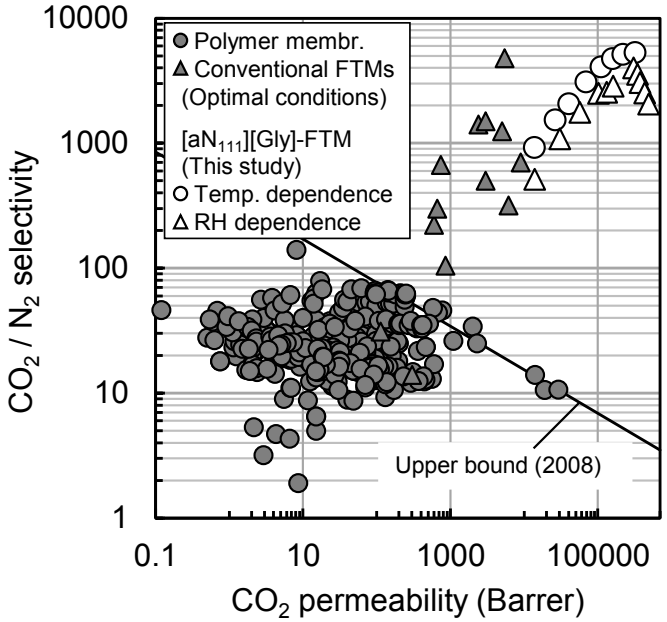

Fig. V.9 Comparison of CO_2 separation performances of various membranes, including [aN_{111}][Gly]-FTM.

V.4 Conclusions

Three AAILs with a different number of amino groups and different sizes were synthesized and their gas absorption properties investigated. The FFVs of the AAILs before and after CO_2 absorption were calculated using MD simulation and the amounts of N_2 absorbed were evaluated on the basis of their FFVs. Based on computational and experimental studies, it was found that the FFV and molar volume of the AAILs became lower with a decrease in size of the ionic liquids. [aN_{111}][Gly], with a small size and two amino groups, showed high CO_2 and low N_2 absorptions. AAIL-FTMs were prepared by using the AAILs and their gas permeation properties investigated. [aN_{111}][Gly]-FTM showed extremely high CO_2 permeability and N_2 barrier properties over wide temperature and RH ranges. Based on the experimental and computational results, it was suggested that the structure of the [aN_{111}][Gly]-CO_2 complex formed via CO_2 absorption can be altered by increasing RH. [aN_{111}][Gly]-FTM showed higher CO_2

permeability and CO_2/N_2 selectivity than conventional FTMs under humid and/or elevated temperature conditions. It exhibited over 300,000 Barrer of CO_2 permeability and a CO_2/N_2 selectivity exceeding 5,000 under optimal conditions. From the present investigation, it can be concluded that a novel AAIL with suitable gas absorption properties for application as a CO_2 separation membrane was successfully synthesized and an FTM with excellent CO_2 permeation properties was successfully fabricated.

References

1. B. F. Goodrich, J. C. de la Fuente, B. E. Gurkan, D. J. Zadigian, E. A. Price, Y. Huang and J. F. Brennecke, *Ind. Eng. Chem. Res.*, 2011, **50**, 111.
2. K. E. Gutowski and E. J. Maginn, *J. Am.Chem. Soc.*, 2008, **130**, 14690.
3. Y. Zhang, S. Zhang, X. Lu, Q. Zhou, W. Fan and X. Zhang, *Chem. Eur. J.*, 2009, **15**, 3003.
4. D. Camper, J. Bara, C. Koval and R. Noble, *Ind. Eng. Chem. Res.*, 2006, **45**, 6279.
5. M. S. Shannon, J. M. Tedstone, S. P. O. Danielsen, M. S. Hindman, A. C. Irvin and J. E. Bara, *Ind. Eng. Chem. Res.*, 2012, **51**, 5565.
6. T. C. Lourenco, M. F. C. Coelho, T. C. Ramalho, D. van der Spoel and L. T. Costa, *Environ. Sci. Technol.*, 2013, **47**, 7421.
7. J. Zhang, S. Zhang, K. Dong, Y. Zhang, Y. Shen and X. Lv, *Chem. Eur. J.*, 2006, **12**, 4021.
8. B. F. Goodrich, J. C. de la Fuente, B. E. Gurkan, Z. K. Lopez, E. A. Price, Y. Huang and J. F. Brennecke, *J. Phys. Chem. B*, 2011, **115**, 9140.
9. Modeling and Simulation Solutions for Chemicals and Materials Research, Materials Studio (Version 6.1), Accelrys software Inc., San Diego, USA. <www.accelrys.com>, 2013.
10. M. J. Frisch, G. W. Trucks, H. B. Schlegel, G. E. Scuseria, M. A. Robb, J. R. Cheeseman, G. Scalmani, V. Barone, B. Mennucci, G. A. Petersson, H. Nakatsuji, M. Caricato, X. Li, H. P. Hratchian, A. F. Izmaylov, J. Bloino, G. Zheng, J. L. Sonnenberg, M. Hada, M. Ehara, K. Toyota, R. Fukuda, J. Hasegawa, M. Ishida, T. Nakajima, Y. Honda, O. Kitao, H. Nakai, T. Vreven, J. A. Montgomery, J. E. Peralta, F. Ogliaro, M. Bearpark, J. J. Heyd, E. Brothers, K. N. Kudin, V. N. Staroverov, R. Kobayashi, J.

Normand, K. Raghavachari, A. Rendell, J. C. Burant, S. S. Iyengar, J. Tomasi, M. Cossi, N. Rega, J. M. Millam, M. Klene, J. E. Knox, J. B. Cross, V. Bakken, C. Adamo, J. Jaramillo, R. Gomperts, R. E. Stratmann, O. Yazyev, A. J. Austin, R. Cammi, C. Pomelli, J. W. Ochterski, R. L. Martin, K. Morokuma, V. G. Zakrzewski, G. A. Voth, P. Salvador, J. J. Dannenberg, S. Dapprich, A. D. Daniels, Farkas, J. B. Foresman, J. V. Ortiz, J. Cioslowski and D. J. Fox, Gaussian 09, Revision A.02, Gaussian, Inc.: Wallingford, CT, 2009.

11. F. Y. Dupradeau, A. Pigache, T. Zaffran, C. Savineau, R. Lelong, N. Grivel, D. Lelong, W. Rosanski and P. Cieplak, *Phys. Chem. Chem. Phys.*, 2010, **12**, 7821.
12. D. Case, T. A. Darden, T. E. Cheatham, C. Simmerling, J. Wang, R. Duke, R. Luo, M. Crowley, R. Walker, W. Zhang, K. M. Merz, B. Wang, S. Hayik, A. Roitberg, G. Seabra, I. Kolossvary, K. F. Wong, F. Paesani, J. Vanicek, X. Wu, S. Brozell, T. Steinbrecher, H. Gohlke, L. Yang, C. Tan, J. Mongan, V. Hornak, G. Cui, D. H. Mathews, M. G. Seetin, C. Sagui, V. Babin and P. Kollman, *Amber 11.* .San Francisco, CA: University of California; 2010.
13. L. Martinez, R. Andrade, E. G. Birgin and J. M. Martinez, *J. Comput. Chem.*, 2009, **30**, 2157.
14. D. van der Spoel, E. Lindahl, B. Hess, A. R. van Buuren, E. Apol, P. J. Meulenhoff, D. P. Tieleman, A. L. T. M. Sijbers, K. A. Feenstra, R. van Drunen and H. J. C. Berendsen, Gromacs User Manual version 4.5.6, www.gromacs.org (2010).
15. G. Bussi, D. Donadio and M. Parrinello, *J. Chem. Phys.*, 2007, **126**, 014101/1.
16. H. J. C. Berendsen, J. P. M. Postma, W. F. van Gunsteren, A. DiNola and J. R. Haak, *The J. Chem. Phys.*, 1984, **81**, 3684.
17. U. Essmann, L. Perera, M. L. Berkowitz, T. Darden, H. Lee and L. G. Pedersen, *J.*

Chem. Phys., 1995, **103**, 8577.

18. W. Humphrey, A. Dalke and K. Schulten, *J. Mol. Graph. Model.*, 1996, **14**, 33.
19. V. S. Bernales, A. V. Marenich, R. Contreras, C. J. Cramer and D. G. Truhlar, *J. Phys. Chem. B*, 2012, **116**, 9122.
20. E. I. Izgorodina, U. L. Bernard and D. R. MacFarlane, *J. Phys. Chem. A*, 2009, **113**, 7064.
21. A. V. Marenich, C. J. Cramer and D. G. Truhlar, *J. Phys. Chem. B*, 2009, **113**, 6378.
22. W. M. Lee, *Polym. Eng. Sci.*, 1980, **20**, 65.
23. A. Bondi, *J. Phys. Chem.*, 1964, **68**, 441.
24. W. S. W. Ho and K. K. Sirkar, Eds. *Membrane Handbook*; Kluwer Academic Publishers: Boston, 1992.
25. C. R. Wilke and P. Chang, *Am. Inst. Chem. Eng. J.*, 1955, **1**, 264.
26. M. Teramoto, K. Nakai, N. Ohnishi, Q. Huang, T. Watari and H. Matsuyama, *Ind. Eng. Chem. Res.*, 1996, **35**, 538.
27. A. S. Kovvali, H. Chen and K. K. Sirkar, *J. Am. Chem. Soc.*, 2000, **122**, 7594.
28. J. Huang, J. Zou and W. S. W. Ho, *Ind. Eng. Chem. Res.*, 2008, **47**, 1261.
29. L. M. Robeson, *J. Membr. Sci.*, 2008, **320**, 390.
30. C. A. Scholes, S. E. Kentish and G. W. Stevens, *Rec. Pat. Chem. Eng.*, 2008, **1**, 52.
31. H. Matsuyama, K. Matsui, Y. Kitamura, T. Maki and M. Teramoto, *Sep. Purif. Technol.*, 1999, **17**, 235.
32. H. Matsuyama, M. Teramoto, K. Matsui and Y. Kitamura, *J. Appl. Polym. Sci.*, 2001, **81**, 936.
33. N. Matsumiya, S. Matsufuji, M. Nakabayashi, K. Okabe, H. Mano and M. Teramoto, *Maku*, 2004, **29**, 66.

34. N. Matsumiya, S. Matsufuji, K. Okabe, H. Mano and M. Teramoto, *Maku*, 2004, **29**, 123.

35. K. Okabe, N. Matsumiya and H. Mano, *Sep. Purif. Technol.*, 2007, **57**, 242.

36. G. J. Francisco, A. Chakma, X. Feng, *J. Membr. Sci.*, 2007, **303**, 54.

37. P. Ji, Y. Cao, H. Zhao, G. Kang, X. Jie, D. Liu, J. Liu and Q. Yuan, *J. Membr. Sci.*, 2009, **342**, 190.

Chapter VI

Polymeric ion-gels containing an amino acid ionic liquid for facilitated CO_2 transport media

VI.1 Introduction

SILMs have a serious disadvantage. The SILMs are prepared by impregnating ionic liquids in porous polymeric supports as liquid state. Since an ionic liquid as held in the porous supports by weak capillary force, they would easily leaked out from the porous support even under low pressurized conditions. To overcome the leakage of an ionic liquid, gelation of ionic liquids have been investigated to improve the pressure resistance of the SILMs. Among the ion-gels, polymeric ion-gels offer virtually unlimited tunability and a unique platform for designing materials.[1] A polymer network at a concentration of less than several tens percent by volume can provide a soft but highly elastic solid. The polymer network acts like a sponge, with the voids filled with IL. Because the voids are much larger than the ions, ion diffusivities are comparable to those in the neat IL.[2-4] Such high diffusivities have also been reported for CO_2 separation membranes.[5-8] However, CO_2 solubility in these RTILs is low, and the low CO_2 permeability of ion-gel membrane composed of RTILs has limited any practical applications.

In this chapter, I present polymer gels containing AAILs (AAIL-gels) for the first time in the world. I demonstrate the superior mechanical strength of the AAIL-gel and the excellent CO_2 permeability of AAIL-gel films.

VI.2 Experimental

VI.2.1 Materials

The AAIL-gel was prepared by conventional free radical polymerization. For ILs to be used as solvents for ion-gels, the compatibility of the polymers and their monomers with the ILs is of paramount importance.[9] The solubility and compatibility of synthetic polymers with ILs is not well understood. Determination of the appropriate combination of an IL and monomer precursors for the polymer formation in an ion-gel remains challenging.[10] Ueki and Watanabe have reported on the phenomenological aspects of polymer solubility in RTILs including the hydrophilic [Emim][BF_4].[10] Because AAIL are extremely hydrophilic ionic liquids, polymers that have good compatibility with [Emim][BF_4] may be expected to be good candidates for use with AAILs. According to the phenomenological aspects, I selected poly(dimethyl-acrylamide) (PDMAAm), poly(vinylpyrrolidone) (PVP), poly(2-hydroxyethylmethacrylate) (PHEMA), poly(methyl-acrylate) (PMA) and poly(ethylacrylate) (PEA) for the fabrication of AAIL-gels. Tetrabutylphosphonium type AAILs including glycine ([P_{4444}][Gly]), serine ([P_{4444}][Ser]), lysine ([P_{4444}][Lys]) and proline ([P_{4444}][Pro]) as their anion part were synthesized and used in this study. From these AAILs, [P_{4444}][Pro] was chosen for use as the solvent component of the AAIL-gel films because [P_{4444}][Pro] features the highest CO_2 permeability.

Tetrabutylphosphonium hydroxide ([P_{4444}][OH], 40 wt% in water) was purchased from Sigma-Aldrich Co. (St Louis, MO, USA). Glycine (99.8%), lysine (>99.0%), serine (>99.0%) and proline (>99.0%) were purchased from Tokyo Chemical Industry Co. (Tokyo, Japan). Methanol (99.8%) was purchased from Wako Pure Chemicals Industry Ltd. (Osaka, Japan). Acetonitrile (99.90%) was purchased from Sigma-Aldrich Co. All

reagents were used as received.

Tetrabutylphosphonium type AAILs (tetrabutylphosphonium glycine ([P_{4444}][Gly]), tetrabutylphosphonium lysine ([P_{4444}][Lys]), tetrabutylphosphonium serine [P_{4444}][Ser], and tetrabutylphosphonium proline ([P_{4444}][Pro])) were synthesized following a neutralization procedure. An aqueous solution of [P_{4444}][OH] was added to a slight excess of an equimolar amino acid (AA) aqueous solution to prepare the [P_{4444}][AA] salts, with water formed as a byproduct. The product was dried *in vacuo* for more than 8 h at 313 K. A mixture of acetonitrile/ethanol was then added to recrystallize and remove unreacted amino acid. The filtrate was evaporated to remove solvent. The reaction ratios were 95.5, 93.2, 99.9 and 99.9% for [P_{4444}][Gly], [P_{4444}][Lys], [P_{4444}][Ser] and [P_{4444}][Pro], respectively. The structures of the resulting [P_{4444}][AA]s were confirmed by ^{1}H-NMR spectroscopy (Bruker Advance 500, Bruker BioSpin) and FT-IR (ALPHA FT-IR Spectrometer, Bruker Optics) measurements. ^{1}H-NMR data and FT-IR data of [P_{4444}][AA]s were shown in the appendix

VI.2.2 Preparation of AAIL-gels

The monomers N,N-dimethylacrylamide (DMAAm), N-vinyl-2-pyrrolidone (NVP), 2-hydroxyethyl-methacrylate (HEMA), methylacrylate (MA) or ethylacrylate (EA), were mixed with an AAIL, a cross-linker (ethylene glycol dimethacrylate) and a photoinitiator (1-hydroxycyclohexyl phenyl ketone) and homogenized by vigorous mixing. The solution was poured into a test tube and irradiated by 365 nm UV light for 3 hours. Confirmation of gelation was evaluated by the test tube-tilting method.[11,12] The as-prepared AAIL-gels were then removed from the test tube.

VI.2.3 Preparation of AAIL-gel films

A typical procedure for preparation of the AAIL gel films is as follows. Monomer (NVP or DMAAm) and $[P_{4444}][Pro]$ were mixed in a 1:1 wight ratio, and the mixture homogenized by vigorous mixing. EGDMA (molar ratio of EGDMA/monomer = 0.3) was then added, and the mixture homogenized again. Finally, HCPK (weight ratio of HCPK/(monomer+EGDMA) = 0.01) was added and the mixing step repeated a final time. The solution was cast onto a 50 × 50 mm Rain-X-coated quartz substrate. Rain-X is a commercially available, hydrophobic coating for glass surfaces, which aids in the removal of the film after photopolymerization is completed. A 300 μm thick PTFE spacer and identical quartz plate was then placed on top to completely spread the monomer. The plates were placed under a 365 nm UV light for 3 h. After the reaction was complete, the plates were separated and the so formed gel film was peeled-off from the plates. The gel film obtained was flexible and freestanding with a thickness of about 300 μm.

VI.2.4 Gas permeability tests

Gas permeability tests were carried out with a similar procedure described in II.2.3, except that no water was added.

VI.3 Results and discussion

VI.3.1 Gelation tests

Table VI.1 shows a summary of the gelation tests including the e- and Q-values for each monomer. As shown in Table VI.1, all the AAILs were gelled with NVP, HEMA and DMAAm as sources of a polymer matrix. However, when EA and MA were used, incomplete gelation of AAIL was observed in most cases. Whereas, $[Emim][BF_4]$, a

typical RTIL having no reactive functional groups, formed gels with all the monomers investigated in this study. Thus, AAIL would inhibit radical polymerization. During radical polymerization in ILs, a number of solvent properties such as the polarity, electron pair acceptor-electron pair donator interactions and Coulomb interactions contribute to the overall solvent influence.[13-15] Hydrogen bonding interactions may also have an effect because the AAIL has strong hydrogen bonding ability. As shown in Table VI.1, there was a threshold in the relationship between the e-value and gelation with the AAIL although no relationship was found with the Q-value. The monomers with e-values less than zero could form gels with the AAILs, however the monomers with e-values greater than zero could not form gels.

Table VI.1 Results of gelation tests for five different monomers with four different phosphonium type AAILs and [Emim][BF_4]

	NVP	HEMA	DMAAm	EA	MA
[P_{4444}][Gly]	Gel	Gel	Gel	P	L
[P_{4444}][Ser]	Gel	Gel	Gel	L	L
[P_{4444}][Lys]	Gel	Gel	Gel	P	Gel
[P_{4444}][Pro]	Gel	Gel	Gel	L	L
[Emim][BF_4]	Gel	Gel	Gel	Gel	Gel
e-value	-1.62	-0.39	-0.26	0.55	0.64
Q-value	0.088	1.78	0.41	0.41	0.45

"Gel" indicates the AAIL was gelled, "L" and "P" mean the AAILs was not or partially gelled, respectively.

Fig. VI.1(a) and VI.1(b) shows the as-prepared AAIL-gels based on PDMMAm and PVP matrixes, respectively. These gels contained the four types of AAILs used in this study. The AAIL-gels prepared with each polymer are referred to as "AAIL-polymer gel". For example, [P_{4444}][Pro]-PDMAAm gel is the ion-gel containing [P_{4444}][Pro] in the PDMAAm matrix.

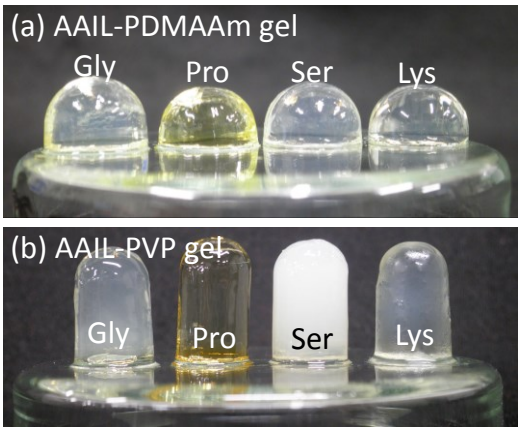

Fig. VI.1 AAIL gels prepared with four AAILs ([P_{4444}][Gly], [P_{4444}][Pro], [P_{4444}][Ser] and [P_{4444}][Lys]) and two monomers ((a) DMAAm and (b) NVP). AAIL content in the gels: 50 wt%.

VI.3.2 Inhibition of radical polymerization in AAILs

I investigated the inhibition of polymerization by the AAILs and found some possibilities relating to the inhibition behaviour; i.e. deactivation of vinyl group by the AAILs and reduction of the propagation rate of the monomers in the AAILs.

VI.3.2.1 Michael addition

Michael addition between a primary or a secondary amine and an acrylate is a well-known reaction.[16,17] Because the AAILs contain a high concentration of amino acid anions, I checked for Michael addition of the amine group to the vinyl group of an acrylate monomer. Because the e-value of methyl acrylate (MA) was the highest among the acrylate monomers investigated in this work, MA was chosen as a representative example. [P_{4444}][Gly] was used as the typical AAIL. The experiment was carried out as follows. Equal amounts of MA and [P_{4444}][Gly] were mixed and homogenized by vigorous mixing. The solution was poured into a test tube irradiated by 365 nm UV light for 24 hours. The occurrence of Michael addition was evaluated by comparing the ^{1}H-NMR

spectrum of the resulting solution with that of the original MA. The ^{1}H NMR spectrum are shown in Fig. VI.2.

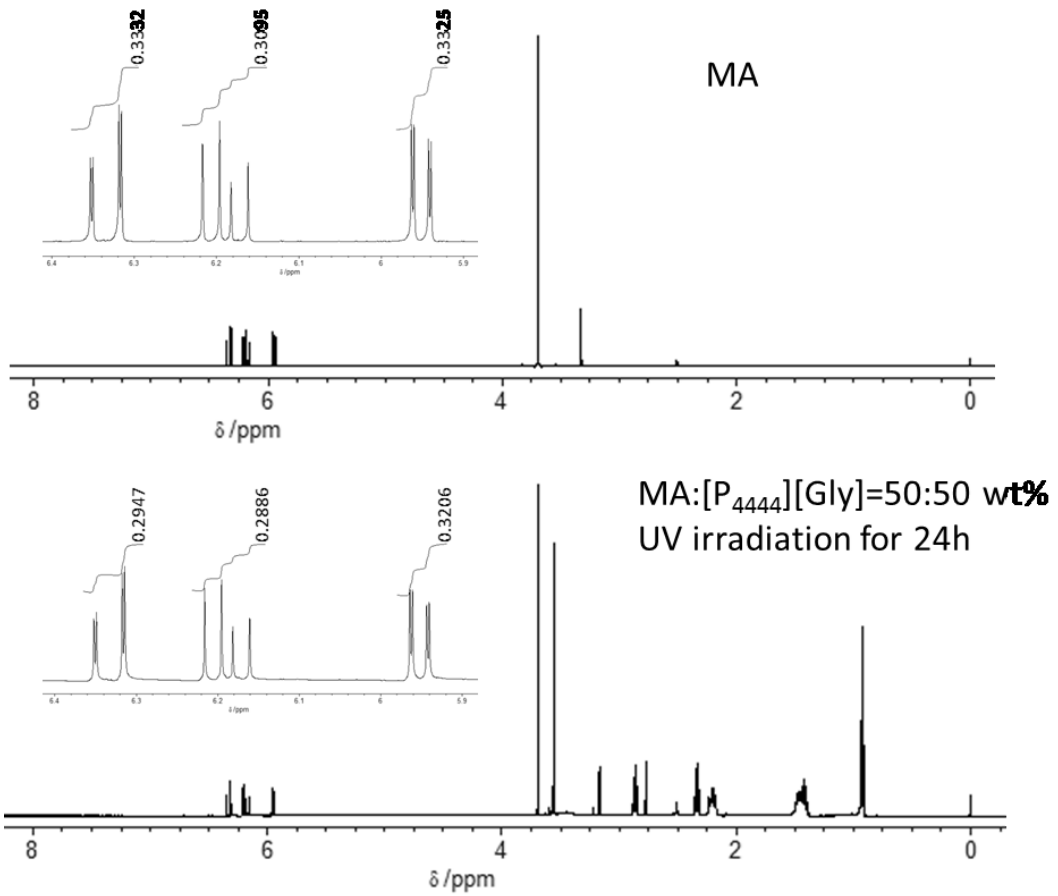

Fig. VI.2 ^{1}H-NMR spectra for MA and the MA/[P_{4444}][Gly] mixture after UV irradiation for 24 h.

Comparing the two spectrum, the integration of the vinyl signal (δ 5.5–7.0 ppm, normalized by the integration of the methyl proton of MA) for the mixture of MA and [P_{4444}][Gly] was not disappeared but decreased to 82% of that for MA. Because the molar ratio of [P_{4444}][Gly]/MA in the 50:50 wt% MA/[P_{4444}][Gly] mixture is 0.257 and glycinate is allowed to react with equimolar of MA, the 18% decrease in the integration of the vinyl signal would indicate the 70% of [P_{4444}][Gly] reacted with MA. From these results there may be a possibility that the deactivation of vinyl group of acrylate monomer by Michael

addition of amino acid anion would be occurred. However, if all the [P_{4444}][Gly] react with MA, about 75% of MA ought to be remained after the reaction under the investigated experimental condition. Therefore, there would be another possibility for the inhibition of gel formation.

VI.3.2.2 Polymerization kinetics

To investigate the polymerization kinetics, the FT-IR spectra during polymerization was monitored in real time by using ReactIR™15 (Mettler Toledo International Inc.). In this experiment, DMAAm and [P_{4444}][Pro] were chosen as representative examples of a vinyl monomer and AAIL, respectively. In addition, a comparative experiment was performed by polymerizing DMAAm in [Emim][BF_4] which was chosen as a representative unreactive IL. The experiments were carried out as follows. A 3:7 weight ratio mixture of DMAAm and [P_{4444}][Pro] was homogenized by vigorous mixing. The solution was poured into a test tube attached to the diamond ATR-IR-fiber probe of a ReactIR™15 and vigorously agitated by a magnetic stirrer. The tip of the probe was immersed in the solution and the test tube was capped with a silicone rubber stopper. The polymerization was initiated by irradiating the solution with 365 nm UV light. Infrared absorption spectra of the samples were measured under continuous UV irradiation. In these experiments, the C=C stretching, in-plane C-H bending and out-of-plane C-H bending of the vinyl group were monitored at 1648, 1421 and 980 cm^{-1}, respectively.

Fig. VI.3 shows the raw IR spectra of pure [P_{4444}][Pro], and processed DMAAm spectra from DMAAm/[P_{4444}][Pro] and DMAAm/[Emim][BF_4] mixtures, extracted by deducting the spectra of each ionic liquid from the corresponding raw IR spectra of the

mixtures before polymerization. As shown in Fig. VI.3, the peaks at 1648, 1421 and 980 cm^{-1} for DMAAm, are indicated by broken black lines, and showed little overlap with the characteristic peaks of $[P_{4444}][Pro]$.

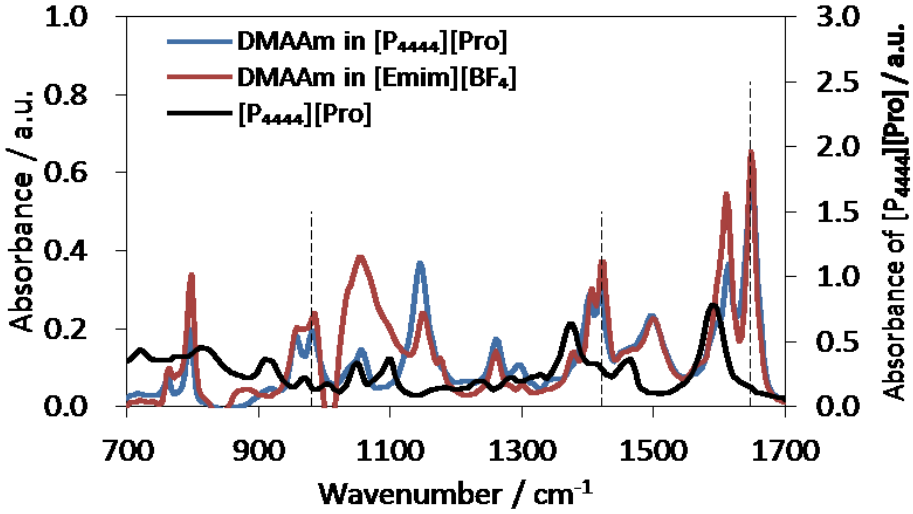

Fig. VI.3 IR spectra of $[P_{4444}][Pro]$ and the DMAAm spectra in DMAAm/$[P_{4444}][Pro]$ and DMAAm/[Emim][BF_4] mixtures.

The results of monitoring the IR peak around 980 cm^{-1} are shown in Fig. VI.4. For polymerization of DMAAm in [Emim][BF_4], the peak corresponding to the out-of-plane C–H bending at 980 cm^{-1} decreased immediately after polymerization was started. Relatively slow attenuation of the corresponding peak intensity was observed during polymerization of DMAAm in $[P_{4444}][Pro]$. The changes of the peak intensities at 1648, 1421 and 980 cm^{-1} during the course of the polymerization reaction are shown in Fig. VI.5. The vertical axis in Fig. VI.5 is the differential absorbance intensity values between at certain periods of reaction and at t = 180 min. I confirmed from the ^{1}H-NMR measurement that the polymerization reaction in $[P_{4444}][Pro]$ was completely finished at t = 180 min; i.e. the vinyl signals (δ 5.5–7.0 ppm) for the mixture of DMAAm and $[P_{4444}][Pro]$ were completely disappeared (Fig. VI.6).

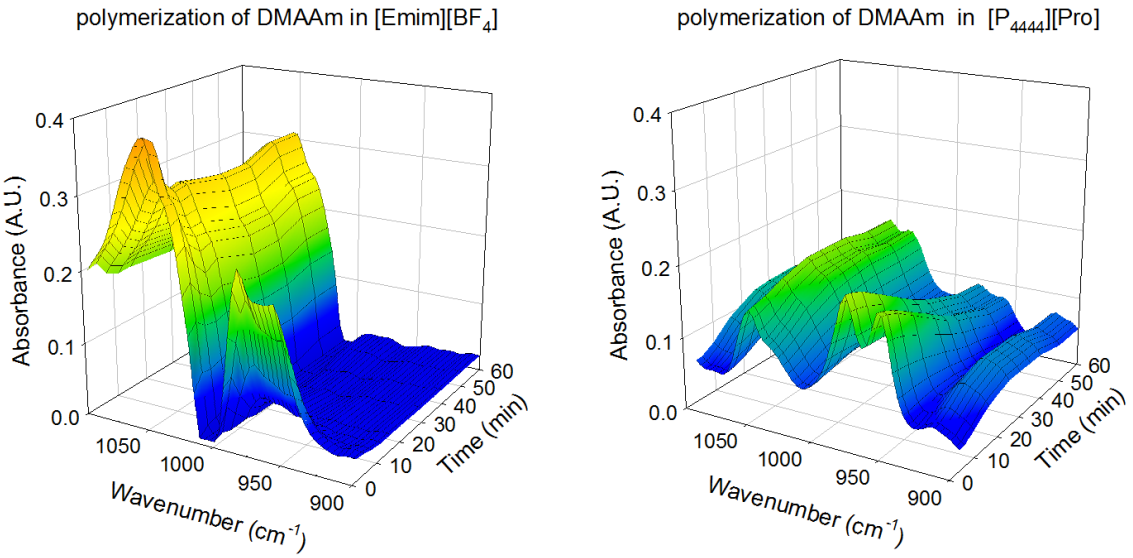

Fig. VI.4 Monitored IR peak around 980 cm^{-1} for polymerization of DMAAm in [Emim][BF_4] (left) and in [P_{4444}][Pro] (right).

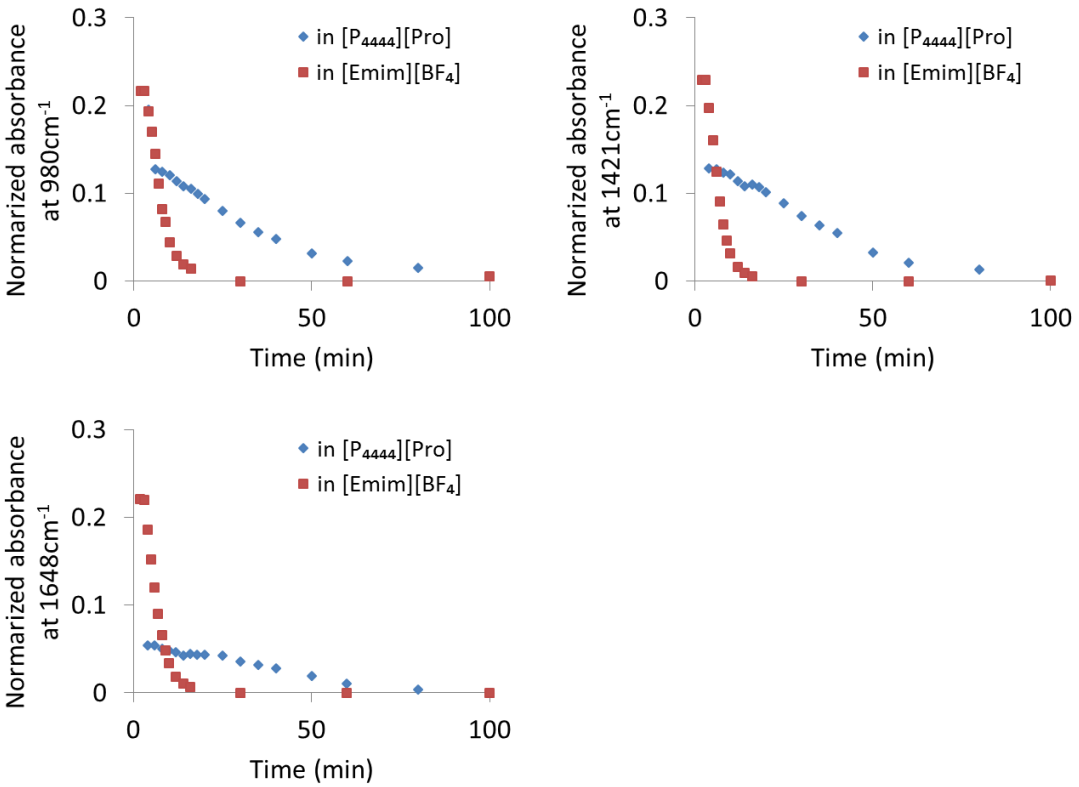

Fig. VI.5 Change of the absorbance intensity at 980, 1421 and 1648 cm^{-1} during polymerization reaction.

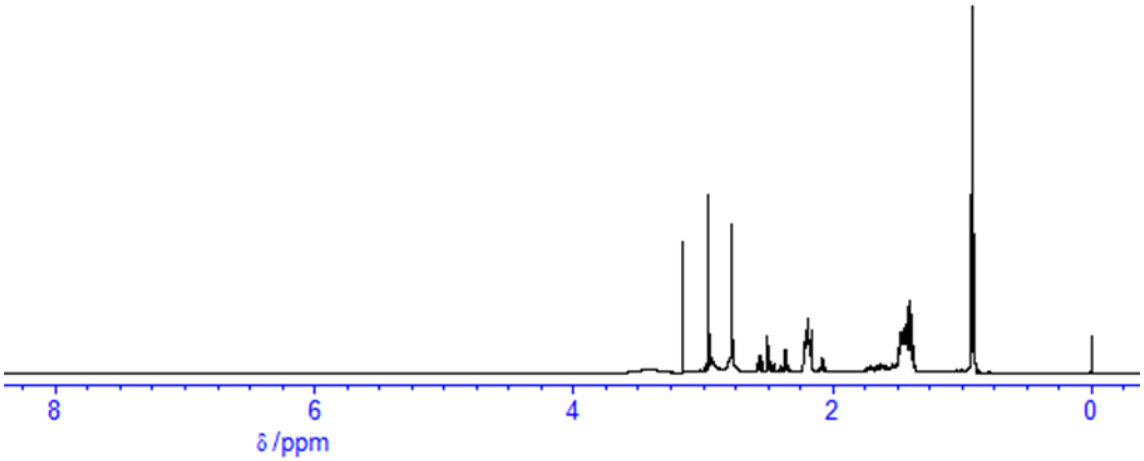

Fig. VI.6 ^{1}H-NMR spectrum for DMAAm in [P_{4444}][Pro] after UV irradiation for 3 h.

As shown in Fig. VI.5, similar trends in the absorbance intensity changes at 980 cm^{-1} were also found at 1648 and 1421 cm^{-1}. These results indicated that the propagation rate of DMAAm was reduced in [P_{4444}][Pro]. From the results shown above, the polymerization rate may be considered to contribute to the degree of gelation of the AAILs.

Some Research on the propagation and termination kinetics of free radical polymerization in ILs has been reported.[13-15,18,19] In these studies, imidazolium-based unreactive ionic liquids were used as the solvent for vinyl monomers and it was shown that the propagation rate increased considerably in the presence of the ILs. As shown in Fig. VI.5, it was confirmed that the polymerization rate of DMAAm in [Emim][BF_4] is rapid, in agreement with previous reports. However, for the polymerization of DMAAm in [P_{4444}][Pro], the polymerization rate decreased drastically, in contrast to the previously reported trend. Solvent properties and interactions such as the polarity, electron pair acceptor-electron pair donator interactions and nonspecific (Coulomb) interactions may contribute to the enhancement of the rate of the free radical polymerization of a vinyl monomer. For the AAILs, hydrogen bonding interactions might also contribute because

AAILs show strong hydrogen bonding.

Regarding the traditional free radical bulk polymerization, Lee *et al.*[20] reported that more electron-deficient acrylate double bonds undergo faster radical addition reactions than electron-rich double bonds. This is also unlike the radical polymerization in AAILs shown in this work; i.e., the monomer with large e-value cannot gel AAILs and vice versa.

The inhibition of radical polymerization in the presence of AAILs is not well understood at this stage, however further experiments are currently in progress to determine the true cause of the observed inhibition. Understanding the mechanism of inhibition may help me to design controlled polymerization systems to further improve the properties of the AAIL-gels. More detailed investigations of the polymerization kinetics are necessary to understand the inhibition of radical polymerization by AAILs.

VI.3.3 Compression tests of AAIL-gels

Figs. VI.7 and VI.8 demonstrate how the polymeric AAIL-gels behave under compression. The AAIL-gels used in this test were the [P_{4444}][Pro]-PDMAAm and [P_{4444}][Pro]-PVP gels. The AAIL content in both gels was 70 wt%. As shown in Fig. VI.7, both ion-gels retained their shape before and after compression by finger-pressure without any leakage of [P_{4444}][Pro] from the polymer matrix. The stress-strain curves of the gels under compression are shown in Fig. VI.8. The [P_{4444}][Pro]-PDMAAm gel ruptured at an applied pressure of less than several hundred kPa. However, the [P_{4444}][Pro]-PVP gel sustained a stress of more than 1 MPa. This high toughness makes the [P_{4444}][Pro]-PVP gel preferable for use in a CO_2 separation membrane.

(a) [P_{4444}][Pro]-PDMAAm gel
(Preparation conditions: DMAAm = 30 wt%, closs-linker/monomer mole fraction = 0.3 (-))

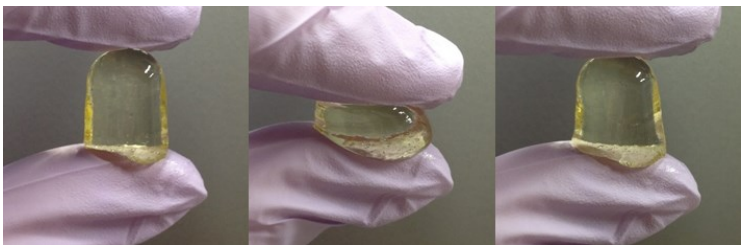

(b) [P_{4444}][Pro]-PVP gel
(Preparation conditions: NVP = 30 wt%, closs-linker/monomer mole fraction = 0.3 (-))

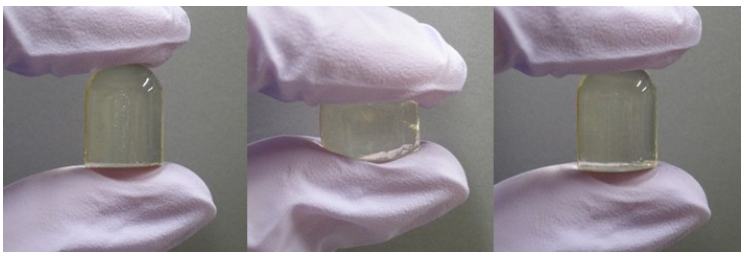

Fig. VI.7 Photographs of finger pressure compression tests of (a) [P_{4444}][Pro]-DMAAm gel and (b) [P_{4444}][Pro]-PVP gel.

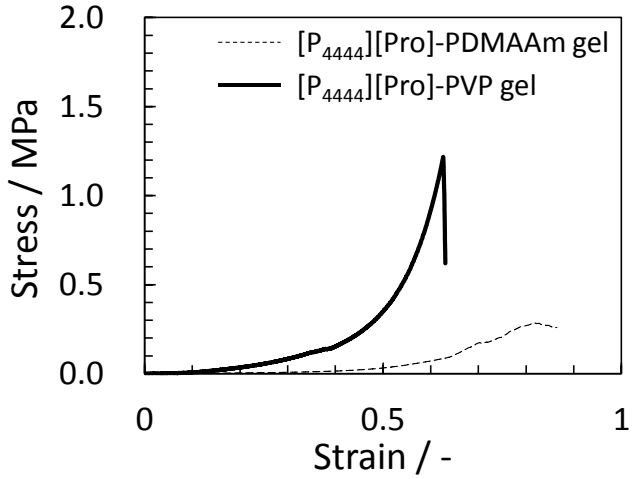

Fig. VI.8 Stress-strain curve of [P_{4444}][Pro]-PDMAAm gel and [P_{4444}][Pro]-PVP gel. The [P_{4444}][Pro] contents in the gels was 70 wt%.

VI.3.4 Gas permeability tests of AAIL-gel films

Figs. VI.9(a) and VI.9(b) show typical AAIL-gel films prepared based on the polymers PDMAAm and PVP and the AAIL [P_{4444}][Pro]. Transparent and flexible gel films were

successfully created with thickness of 300 μm. Owing to the superior toughness of the [P_{4444}][Pro]-PVP gel shown in Fig. VI.8, I selected PVP as the matrix for an AAIL-gel film for testing as a CO_2 separation membrane. Three different [P_{4444}][Pro]-PVP gel films were prepared by changing the ratio of the NVP to NVP/[P_{4444}][Pro] mixture.

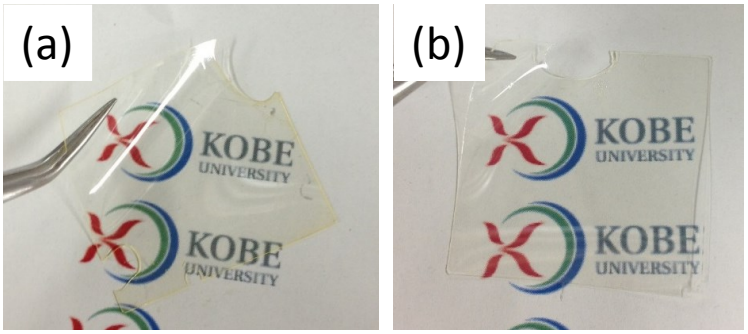

Fig. VI.9 Photographs of (a) [P_{4444}][Pro]-PDMAAm and (b) [P_{4444}][Pro]-PVP gel films. The [P_{4444}][Pro] content in the gel films were 50 wt%.

Fig. VI.10 shows the effect of AAIL weight fraction (wt%) on the gas permeabilities and selectivity of the [P_{4444}][Pro]-PVP gel films. Both the CO_2 and N_2 permeabilities increased with the increase of AAIL content. At a [P_{4444}][Pro] content of 70 wt%, the CO_2 permeability of the AAIL-gel film was about 6700 Barrer. The permeability and selectivity data for the AAIL-gel films prepared in this work are plotted along with the data for SILMs, ion-gel films (RTIL-gel films), polymeric ionic liquid membranes (poly(RTIL) membranes) and supported AAIL membranes (AAIL-FTMs) in Fig. VI.11.[5-8,21-37] In this figure, a well-known "Robeson upper bound" for dense polymer membranes is also shown.[38] As shown in Fig. VI.11, most of the performances of the AAIL-gel films are higher than the upper bounds for polymer membranes as well as the performances of SILMs, RTIL-gel films and poly(RTIL) membranes. The superior transport properties of AAIL-gel films stem from the fact that the AAIL in the gel act as a CO_2 carrier. That

is to say, the CO_2 permeation mechanism of the AAIL-gel films are facilitated transport mechanism. This was supported by the relationship between the CO_2 permeability and CO_2 partial pressure. In Fig. VI.12, the relationship between the CO_2 permeability of $[P_{4444}][Pro]$-PVP gel film and CO_2 partial pressure was plotted. It is clearly shown that the CO_2 permeability was decreased with the increase of CO_2 partial pressure. This is well known tendency for FTMs. The CO_2 permeability of FTMs decreased with the increase of CO_2 partial pressure owing to the carrier saturation with CO_2 under high CO_2 partial pressure conditions. From the other point of view, as shown in Fig. VI.11, the CO_2 permeation performance of the AAIL-gel films were very close to those of the AAIL-FTMs. This result also supports the facilitated CO_2 transport mechanism of the AAIL-gel film. A little inferior performance of the AAIL-gel films might be caused by the diffusion resistance due to the PVP matrix in the gel. In fact, the CO_2 permeation performance of the AAIL-gel films approaches those of AAIL-FTMs with the decrease of the polymer ratio in the AAIL-gel. Such trend was also appeared for the membranes containing RTILs. The most SILMs show higher CO_2 permeability than RTIL-gel films which have the better performance than poly(RTIL) membranes. These trend also due to the diffusion resistance caused by the polymer matrix in the membranes. In other words, the local environment in the gel was not significantly affected to the diffusion of the CO_2-AAIL complex. Therefore, the AAIL-gel films exhibited excellent transport properties, close to those of pure AAIL impregnated SILM. The polymeric AAIL-gel maintains liquid-like permeability within a solid-state material.

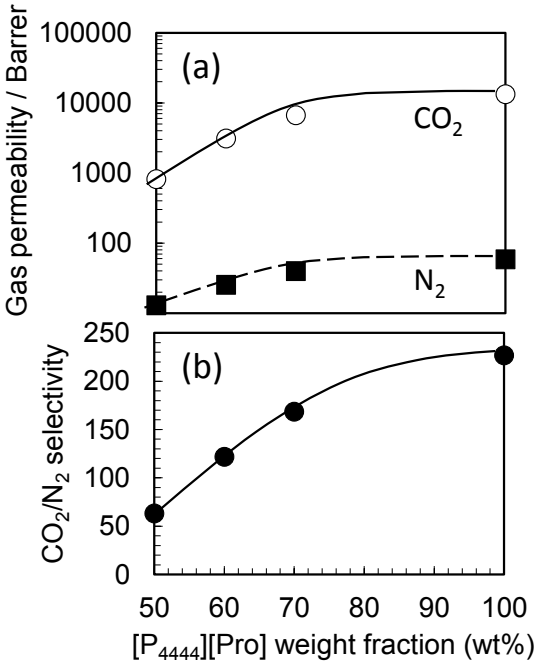

Fig. VI.10 Effect of [P_{4444}][Pro] weight fraction in [P_{4444}][Pro]-PVP gel film on (a) the CO_2 and N_2 permeabilities and (b) CO_2/N_2 selectivity (T = 373 K, Feed mixed gas: CO_2/N_2 (2.5/97.5vol%), Sweep gas: Helium, feed-side and sweep-side pressure were atmospheric pressure, CO_2 partial pressures in feed and sweep gases were 2.5 kPa and 0 kPa, respectively, RH = 0%). The results in 0wt% of monomer weight fraction are those of SILM containing [P_{4444}][Pro] as the AAIL.

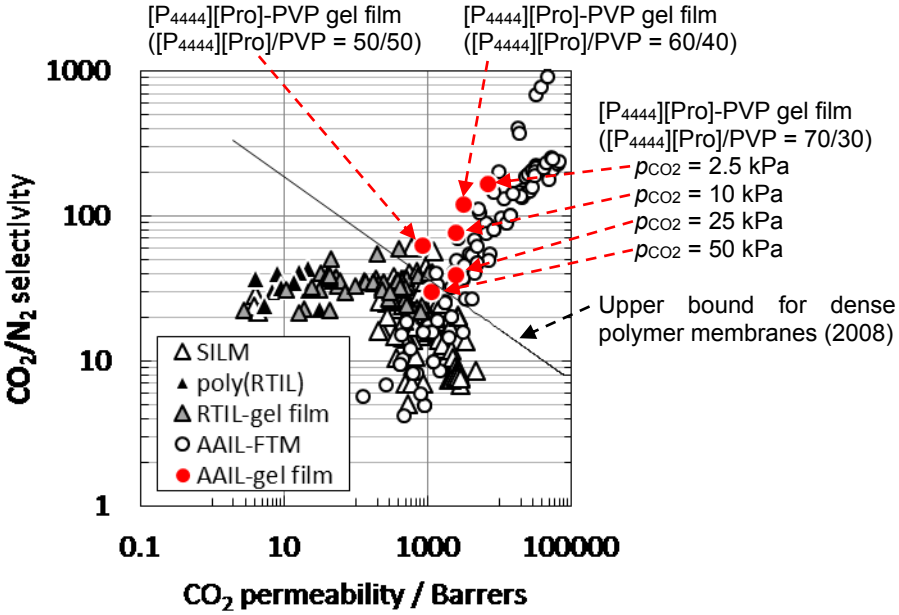

Fig. VI.11 Comparison of gas separation performance for various ionic liquid-related membranes.

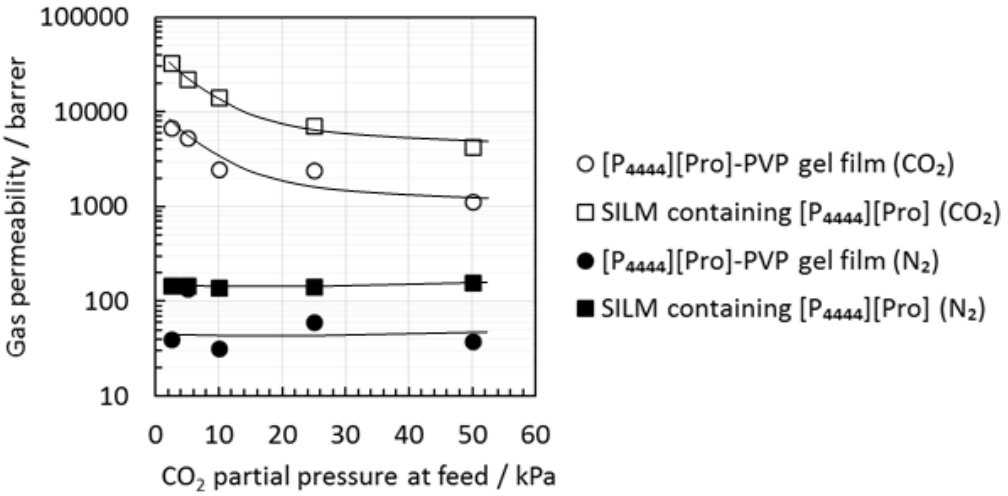

Fig. VI.12 CO_2 partial pressure dependencies on CO_2 permeability of the $[P_{4444}][Pro]$-PVP gel film of which $[P_{4444}][Pro]$ content was 70wt% (T= 373 K, Feed mixed gas: CO_2/N_2 (2.5/97.5, 10/90, 25/75 and 50/50vol%), Sweep gas: Helium, feed-side and sweep-side pressure were atmospheric pressure, CO_2 partial pressures in feed gas were 2.5, 10, 25 and 50 kPa and in sweep gas was 0 kPa, respectively, RH = 0%).

Unfortunately, I was not able to measure the exact gas permeability of the gel film under pressurised conditions. However, as shown in Fig. VI.8, the $[P_{4444}][Pro]$-PVP gel remained intact under a pressure of 1 MPa. This proof-of-concept study demonstrates the viability of AAIL-gels for use as a gas separation media. Improvements in both the AAIL and polymer matrix should provide a CO_2 separation membrane with excellent CO_2 permeability over an extremely wide pressure range. Ion-gels containing reactive ionic liquids such as AAILs would likely be useful in other separation technologies such as solid-liquid extraction medium and gas sorbents.

VI.4 Conclusions

Novel polymer gels containing an AAIL were fabricated by free radical polymerization of vinyl monomers. The AAIL-gels retained their shape before and after compression by

finger-pressure without any leakage of AAIL from the polymer matrix. [P_{4444}][Pro]-PVP gel sustained a stress of more than 1 MPa. In addition, transparent and flexible gel films were successfully created with thickness of 300 μm. At a [P_{4444}][Pro] content of 70 wt%, the CO_2 permeability of the AAIL-gel film was about 6700 Barrer. From the investigation of CO_2 partial pressure dependencies on gas permeability, it was revealed that CO_2 permeation mechanism of the AAIL-gel films are facilitated transport mechanism. The AAIL-gel films exhibited excellent transport properties, close to those of pure AAIL impregnated SILM. The polymeric AAIL-gel maintains liquid-like permeability within a solid-state material.

References

1. J. Lu, F. Yan and J. Texter, Prog. Polym. Sci., 2009, **34**, 431.
2. M. A. B. H. Susan, T. Kaneko, A. Noda and M. Watanabe, J. Am. Chem. Soc., 2005, **127**, 4976.
3. K. Ueno, K. Hata, T. Katakabe, M. Kondoh and M. Watanabe, J. Phys. Chem. B, 2008, **112**, 9013.
4. T. P. Lodge, Science, 2008, **321**, 50.
5. S. U. Hong, D. Park, Y. Ko and I. Baek, Chem. Commun., 2009, 7227.
6. J. E. Bara, R. D. Noble and D. L. Gin, Ind. Eng. Chem. Res., 2009, **48**, 4607.
7. T. K. Carlisle, G. D. Nicodemus, D. L. Gin and R. D. Noble, J. Membr. Sci., 2012, **397-398**, 24.
8. J. C. Jansen, K. Friess, G. Clarizia, J. Schauer and P. Izak, Macromolecules, 2011, **44**, 39.
9. A. Noda and M. Watanabe, Electrochim. Acta, 2000, **45**, 1265.
10. T. Ueki and M. Watanabe, Bull. Chem. Soc. Japan, 2012, **85**, 33.
11. J. Kagimoto, N. Nakamura, T. Kato and H. Ohno, Chem. Commun., 2009, 2405.
12. S. Taguchi, T. Matsumoto, T. Ichikawa, T. Kato and H. Ohno, Chem. Commun., 2011, **47**, 11342.
13. S. Harrisson, S. R. Mackenzie and D. M. Haddleton, Chem. Commun., 2002, 2850.
14. J. Barth, M. Buback, G. Schmidt-Naake and I. Woecht, Polymer, 2009, **50**, 5708.
15. A. Jelicic, S. Beuermann and N. Garcia, Macromolecules, 2009, **42**, 5062.
16. D. C. Cole, Tetrahedron, 1994, **50**, 9517.
17. E. S. Read, K. L. Thompson and S. P. Armes, Polym. Chem., 2010, **1**, 221.
18. I. Woecht, G. Schmidt-Naake, S. Beuermann, M. Buback and N. Garcia, J. Polym.

Sci., Part A: Polym. Chem., 2008, **46**, 1460.

19. S. Beuermann, M. Buback, P. Hesse and I. Lacik, Macromolecules, 2006, **39**, 184.
20. T. Y. Lee, T. M. Roper, E. S. Jonsson, C. A. Guymon and C. E. Hoyle, Macromolecules, 2004, **37**, 3606.
21. J. E. Bara, S. Lessmann, C. J. Gabriel, E. S. Hatakeyama, R. D. Noble and D. L. Gin, Ind. Eng. Chem. Res., 2007, **46**, 5397.
22. J. E. Bara, C. J. Gabriel, E. S. Hatakeyama, T. K. Carlisle, S. Lessmann, R. D. Noble and D. L. Gin, J. Membr. Sci., 2008, **321**, 3.
23. Y.-Y. Gu and T. P. Lodge, Macromolecules, 2011, **44**, 1732.
24. S. M. Mahurin, T. Dai, J. S. Yeary, H. Luo and S. Dai, *Ind. Eng. Chem. Res.*, 2011, **50**, 14061.
25. T. K. Carlisle, J. E. Bara, A. L. Lafrate, D. L. Gin and R. D. Noble, *J. Membr. Sci.*, 2010, **359**, 37.
26. Y. C. Hudiono, T. K. Carlisle, J. E. Bara, Y. Zhang, D. L. Gin and R. D. Noble, *J. Membr. Sci.*, 2010, **350**, 117.
27. B. A. Voss, J. E. Bara, D. L. Gin and R. D. Noble, *Chem. Mater.*, 2009, **21**, 3027.
28. J. E. Bara, T. K. Carlisle, C. J. Gabriel, D. Camper, A. Finotello, D. L. Gin and R. D. Noble, *Ind. Eng. Chem. Res.*, 2009, **48**, 2739.
29. J. E. Bara, C. J. Gabriel, T. K. Carlisle, D. E. Camper, A. Finotello, D. L. Gin and R. D. Noble, *Chem. Eng. J.*, 2009, **147**, 43.
30. J. E. Bara, D. L. Gin and R. D. Noble, *Ind. Eng. Chem. Res.*, 2008, **47**, 9919.
31. J. E. Bara, E. S. Hatakeyama, D. L. Gin and R. D. Noble, *Polym. Adv. Technol.*, 2008, **19**, 1415.
32. J. E. Bara, E. S. Hatakeyama, C. J. Gabriel, X. Zeng, S. Lessmann, D. L. Gin and R.

D. Noble, *J. Membr. Sci.*, 2008, **316**, 186.

33. Y. Gu, E. L. Cussler and T. P. Lodge, *J. Membr. Sci.*, 2012, **423-424**, 20.
34. P. Scovazzo, *J. Membr. Sci.*, 2009, **343**, 199.
35. J. J. Close, K. Farmer, S. S. Moganty and R. E. Baltus, *J. Membr. Sci.*, 2012, **390-391**, 201.
36. L. C. Tome, M. A. Aboudzadeh, L. P. N. Rebelo, C. S. R. Freire, D. Mecerreyes and I. M. Marrucho, *J. Mater. Chem. A*, 2013, **1**, 10403.
37. P. Scovazzo, J. Kieft, D. A. Finan, C. Koval, D. DuBois and R. Noble, *J. Membr. Sci.*, 2004, **238**, 57.
38. L. M. Robeson, *J. Membr. Sci.*, 2008, **320**, 390.

Chapter VII

Conclusions

In this study, to overcome the disadvantages of the conventional FTMs, I fabricated novel FTMs including aTSILs with suitable properties as a CO_2 carrier and investigated their CO_2 permeation properties under various conditions. In application the aTSILs to the FTMs, the comprehension of relationship between the physicochemical properties of the aTSILs and the CO_2 permeation properties of the aTSIL-FTMs is very important. Therefore, the CO_2 permeation properties of the aTSIL-FTMs were investigated both experimentally and theoretically on the basis of the physicochemical properties of the aTSILs. In addition, based on the relationship, I proposed design guidelines of an aTSIL with stable structure as a CO_2 carrier of the FTMs under several conditions. The conclusions of this study are summarized below.

1. Fabrication of amino acid ionic liquid-based facilitated transport membranes for CO_2 separation

Novel CO_2-selective membranes with excellent CO_2 permeability were fabricated with AAILs. I synthesized a series of tetrabutylphosphonium-type AAILs and prepared AAIL-FTMs containing the synthesized AAILs. AAILs act as not only a diffusion medium but as a CO_2 carrier and remarkably facilitate CO_2 permeation under dry and low humidity conditions. Among the AAIL-FTMs, FTM containing AAIL with prolinate as an anion showed the highest CO_2 permeation property under dry condition. As the results of hygroscopicity and water-holding property measurements, it was suggested

that the highest performance of the AAIL-FTM containing the prolinate type AAIL is due to the highest water-holding property of the AAIL. That is to say, it can be said that water included AAILs enhances the CO_2 transport through the AAIL-FTMs.

2. Fundamental investigation of the factors controlling the CO_2 permeability of facilitated transport membranes containing amine-functionalized task-specific ionic liquids

I synthesized three types of AAILs containing various glycinate anions. Among them, the AAILs that has CO_2 reactivity showed drastically increased viscosity with CO_2 absorption. From the FT-IR analysis, this increase of the viscosity was due to formation of hydrogen bonds among the CO_2 complexes. The CO_2 permeability at a low temperature under dry conditions was improved by using the IL which do not form hydrogen bond among the IL-CO_2 complexes. I propose the following to fabricate a FTM with high CO_2 permeability over a wide temperature range: 1) the aTSIL has somewhat higher CO_2 absorption ability, 2) the aTSIL does not change its viscosity with CO_2 absorption, and 3) the aTSIL has lower viscosity before CO_2 absorption.

3. Improvements in the CO_2 permeation selectivities of amino acid ionic liquid-based facilitated transport membranes by controlling their gas absorption properties

The effects of the cation size of AAILs on their gas absorption and gas permeability properties were investigated. An AAIL with smallest size cation in this study showed the lowest N_2 absorption amount because the AAIL had the smallest molar volume. Therefore, a FTM including the AAIL with the smallest size cation showed the best N_2 barrier property and CO_2/N_2 selectivity under dry conditions. From these results, it can

be said that the N_2 barrier property of the AAIL-FTMs can be improved by using an AAIL with small size cation. I could propose a methodology for improving the CO_2/N_2 selectivity of AAIL-FTMs based on reducing their N_2 permeabilities.

4. An amino acid ionic liquid-based facilitated transport membrane with excellent CO_2 permeation properties under humid and/or elevated temperature conditions

To improve the CO_2 separation performance of the AAIL-FTMs, a novel AAIL with suitable gas absorption properties for application as a CO_2 separation membrane was synthesized. The novel AAIL with a small size and two amino groups showed high CO_2 and low N_2 absorption amounts. In addition, an AAIL-FTM including the novel AAIL showed extremely high CO_2 permeability and N_2 barrier property under wide temperature and RH conditions. The CO_2 permeability and selectivity of the AAIL-FTM was higher than conventional FTMs under humid and/or elevated temperature conditions, which exhibited over 300,000 Barrer of CO_2 permeability and a CO_2/N_2 selectivity exceeding 5,000 under optimal conditions. From the investigation, it can be said that the increase of amino groups in the AAILs and the decrease of molecular size of the AAILs are effective way to improve the CO_2 separation performance of the AAIL-FTMs.

5. Polymeric ion-gels containing an amino acid ionic liquid for facilitated CO_2 transport media

Novel polymeric ion-gel containing an AAIL as its solvent was fabricated. An AAIL-gel containing a PVP as a polymer matrix showed high mechanical strength, which sustained a stress of more than 1 MPa. As the AAIL-gels has high formability, the gel

films which indicate transparent and flexible were therefore successfully prepared. The AAIL-gel film containing 70 wt% of AAIL showed high CO_2 permeability, which was 6700 Barrer. This is because AAIL in the gel film act as not only diffusion medium but a CO_2 carrier. As mentioned above, it can be said that the polymeric AAIL-gel is preferable material for CO_2 separation membrane.

List of Publications

Chapter II Amino acid ionic liquid-based facilitated transport membranes for CO_2 separation, **Shohei Kasahara**, Eiji Kamio, Toru Ishigami, Hideto Matsuyama, *Chem. Commun.*, 2012, **48**, 6903-6905.

Effect of water in ionic liquids on CO_2 permeability in amino acid ionic liquid-based facilitated transport membranes, **Shohei Kasahara**, Eiji Kamio, Toru Ishigami, Hideto Matsuyama, *J. Membr. Sci.*, 2012, **415-416**, 168-175.

Chapter III Fundamental investigation of the factors controlling the CO_2 permeability of facilitated transport membranes containing amine-functionalized task-specific ionic liquids, **Shohei Kasahara**, Eiji Kamio, Akihito Otani, Hideto Matsuyama, *Ind. Eng. Chem. Res.*, 2014, **53**, 2422-2431.

Chapter IV Improvements in the CO_2 permeation selectivities of amino acid ionic liquid-based facilitated transport membranes by controlling their gas absorption properties, **Shohei Kasahara**, Eiji Kamio, Hideto Matsuyama, *J. Membr. Sci.*, 2014, **454**, 155-162.

Chapter V An amino acid ionic liquid-based facilitated transport membrane with excellent CO_2 permeation properties under humid and/or elevated

temperature conditions, **Shohei Kasahara**, Eiji Kamio, Abdul Rajjak Shaikh, Hideto Matsuyama, in submitted.

Chapter VI Polymeric ion-gels containing an amino acid ionic liquid for facilitated CO_2 transport media, **Shohei Kasahara**, Eiji Kamio, Ayumi Yoshizumi, Hideto Matsuyama, *Chem. Commun.*, 2014, **50**, 2996-2999.

Other Publication

A facilitated transport ion-gel membrane for propylene/propane separation using silver ion as a carrier, **Shohei Kasahara**, Eiji Kamio, Reiko Minami, Hideto Matsuyama, *J. Membr. Sci.*, 2013, **431**, 121-130.

Acknowledgement

First of all, I would like to express my sincere gratitude to Prof. Hideto Matsuyama for the support and the opportunity to perform my study under his supervision. Through your leading I could learn a lot about my study and myself. All that you taught me will always affect me in my future life.

I am truly grateful for assistant Prof. Eiji Kamio. You have been a continual source of support and encouragement. Your attitude of research and life always impressed me. I respect you both as a researcher and a person. Therefore, I could exert myself to be like you. Without your leading and your kind help, I could not achieve my accomplishments here. I will never forget this favor as long as my life.

I sincerely thank Prof. Atsunori Mori and Prof. Satoru Nishiyama for your kindness during the reviewing and examining of this thesis and giving constructive comments to improve upon it. I also owe my gratitude to the members in Prof. Matsuyama's laboratory. Thank you for your constructive comments for my study and your kindness.

I would like to offer my special thanks to Natsumi Miya for your mental support and cooperation. With you around, I could always freshen my thinking. Thank you for always listening to me and being there for me.

Finally, I am forever grateful for my parents. While I am truly grateful for both the financial and practical help you have given me, the most important thing has been your mental support. I would not have accomplished my PhD thesis without you.

Shohei Kasahara

Graduate School of Engineering

Kobe University, 2014

Appendix

The resulted ^{1}H-NMR results and FT-IR spectra are shown below.

[P_{4444}][Gly]

^{1}H-NMR (DMSO, δ/ppm relative to TMS): δ = 0.92 (t, 12H, J = 7.1; a), 1.37-1.50 (m, 16H; b,c), 2.08 (s, 1H; DMSO), 2.16-2.22 (m, 8H; d), 2.50-2.51 (m, 1H, acetonitrile), 2.64 (s, 2H; N-CH_2-CO_2), 3.16 (s, 3H; methanol), 3.39 ppm (broad; water)

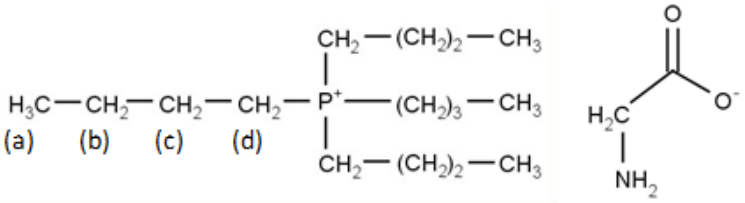

[Emim][Gly]

^{1}H-NMR (DMSO, δ/ppm relative to TMS): δ = 1.41 (t, 3H, J = 7.4; a), 2.51 (s, 0H; DMSO), 2.73 (s, 2H; N-CH_2-CO_2), 3.20 (broad; water), 3.87 (s, 3H; b), 4.22 (q, 2H, J = 11.2; c), 7.75 (s, 1H; d), 7.84 (s, 1H; e), 9.68 (s, 1H; f)

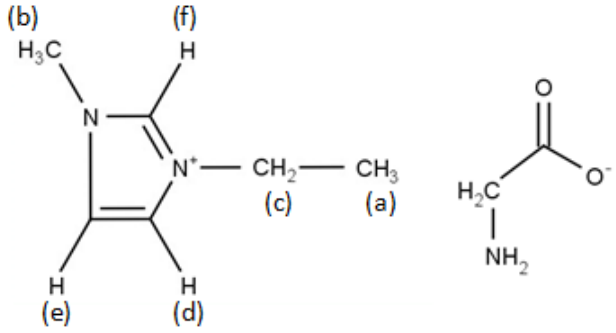

[P_{4444}][Ala]

^{1}H-NMR (DMSO, δ/ppm relative to TMS): δ = 0.93 (t, 12H, J = 7.1; a), 0.99 (d, 3H, J = 3.5; CH_3-C-N), 1.37-1.51 (m, 16H; b, c), 2.14-2.25 (m, 8H; d), 2.50-2.52 (m, 2H; acetonitrile), 2.78 (q, 1H, J = 10.4; CH), 3.17 (s, 2H; methanol), 3.37 ppm (broad; water)

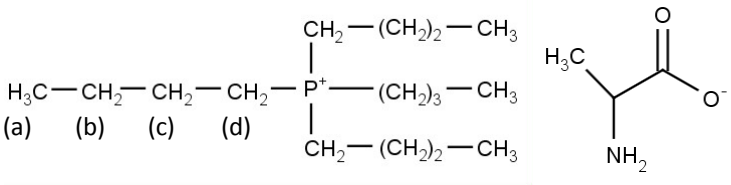

[P_{4444}][Ser]

^{1}H-NMR (DMSO, δ/ppm relative to TMS): δ = 0.93 (t, 12H, J = 7.3; a), 1.36-1.52 (m, 16H; b, c), 2.11-2.25 (m, 8H; d), 2.50-2.52 (m, 3H; acetonitrile), 2.78 (t, 1H, J = 10.9; CH-O), 3.12 (t, 1H, J = 13.9; CH-N), 3.18 (s, 2H; methanol), 3.26 (q, 1H, J = 5.3; CH-O), 3.35 ppm (broad; water)

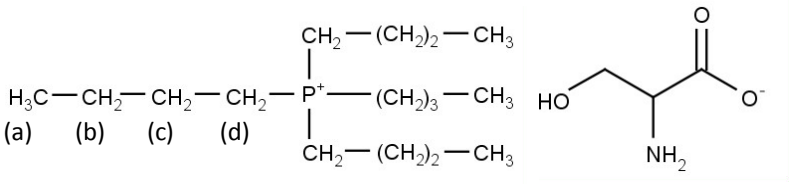

[P_{4444}][Pro]

^{1}H-NMR (DMSO, δ/ppm relative to TMS): δ = 0.92 (t, 12H, J = 6.9; a), 1.34-1.54 (m, 18H; b, c), 1.6 (broad, 1H), 1.69-1.78 (m, 1H), 2.15-2.25 (m, 8H; d), 2.48-2.56 (m, 2H; acetonitrile), 2.88-2.94 (m, 1H), 3.02 (broad, 1H), 3.17 (s, 1H; methanol), 3.50 ppm (broad; water)

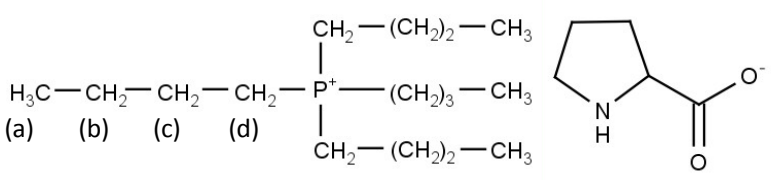

[P_{4444}][mGly]

^{1}H-NMR (DMSO, σ/ppm relative to TMS)

σ = 0.92 (t, 12H, J = 7.3; a), 1.05 (t, 6H, J = 6.0; ethanol), 1.37-1.51 (m, 16H; b,c), 2.19 (s, 3H; N-CH_3), 2.20-2.28 (m, 8H; d), 2.65 (s, 2H; N-CH_2-CO_2), 3.44 ppm (dd, 4H; ethanol)

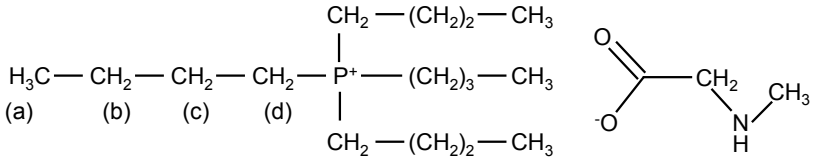

[P_{4444}][dmGly]

^{1}H-NMR (DMSO, σ/ppm relative to TMS)

σ = 0.92 (t, 12H, J = 7.1; a), 1.37-1.51 (m, 16H; b,c), 2.12 (s, 6H; N-$(CH_3)_2$), 2.17-2.23 (m, 8H; d), 2.50-2.51 (m, 1H, DMSO), 2.52 (s, 2H; N-CH_2-CO_2), 3.17 ppm (s, 2H; water)

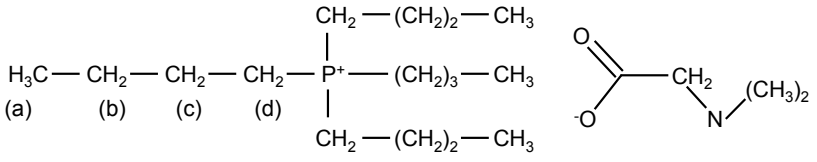

[P_{4444}][2-CNpyr]

^{1}H-NMR (DMSO, σ/ppm relative to TMS)

σ = 0.92 (t, 12H, J = 7.1; a), 1.37-1.49 (m, 16H; b,c), 2.13-2.19 (m, 8H; d), 5.82 (dd, 1H, J = 3.15, 1.58; H on the cyanopyrrolide ring), 6.43 (dd, 1H, J = 3.15, 1.26; H on the

cyanopyrrolide ring), 6.67 ppm (t, 1H, J = 1.26; H on the cyanopyrrolide ring)

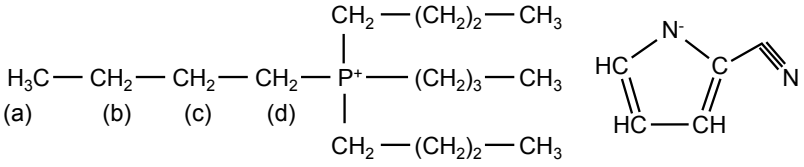

[P_{66614}][Gly]

^{1}H-NMR (DMSO, σ/ppm relative to TMS)

σ = 0.80-0.97 (m, 12H), 1.21-1.34 (m, 32H), 1.35-1.42 (m, 8H), 1.43-1.51 (m, 8H), 2.15-2.29 (m, 8H), 2.50-2.52 (m, 1H; DMSO), 2.64 ppm (s, 2H; N-CH_2-CO_2)

[P_{2225}][Gly]

^{1}H-NMR (DMSO, σ/ppm relative to TMS)

σ = 0.89 (t, 3H, J = 7.4), 1.08-1.17 (m, 9H), 1.29-1.41 (m, 4H), 1.45-1.53 (m, 2H), 2.18-2.30 (m, 8H), 2.65 ppm (s, 2H; N-CH_2-CO_2)

[N_{4444}][Gly]

^{1}H-NMR (DMSO, σ/ppm relative to TMS)

σ = 0.94 (t, 12H, J = 7.3; a), 1.28-1.35 (m, 8H; b), 1.55-1.61 (m, 8H; c), 2.65 (s, 2H; N-CH_2-CO_2), 3.16-3.20 ppm (m, 8H; d)

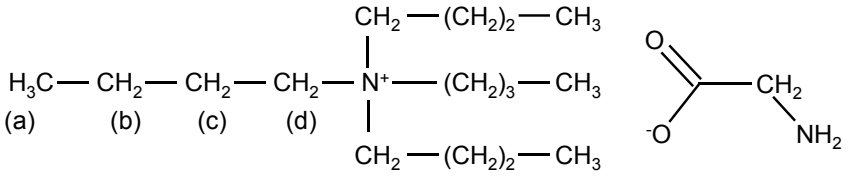

[N_{1111}][Gly]

^{1}H-NMR (DMSO, σ/ppm relative to TMS)

σ = 2.69 (s, 2H; N-CH_2-CO_2), 3.15 ppm (s, 12H; N-CH_3)

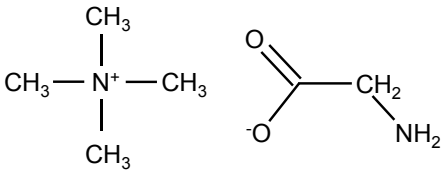

[aN_{111}][Gly]

^{1}H-NMR (DMSO, σ/ppm relative to TMS)

σ = 2.75 (s, 2H; N-CH_2-CO_2), 3.33 (s, 9H; N-CH_3), 6.79 ppm (s, 2H; N-NH_2)

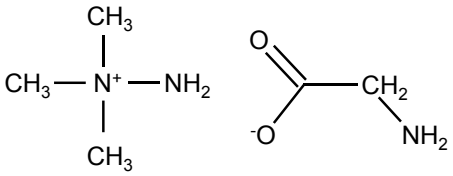

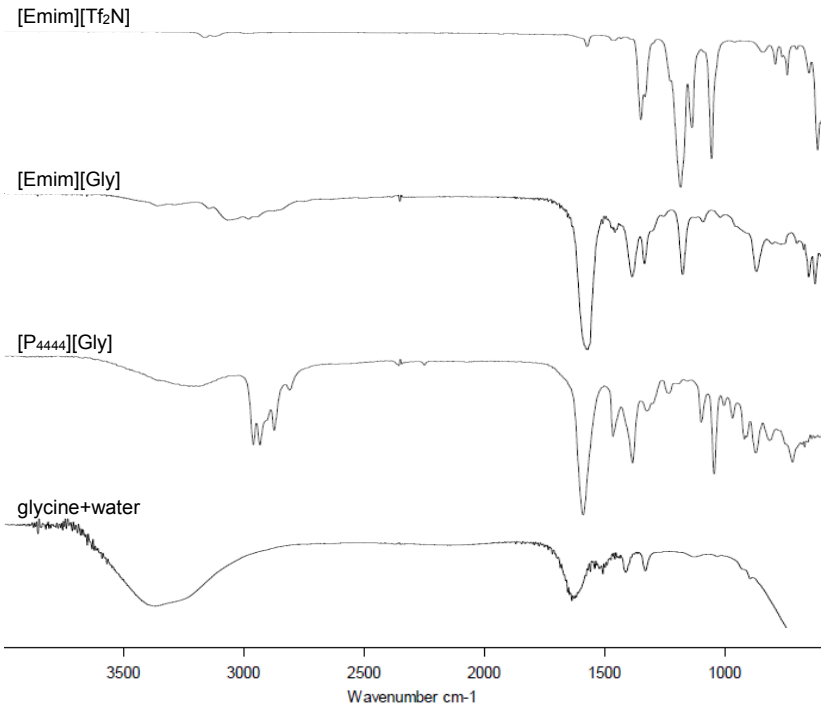

Fig. a1 FT-IR spectra of [Emim][Tf_2N], [Emim][Gly], [P_{4444}][Gly] and glycine aqueous solution.

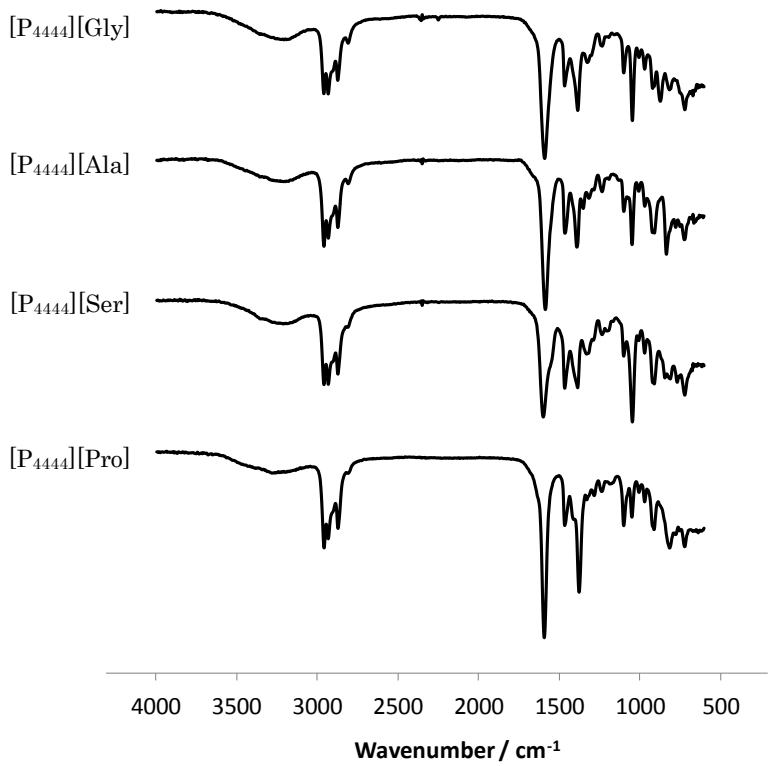

Fig. a2 FT-IR spectra of [P_{4444}][Gly], [P_{4444}][Ala], [P_{4444}][Ser] and [P_{4444}][Pro].

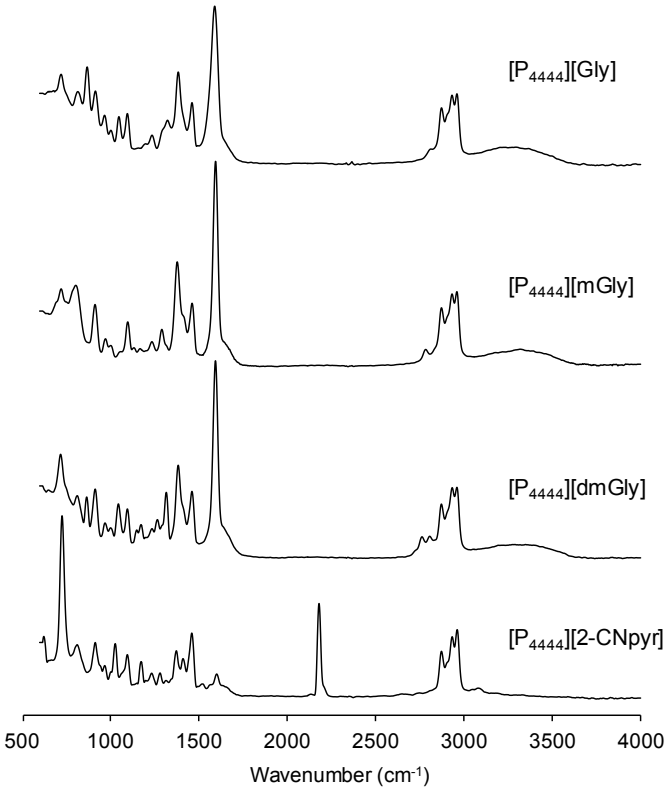

Fig. a3 FT-IR spectra of [P_{4444}][Gly], [P_{4444}][mGly], [P_{4444}][dmGly] and [P_{4444}][2-CNpyr].

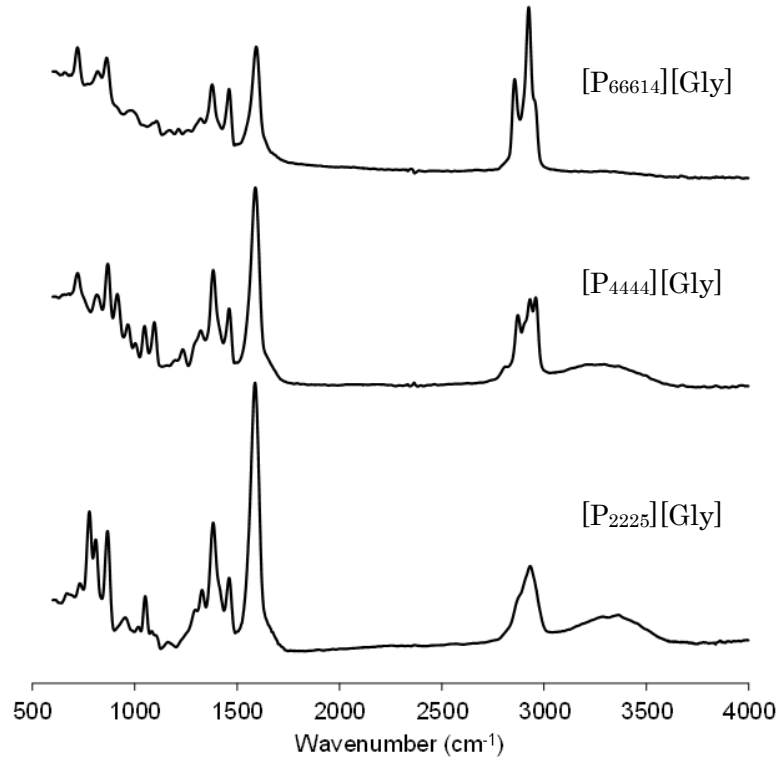

Fig. a4 FT-IR spectra of [P_{66614}][Gly], [P_{4444}][Gly] and [P_{2225}][Gly].

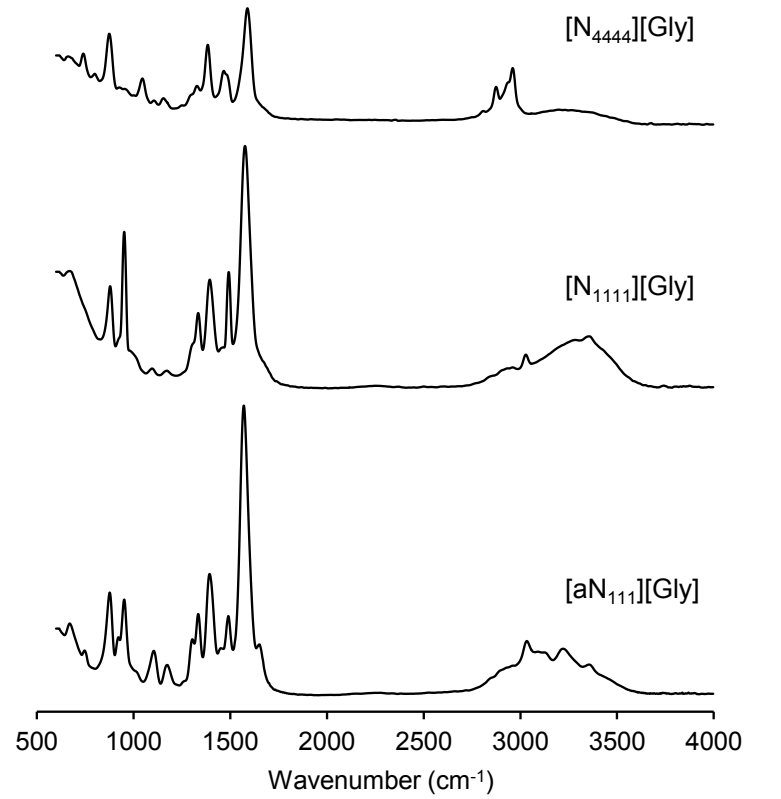

Fig. a5 FT-IR spectra of [N_{4444}][Gly], [N_{1111}][Gly] and [aN_{111}][Gly].

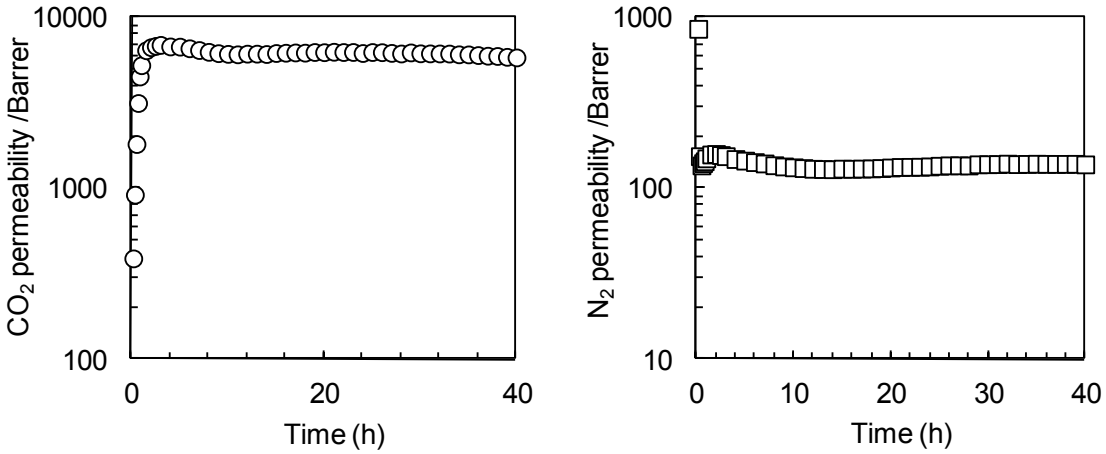

Fig. a6 Time course of (a) CO_2 and (b) N_2 permeability through $[P_{4444}][Gly]$-FTM (T = 373.15 K, CO_2 = 10 mol%, N_2 = 90 mol%, without moisture, $P_F = P_S$ = 101.3 kPa).

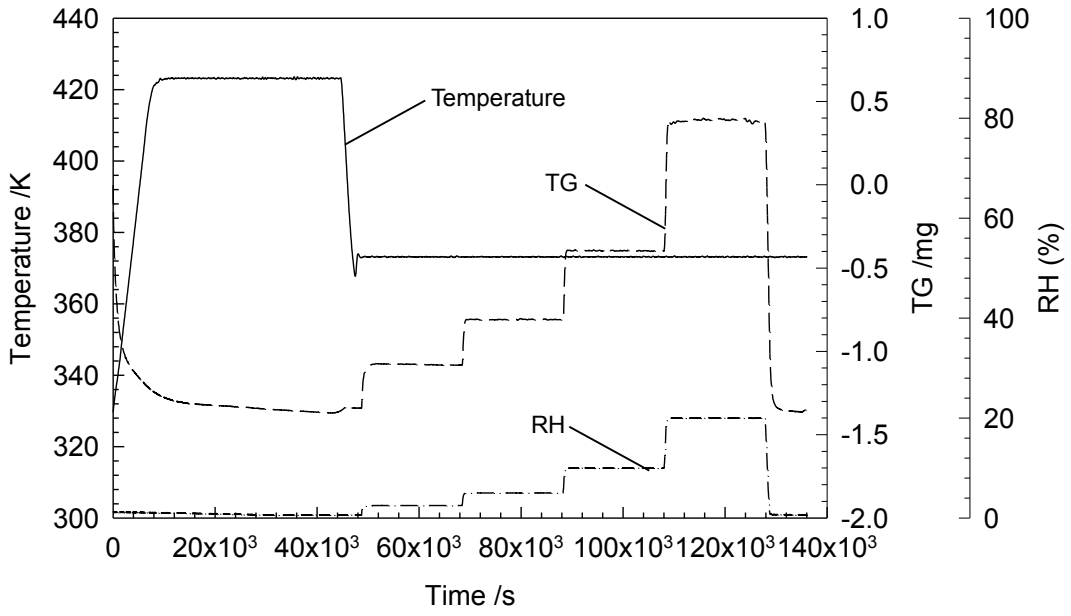

Fig. a7 Relationship among temperature, RH and TG of $[P_{4444}][Gly]$.

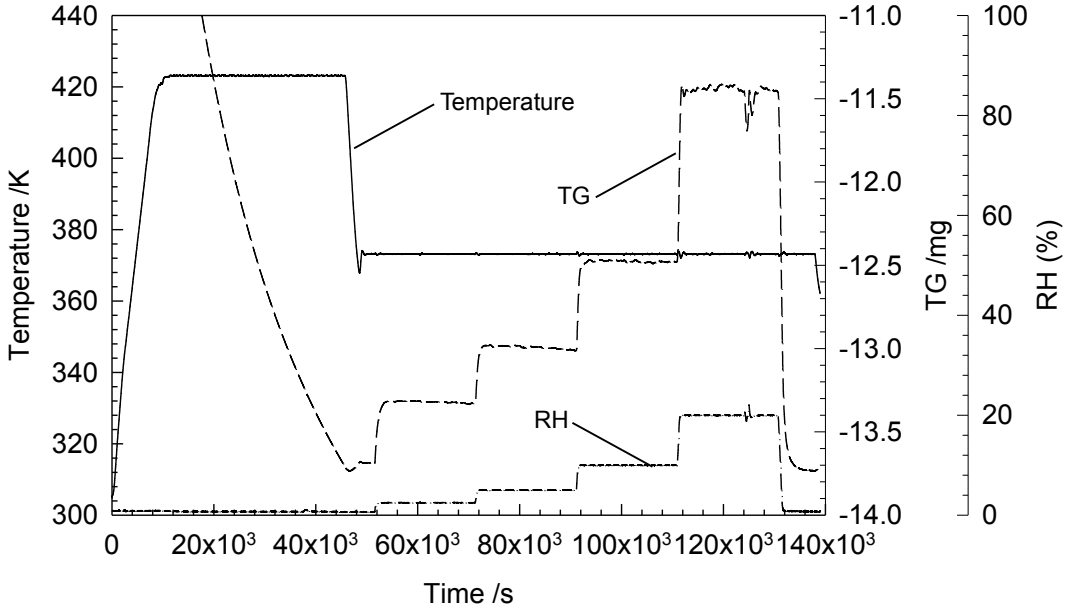

Fig. a8 Relationship among temperature, RH and TG of [Emim][Gly].

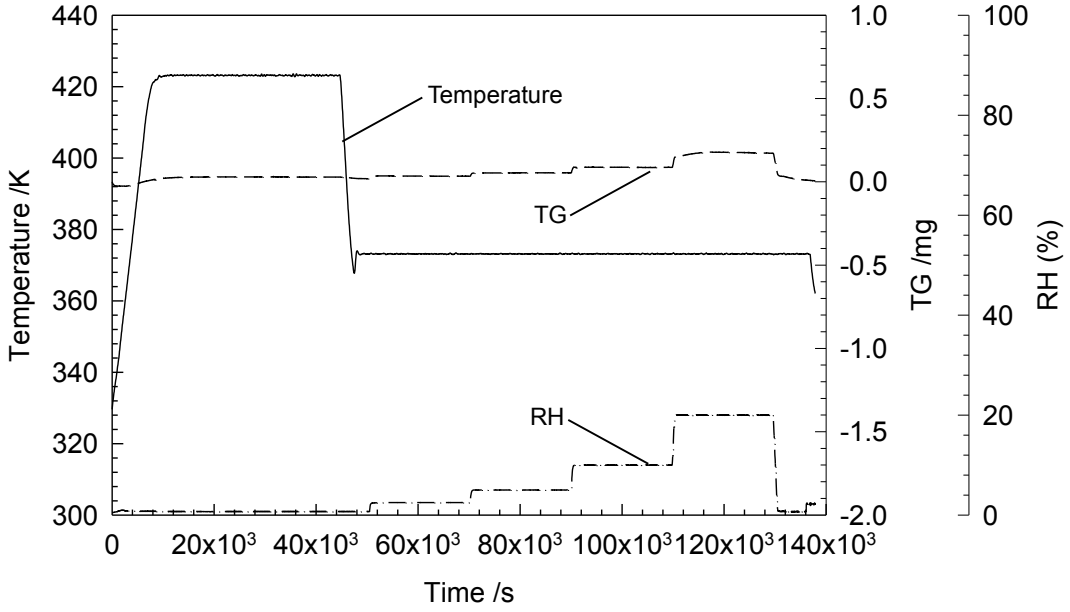

Fig. a9 Relationship among temperature, RH and TG of [Emim][Tf_2N].

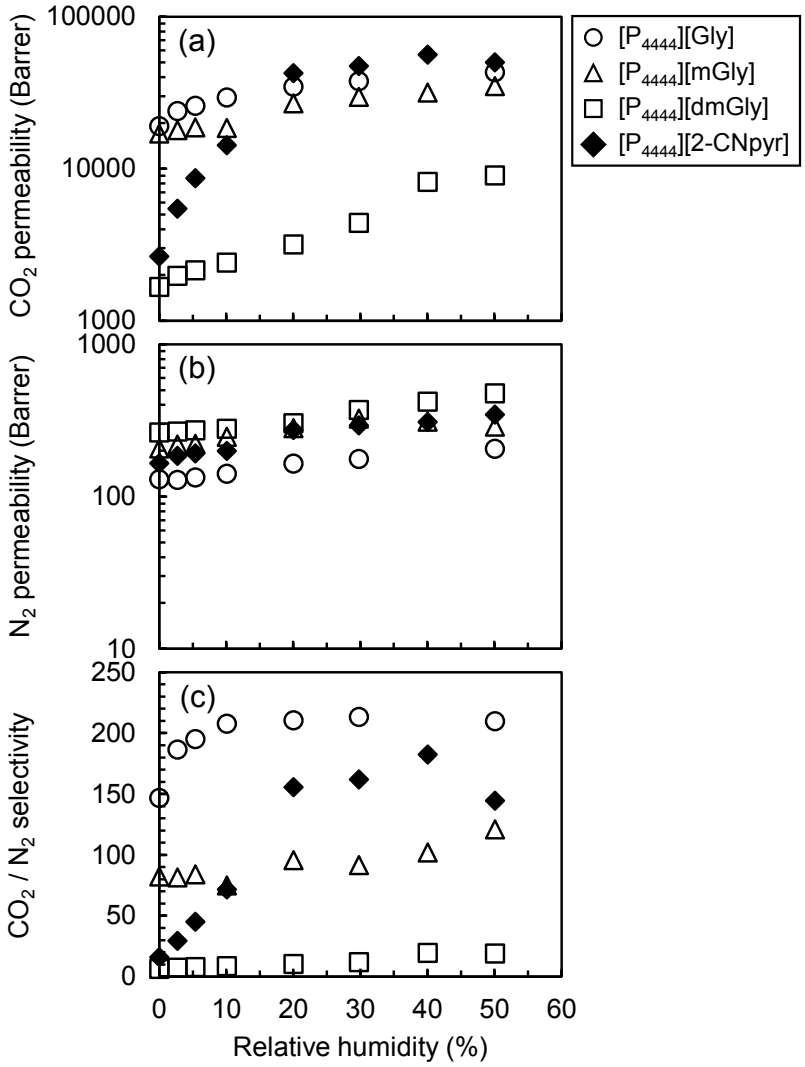

Fig. a10 Relative humidity dependences on (a) CO_2 permeability, (b) N_2 permeability and (c) CO_2/N_2 selectivity for [P_{4444}][Gly]-, [P_{4444}][mGly]-, [P_{4444}][dmGly]-, and [P_{4444}][2-CNpyr]-based membranes.

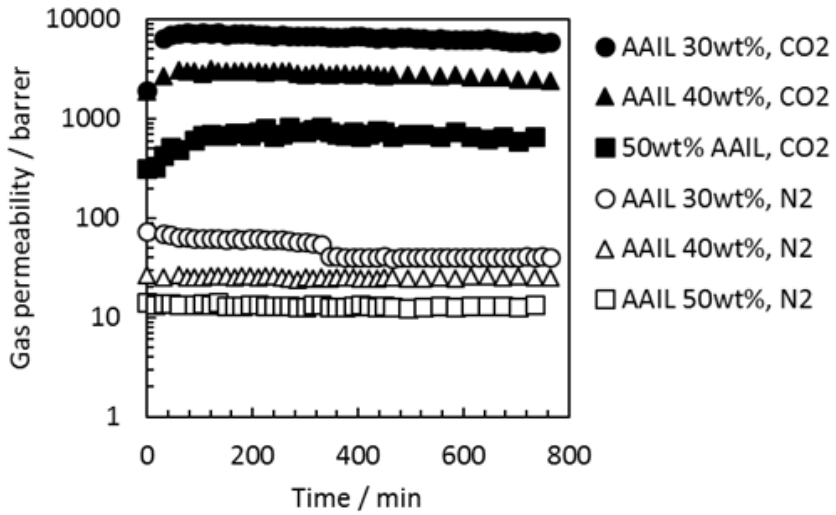

Fig. a11 Time course of CO_2 and N_2 permeability through $[P_{4444}][Pro]$-PVP gel film (T= 373 K, Feed mixed gas: CO_2/N_2 (2.5/97.5vol%), Sweep gas: Helium, feed-side and sweep-side pressure were atmospheric pressure, CO_2 partial pressures in feed and sweep gases were 2.5 kPa and 0 kPa, respectively, RH = 0%).

Doctoral Dissertation, Kobe University
"Study on development of CO_2 reactive ionic liquid-based facilitated transport membranes for CO_2 separation", 177 pages
Submitted on 7, 7, 2014
The date of publication is printed in cover of repository version published in Kobe University Repository Kernel.